NOISE IN NOISE OUT - SINGLE MOLECULE STUDIES OF MOLECULAR MOTORS

BY

MARCO TJIOE

DISSERTATION

Submitted in partial fulfillment of the requirements
for the degree of Doctor of Philosophy in Biophysics and Computational Biology
in the Graduate College of the
University of Illinois at Urbana-Champaign, 2017

Urbana, Illinois

Doctoral Committee:

Professor Paul R. Selvin, Chair
Professor Yann R. Chemla
Professor Brian L. DeMarco
Assistant Professor Kai Zhang

ABSTRACT

Many cellular functions rely on the movements of molecular motors. Single molecule studies of these motors allow investigation into their step-sizes and stall forces. Such studies inevitably involve noise, which is inherent in the biological and imaging systems probing these motors. Having to work with noise in the system, we develop a parameter, called the FIONA Index, which serves as a guide for data quality based on noise per step-size (NPS) and frames per step (FPS). Attempting to bring the noise out of the system, we develop Magnetic Cytoskeleton Affinity (MiCA) purification to remove excess dyes that prevent clear observation of individual motors. We show that with appropriate treatment of noise, complex systems can be assembled to study how multiple motors work together.

ACKNOWLEDGEMENTS

This work is possible only with the help of individuals who support me throughout my graduate journey. I would like to thank my advisor, Paul Selvin, who lets me work on projects I am passionate about, while at the same time teaching me how to prioritize, do science, and think like a scientist. I am also thankful for my thesis and prelim committee, Prof. Yann Chemla, Prof. Brian DeMarco, Assistant Prof. Kai Zhang, Prof. Martin Gruebele and Prof. SuA Myong, for taking the time to sit in and review my thesis and prelim, and for the flexibility with changes in the thesis defense date.

I am grateful for the funding support by NSF PHY-1430124 and NIH GM108578 to PRS, University of Illinois Physics Department, and Gregorio Weber Graduate Award, which have allowed me to focus on the science at hand.

I would like to thank previous and current lab members: Paul Simonson, Eli Rothenberg, Benjamin Blehm, Melinda Hoffman, Janet Sheung, Hannah Deberg, Dylan Reid, Pinghua Ge, Ruobing Zhang, Hyeongjun Kim, Murat Baday, En Cai, Tobias Rosenkranz, Pallavi T. Rosenkranz, Kai Wen Teng, Sang Hak Lee, Yuji Ishitsuka, Andre Thomaz, Duncan Nall, Chaoyi Jin, Yeoan Youn, Pin Ren, Yongjae Lee, and Saurabh Shukla, for the invaluable discussions, technical support and expertise, and camaraderie that help make graduate life much less stressful than it would have.

I would also want to thank our collaborators: Kathy Trybus, Carol Bookwalter, Ahmet Yildiz, Vladislav Belyy, Sinan Can, Ronald Vale, Richard McKenney, Walter Huynh, Yann Chemla and Barbara Stekas for providing the kinesin and dynein used throughout this thesis work, for the SIC stepfinder program used in the first chapter of this work, and for the help in optical trapping.

I had the chance to work with many talented undergraduates throughout my graduate career. I want to thank Everett Vacek, Hyeon Ryoo, Aaron Cravens, Vi Vi Phung, Soojinn Hyung, Nakyung Lee and Joyeon Kim for all the help in preparing PEG coverslips, doing experiments, and conducting analysis that allow me to complete the research projects at much faster pace.

To two of the most important people in my world, my parents Suwarjono Tjioe and Tan Tjin Tjin; I would like to thank you for your unconditional love and support, your exemplary attitude towards work, and your humility. Without you, I am not me. To my brother and sister, Martin and Fidelia, thank you for sharing much life wisdom with me, which has allowed me to stay grounded even when the going gets rough. To my cherished partner, Chye Hong, thank you for your constant companionship. You never fail to put my heart at ease every time we meet and chat. You teach me how to relate better to others.

Last but not least, I would like to thank friends at Tzu Chi, Styrecycle, Meadowbrook Health Center, and Crisis Nursery for helping me find meaning in life through service. You teach me that there is always a bigger picture if we are willing to take a step back and look.

TABLE OF CONTENTS

Noise does not cancel out noise; silence does

Mahatma Gandhi

CHAPTER 1

NOISE IN: THE FIONA INDEX - A GUIDE TO OPTIMIZE NOISE AND FRAME RATE FOR MOLECULAR MOTOR STEPPING EXPERIMENTS

The important thing is not to be too comfortable when you're writing. Noise in the street? That's good. The computer goes down? That's good. All these things are good. It has to be a little bit of a struggle.

E. L. Doctorow

1.1 Abstract

Measurements of molecular motor step-sizes are always accompanied by noise. To date there is no guideline to the level of acceptable noise for step-size analysis. In this study we look at how noise affects data quality at varying frame rate, finding that as noise increases, frame rate needs to increase exponentially to maintain accurate step-size measurement. We developed a parameter, called the FIONA Index, which serves as a guide for data quality based on noise per step-size (NPS) and frames per step (FPS), and if necessary, to eliminate those traces which do not meet this quality. A rough guideline is to get a FIONA Index of ~ 1. To detect steps, we use the Schwarz Information Criterion (SIC) step-finder, as we find that the SIC step-finder has the most consistent performance across all noise levels compared to either the Student's t-test or the Hidden Markov Method. As an example, we evaluate the FIONA Index for kinesin, although it should be applicable to any molecular motor.

1.2 Introduction

Single-molecule tracking (SMT) with high precision are required for dynamic studies of molecular motors, such as that of myosin, kinesin and dynein. This often means low noise and fast temporal resolution (or equivalently, frame rate) in order to clearly delineate steps. Too slow temporal resolution will yield too long of a step size because of an admixture of multiple step-sizes; too fast temporal resolution and there won't be enough signal (photons) to get the precision desired.

Fluorescence Imaging with One Nanometer Accuracy (FIONA) was invented to accurately pinpoint the position of a fluorescent probe, achieving ~ 1.5 nm spatial accuracy using frame rates from 2 Hz[1,2] to 1000 Hz[3]. Getting the best step-size data does not come simply through using the fastest frame rate, because increasing frame rate inadvertently increases noise as the number of photons collected decreases. There is thus a fine interplay between frame rate and noise. The lack of a guideline for an acceptable level of noise at a given frame rate has led to uncertainty in determining these experimental parameters, and the inability to objectively filter out poor quality data.

No study has been done to investigate the optimal combinations of frame rate and noise for step-size experiments. Several studies have been conducted to extract true step-sizes of molecular motors [4–8], but they did not probe the relationship between frame rate and noise. Other studies examined noise, but only to obtain true velocity and trajectory, not step-size [9,10]. The study that comes closest to evaluating the effect of frame rate and noise for a step-size experiment was done by Carter et al., who examined the performance of different step-finding algorithms −t-test, velocity threshold, chi-squared minimization and a derivative of Gaussian wavelet− at different noise levels[9]. They found that the performance of all step-finding algorithms decreases with increasing noise, and concluded that the chi-squared minimization was their method of choice for step finding over a wide range of noise. This study, however, did not specifically establish what level of noise is acceptable at each frame rate, which is the objective of this paper.

We started with evaluating the performance of three different step-finding algorithms− Student's t-test, Hidden Markov Model (HMM), and Schwarz Information Criterion (SIC) − to quantify and predict the likelihood of a step-finding algorithm to find the "true" step-size at a given noise level and frame rate. We find the SIC is the best. Furthermore, we introduced a simple measure that relates frame rate to noise, which we call the FIONA Index. The FIONA Index is defined as:

$$FIONA\ Index = \frac{FPS}{4\ e^{3.25\ NPS}} \qquad (1)$$

where FPS is frames per step, a quantity related to the frame rate, and NPS is noise per step-size.

As discussed later, the equation is made such that when the FIONA Index less is than one, the FPS is less than the minimum needed at a given NPS, which means the frame rate is too low for its noise, hence its time-resolution needs to be increased. For such traces, the measured step-sizes are predicted to be larger than the true step-size. On the other hand, a trace with a FIONA Index more than one should yield the correct step-size of the molecular motor under study (subject to other experimental

parameters, such as stage drift). Different traces will have different FIONA Indices due to variation in noise and molecular motors velocity. A significant advantage of knowing the FIONA Index is that certain data runs that have a FIONA Index less than one can be eliminated and the "correct" step-size then calculated.

In this paper we focus on kinesin-1, the conventional kinesin, although our calculations should be valid for any molecular motor. With kinesin–1, the "true" step-size is 8.3 nm[2,10], meaning its center of mass traverses 8.3 nm each time kinesin steps. A typical kinesin velocity in the cell is around 800 nm/sec, or 100 steps/sec [3,11,12], with a rate dependent on the ATP concentration for *in vitro* measurements. As we find from our simulations, the relationship between optimal frame rate and noise is not linear, but rather fits to an exponential relationship (see equation 1).

1.3 Materials and Methods

1.3.1 Kinesin stepping simulation

We turn to simulation to produce traces with known step-size so that we can objectively evaluate the performance of the step-finding algorithms. To simulate kinesin stepping in one dimension, we use Matlab to generate a master stepping trace consisting 5 million frames with an average dwell of 4620 frames/step (FPS). We use such high average dwell for the master trace to allow traces with shorter dwells to be produced. At every simulated frame, kinesin is allowed to take an 8 nm step with a probability of 1/4620. Note that here we use 8 nm instead of the precise 8.3 nm kinesin step-size for the sake of simplicity, with no loss in precision. At the end of the simulation for the master trace, kinesin has taken 1142 steps with a displacement of 9136 nm.

With the master trace, we then produce 35 other traces with FPS between 1 and 1000 by taking regular position intervals of the master trace. This is akin to collecting data at the fastest frame rate, and generating traces at slower frame rate using positions at the fastest frame rate. To be specific, FPS 1 trace contains positions taken from frame 1, 4620, 9240, to 4998840 of the FPS 4620 trace. FPS 2 trace contains displacements from frame 1, 2310, 4620, to 4998840 of the FPS 4620 trace. The number of kinesin steps is the same for all traces, just that there are more frames for the higher FPS.

Once the 35 traces from FPS 1 to 1000 are produced, we add a normally distributed random noise with amplitude between 0 nm to 14 nm to each trace, which means that the noise added varies from 0 to 1.75 times larger than the step-size (8 nm). This dimensionless quantity, the noise per step-size (NPS), enables us to generalize our result to molecular motors that have step-sizes other than 8 nm. For noise, what matters has less to do with the absolute magnitude of the noise than its relative magnitude with respect to the step-size. A noise of 4 nm and 20 nm has the same effect for motors with step-size of 8 nm and 40 nm respectively since their NPS are both 0.5.

1.3.2 Step-detection methods

There are many step-finding algorithms, and identifying the best algorithm is essential to get accurate step-sizes at various noise and frame rate. As mentioned previously, a review by Carter et al.[9] compared the performance of Student T-test method[8], Velocity Threshold (VT) method[13], Chi-Squared minimization method[14] and derivative of Gaussian wavelet (dG wavelet) method[15] and concluded that Chi-Squared minimization is the method of choice for step finding under the performance metric used. Since the review by Carter et al., two other step-finding algorithms: Hidden Markov Model[6,7] and SIC step-finder[5] were reported, and both claim to perform better than the Chi-Squared minimization method under similar performance metric as described by Carter et al.[9].

In this study, we compare three different step-detection methods: 1) Student's t-test, 2) Hidden Markov Model and 3) SIC step-finder.

1.3.2.1 Student's t-test

We implemented the Student's t-test algorithm using Interactive Data Language (IDL) from Exelis Visual Information Solutions. For each stepping point, an equal number of points before and after this stepping point are compared and for every point, a student's t-test is performed using the equation:

$$t = \frac{\bar{x}_1 - \bar{x}_2}{\sqrt{\frac{s_1^2}{N} + \frac{s_2^2}{N}}}$$

where N is the number of points in each sample, s_1^2 and s_2^2 are the unbiased estimator of the sample variances, and $\bar{x}_1$ and $\bar{x}_2$ are the sample means. The output is the t-statistic and has a value between 0 and 1. A plot of the t-statistic vs. frame will yield a downward or upward peak indicating potential step locations. Small values for the t-test, usually 0.10, 0.05 or 0.01, imply that the means, $\bar{x}_1$ and $\bar{x}_2$, are significantly different with 90%, 95%, or 99% confidence interval respectively. Downward peaks (forward step) or upward peaks (backward step) in the significance values are identified as steps when their magnitudes are smaller than the significance threshold. We vary the significance threshold from 0.01 to 0.05, corresponding to a confidence range of 95% to 99% that the two populations are significantly different. We also vary N from 2 (at least two points are needed to calculate a standard deviation) to 10 (large enough sampling to test if two populations are significantly different) with unit increments. Step-fits are obtained for all significance threshold and N values; the step-fit with the lowest chi-square are chosen to be the best fit.

1.3.2.2 Hidden Markov model

HMMs are extensively used for computer voice recognition[16] sequence analysis of DNA[17] and analysis of single ion channel recordings[18–21]. A thorough discussion of the improved Hidden Markov Model for molecular motors is laid out by Müllner et al. and Syed et al.[6,7]. Implementation of HMM requires little-or-no user input for step finding. There are two major tasks in Hidden Markov Model analysis: the first is to estimate the model parameters, which include dwell times and step-size distribution. This is done through maximum likelihood (ML) estimation. The second is to obtain idealized time course of the motor activity once the model parameters are known. This is done using Viterbi algorithm[6].

Müllner et al. and Syed et al. developed robust algorithms that improved on previously available Markovian-based techniques. Their algorithm allows analysis of molecular motors with arbitrary distribution of step-sizes, better modeling of the data acquisition process, and one that accounts for the random baseline drifts. They call their method variable step-size, integrating detector HMM (VSI-HMM)[6,7]. We use the Matlab implementation of this algorithm for the HMM analysis of our simulated data.

1.3.2.3 Schwarz Information Criterion (SIC) step-finder

Kalafut et al. described a step detection method making use of the Schwarz Information Criterion (SIC) to decide the number and location of steps[5]. This method takes no user input and step detection is automatic and objective. The SIC is used to prevent over-fitting by introducing penalties for over-fitting. This is useful for discriminating between models with differing number of parameters, as is the case for stepping traces when an additional step means an additional parameter. Without a penalty, statistical tests like the likelihood-ratio tests tend to favor models with more parameters.

Kalafut et al. derived the SIC statistic for step detection by treating the stepping data as a series of independent trials of Gaussian random variables with identical variances, yielding:

$$SIC(j_1, \dots, j_k) = (k+2)\log n + n\log \hat{\sigma}^2_{j_1,\dots,j_k} + n\log 2\pi + n$$

where $j_1, \dots, j_k$ are the assumed step locations, $\hat{\sigma}^2_{j_1,\dots,j_k}$ is the maximum likelihood estimator of the variance calculated with the assumed step locations, and n is the number of data points. The terms n and $n\log 2\pi$ are constant and may be dropped, since only relative values of the SIC is important.

The process of step-detection using SIC stepfinder involves calculating the SIC statistic for all the data points. The point having the lowest value of SIC statistic is the step location for a one-step fit. This SIC statistic for one-step hypothesis is compared with SIC statistic for no-step hypothesis. If no-step SIC is lower, the step finding process is terminated and no step is concluded for the trace. Otherwise, the one-step hypothesis is accepted and the process is repeated again looking for a second step and comparing

the SIC statistic for two-step vs. one-step. This continues until the SIC statistic for the k-step is lower than the (k+1)-step, in which case the step finding process is terminated and the trace is fitted with k steps.

1.3.3 Metrics to determine the performance of step-finding algorithms

There are different ways to assess the performance of step-finding algorithms. Carter et al. uses three metrics: fraction of true steps found, fraction of fitted steps correctly placed, and fraction of steps with the correct step-size (8 nm)[9]. Here we use a different metric directly relevant to the molecular motor research: the predicted step-size of the molecular motor. This is not trivial considering the output for each step-finding algorithm is not just a single value for the step-size, but a distribution of step-sizes. We find that the predicted step-size can be estimated by fitting two Gaussians to the step-size histogram, constraining the center of the second Gaussian (corresponding to missed steps) to twice the center of the first Gaussian. The predicted step-size of the motor is taken to be the center of the first Gaussian. Using these predicted step-sizes, we can compare the performances of the three step-finding algorithms under study.

1.3.4 Kinesin motility assay

Kinesin walking assay is performed using Qdot® 655 streptavidin conjugate from Thermo Scientific (Q10121MP) bound to truncated kinesin expressed with biotin and His-tag (K432-Bio-H6). Qdot and kinesin is mixed in 1 to 3 ratio using BRB10-BSA buffer (10 mM PIPES, 1 mM EGTA, 1 mM MgCl2, pH 6.9, with 10 mg/mL BSA). Experiments are done on polyethylene glycol (PEG) coverslip with 5% biotin-PEG. Briefly, one chamber volume of 6 M streptavidin (43–4302, Life Technologies) are flowed into the sample chamber and incubated for > 2 mins. The chamber is then washed with two chamber volumes of BRB10-BSA. Next, two chamber volumes of HiLyte 488-biotin-microtubule (1:3:25 HiLyte 488 tubulin : biotin-tubulin : tubulin from Cytoskeleton, Inc.) is flowed in and incubated for > 2 mins. Two chamber volumes of Taxol-biotin buffer (20 M Taxol (Cytoskeleton, Inc.), 100 M biotin (B4501, Sigma Aldrich)) is then flowed in to block the remaining binding sites of streptavidin. Lastly, imaging buffer containing 200 nM MgATP, 375 nM Qdot-kinesin, 1 mM THP (71194, EMD Millipore), 20 µM Taxol, 100 nM PCD (P8279, Sigma-Aldrich), 10 mM PCA (37580, Sigma Aldrich), 100 µM biotin (B4501, Sigma-Aldrich), 2 Units/mL Creatine Kinase (10127566001, Roche Applied Science) and 2 mM Creatine Phosphate (10621714001, Roche Applied Science) is flowed into the chamber. The sample chamber is later imaged using total internal reflection (TIRF) microscopy.

1.3.4.1 Data collection at varying frame rate

When data acquisition is not fast enough, it becomes harder to obtain the true step-size of the molecular motors. To study the exact effect of varying frame rate on the predicted step-size of kinesin, we conduct the kinesin-walking assay with frame rates of 4 Hz, 10 Hz, 20 Hz, 40 Hz, and 100 Hz.

1.3.4.2 Analysis through integrating frames

Frame rates can also be manipulated post-experimentally by summing together multiple frames, creating new sets of data with lower frame rates from the original data. This allows us to study the effect of varying frame rates using the same data set, thus avoiding user biases that may arise when we are cropping points to be analyzed.

Using data from the fastest frame rate (100 Hz), we create new sets of data by integrating the frames 5x, 25x, 125x and 625x, creating data with frame rates of 20 Hz, 4 Hz, 0.8 Hz and 0.16 Hz.

1.4 Results

1.4.1 Determining NPS and threshold FPS

In order to formulate the FIONA Index, we need to know two quantities: NPS and threshold FPS. The NPS is simply the noise level divided by the expected step-size (8 nm). We define the threshold FPS to be the minimum FPS needed to yield successful step finding at a given noise. We define a successful step-finding algorithm to be successful when the predicted step-size falls within 10% of the true step-size. So, for the case of 8 nm step-size, the range is 7.2 nm - 8.8 nm. This is applicable to all the step-fitting algorithms.

With this definition, we systematically find the threshold FPS for each noise level from 1 nm to 14 nm, corresponding to NPS of 0.125 to 1.75. Figure 1.1 shows the simulation and step-finding using SIC-stepfinder for two noise levels: 1 nm and 12 nm. The threshold FPS increases from 6 to 600 when the noise increases from 1 nm to 12 nm. As noise increases, we need more and more frames between steps because noise blurs each stepping instance, making it more difficult to be sure that a step is a step and not a noise.

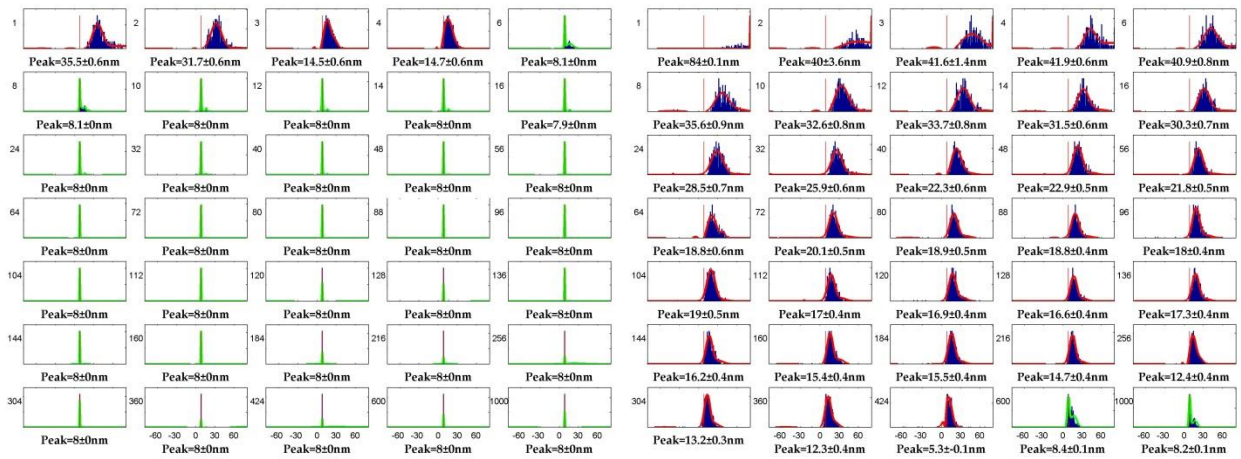

(a) Noise 1 **(b) Noise 12**

Figure 1.1: Simulation and step-fitting with SIC-stepfinder at frames per step (FPS) between 1 to 1000 and noises of (a) 1 nm and (b) 12 nm. The step-size histograms are fitted to two Gaussians at each negative and positive step-size. Green fits are assigned to FPS windows with predicted step-sizes of 8 nm ± 0.8 nm, while red fits are assigned to those outside the range. As noise increases, more FPS is needed to get the right step-size. The threshold FPS for noise 1 and 12 are 6 and 600 respectively.

1.4.2 Relationship between threshold FPS and NPS

Intuitively, we know that as the noise per step-size (NPS) increases, the threshold FPS will increase. What we do not know is how fast the threshold FPS increases with NPS. This varies significantly from one step-finding algorithm to another, as shown in Figure 1.2.

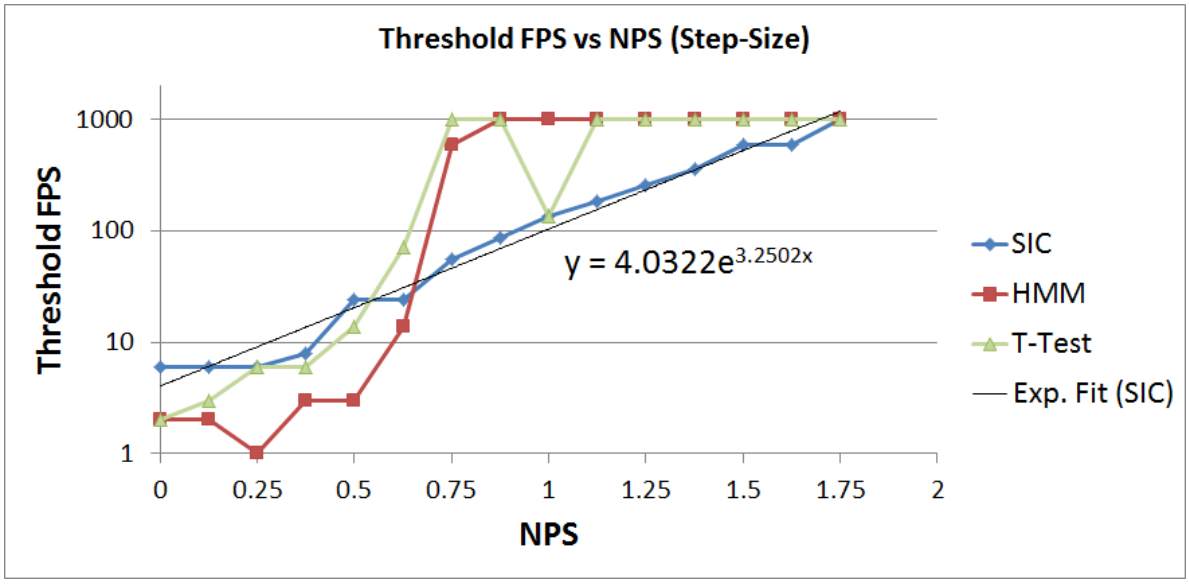

Figure 1.2: A semi-log plot of threshold FPS at different NPS for T-test, HMM and SIC stepfinder. Lower threshold FPS means better step-finding for a given level of noise. At low noise (NPS < 0.625), HMM and Student's T-test are better than SIC-stepfinder, with HMM being the best. At high noise (NPS > 0.625) SIC-stepfinder is better at detecting steps. The consistent performance of SIC-stepfinder across a wide range of noise enables an exponential fit.

For the Student's T-test, the threshold FPS starts at 2 at zero noise, and increases rapidly to FPS greater than 1000 at NPS 0.75. As discussed in Appendix A.1, the threshold FPS at zero noise should be a number greater than 1 frame per step due to the exponential nature of the dwell time. Note that we report any threshold FPS greater than 1000 to be 1000 since our simulation stops at FPS 1000. Student's T-test tends to overfit noise as a series of back and forth steps with no net displacement, as shown in Appendix Figure A.3. This started at NPS 0.375, and renders result from the Student's T-test unreliable for NPS greater than 0.375 because it reports both negative and positive step-sizes when the real step only contains positive step.

For HMM, the threshold FPS starts at 2 at zero noise and stays around 2 to 3 until NPS 0.5. After that it increases quickly to 1000 at NPS 0.875. HMM is generally better than Student's T-test at all noise regime because it reports only positive step-sizes, which means that it does not overfit the traces. The noise regime for accurate step-fitting with HMM is between NPS 0 and 0.75. (See also Figure 3 in Sheyum et al7 and associated discussion of HMM at high noise.)

For SIC-stepfinder, the threshold FPS starts at 6 at zero noise, and increases gradually to 1000 at NPS 1.75. SIC-stepfinder is more reliable than Student's T-test because it reports only positive step-sizes at all noise level, as shown in supplemental Appendix Figure A.3. Compared to HMM, SIC-stepfinder performs worse at very low noise, but it quickly catches up at NPS larger than 0.625. The predictable, gradual increase of the threshold FPS for SIC-stepfinder makes it a better step-finding algorithm than T-test and HMM as it allows us to formulate an equation linking FPS to NPS over a large noise range. As shown later in Figure 1.5, the NPS for a kinesin walking experiment can range anywhere between 0.2 to

1.4, a wide range where the SIC-stepfinder works well. We therefore choose SIC-stepfinder as our routine step-finding algorithm, and will use it for the step-size analysis of the kinesin stepping experiments and to formulate the FIONA Index. This will help us eliminate those traces --which should be eliminated-- in order to end up with a more accurate value for the final step size from an experimental set of data.

1.4.3 Formulation of FIONA Index

The consistency in the performance of SIC-stepfinder across a wide noise spectrum prompts us to use SIC-stepfinder to formulate FIONA Index. T-test or HMM can also be used to formulate the FIONA Index, though the resulting formula will be different. It is important to note that FIONA Index formulated with one step-finding algorithm is useful to evaluate traces analyzed only with that particular step-finding algorithm.

In Figure 1.2, we see that the Threshold FPS vs. NPS graph for SIC-stepfinder can be fitted with an exponential fit, yielding the equation:

$$Threshold\ FPS = 4\ e^{3.25\ NPS}$$

We define the FIONA Index simply as the ratio between the left-hand-side vs. right-hand-side of the equation above, with threshold FPS being a special case of FPS.

$$FIONA\ Index = \frac{FPS}{4\ e^{3.25\ NPS}} \qquad (1)$$

When the FPS equals threshold FPS at a given NPS, the FIONA Index will be 1; When the FPS is less than the threshold FPS, FIONA Index will be smaller than one. Since threshold FPS is defined as the minimum FPS needed to yield successful step-finding, a FIONA Index less than 1 means poor step-finding that will give larger predicted step-size than expected.

During the analysis of a kinesin walking trace, the FPS and NPS can be calculated with the following equations:

$$\boldsymbol{FPS = \frac{N_{frames}}{N_{steps}}} \qquad (2)$$

$$\boldsymbol{NPS = \frac{\sqrt{\frac{1}{N}\sum_{i=1}^{N}\left(x_i - x_{fit_i}\right)^2}}{S}} \qquad (3)$$

where N_{frames} is the number of frames, N_{steps} is the number of steps, S is the step-size, x is the walking trace, and x_{fit} is the fitted trace. N_{steps} can be calculated in two ways, one is by simply getting the number of steps fitted by the step-finding algorithm, and another by taking displacement divided by the expected step-size (8 nm). The FPS that generates the lowest FIONA Index is used. When FIONA Index is more than 1, there are enough frames collected that the trace FPS is greater than the threshold FPS, yielding predicted step-size close to 8 nm. When FIONA Index is less than 1, the trace FPS is lower than threshold FPS, and the predicted step-size is likely greater than 8 nm.

To verify that the formulation for FIONA Index in Equation (1) is applicable to step-sizes other than 8 nm, we repeat the kinesin walking simulation using step-sizes of 1.5 nm and 35 nm and show in Appendix Figure A.5 that we get similar formulation as in Equation (1).

Equation (1) shows the formulation of the FIONA Index based on step-size histogram, yielding threshold FPS vs NPS graph in Figure 1.2. Similar threshold FPS vs NPS graph based on dwell-time instead of step-size histogram can be generated, and this is shown in supplemental Figure A.9. This will yield a different and more stringent formulation of the FIONA index and can be used when the dwell-time is important.

1.4.4 Applying FIONA Index to kinesin stepping data

Once the FIONA Index is formulated, we can start applying it to evaluate the data quality of a kinesin walking assay. Here we typically use low ATP concentration (200 nM) and a frame rate around 12.5 Hz, or a time-resolution of 80 msec.

For each kinesin stepping trace obtained through experiment, we get a displacement vs. frame graph as shown in Figure 1.3(a). The blue line is the experimental data of the stepping trace, and the red line is the fit to the data (the step-fit). The step-sizes are noted next to the steps of the step-fit. Since the number of frames is 1089 and the number of steps is 45, the FPS can be calculated with equation (2), yielding 1089/45 = 24.2.

To calculate NPS, we refer to the residual graph in Figure 1.3(b). The residual is the difference between the step-trace and the step-fit. In Figure 1.3(b), the residual falls between –5 nm to 5 nm, with a standard deviation of 2.6 nm. This is the noise. Since the expected step-size is 8 nm, we can calculate the NPS using equation (3), yielding 2.6 nm/8 nm = 0.325.

Knowing FPS and NPS, we can calculate FIONA Index using equation (1), yielding FIONA Index = 2.1, which is clearly greater than 1.

When the FPS and NPS is plotted on Figure 1.3(c), we get a good sense of where the FPS and NPS stands with respect to the FIONA Index = 1 line. Any points above this line will have FIONA Index > 1, which is good for step-size prediction. Any points below this line will have FIONA Index < 1. For this trace with high FIONA Index, the FPS vs. NPS point lies above the FIONA Index = 1 line.

Due to the high FIONA Index of this trace, its predicted step-size should come very close to the true step-size, which is 8.3 nm. Indeed, when the step-size histogram is plotted on Figure 1.3(d) and fitted to a double Gaussian curve for both positive and negative step-sizes, the predicted step-size is 8.0 nm.

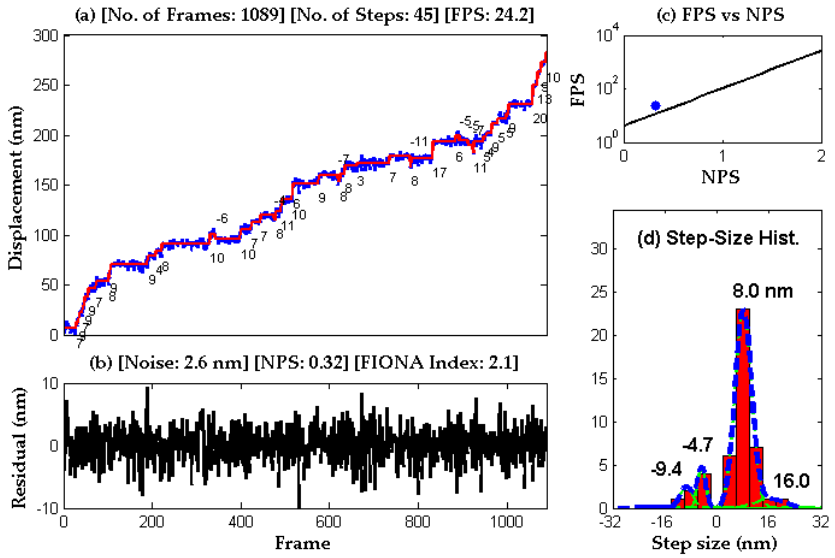

Figure 1.3: (a) A typical stepping trace of kinesin with high FIONA Index (= 2.1). Blue is the step-trace. Red is step-fit. The numbers next to the step fits are the step-sizes. (b) Residual graph subtracting the step-trace by the step-fit. (c) A semi-log graph of FPS vs. NPS. The straight line represents the line where FIONA Index = 1 and the blue dot plots the position of the FPS and NPS of the stepping-trace (d) Step-size histogram of the step-sizes obtained from the step-fits.

A trace from the same experiment as Figure 1.3 but with a low FIONA Index is shown in Figure 1.4(a). The FPS in this trace is 86.1, higher than that of Figure 1.3. Higher FPS usually leads to higher FIONA Index, but for this trace, the noise is really large, i.e. 10.5 nm as shown in Figure 1.4(b). This leads to high NPS of 1.31, leading to low FIONA Index of 0.3.

When the FPS vs. NPS graph is plotted on Figure 1.4(c), the FPS vs. NPS point lies below the FIONA Index = 1 line. With a low FIONA Index, the predicted step-size should be larger than the true step-size. From Figure 1.4(d), we find that the predicted step-size is 12.6 nm, which is higher than the true 8.3 nm step-size.

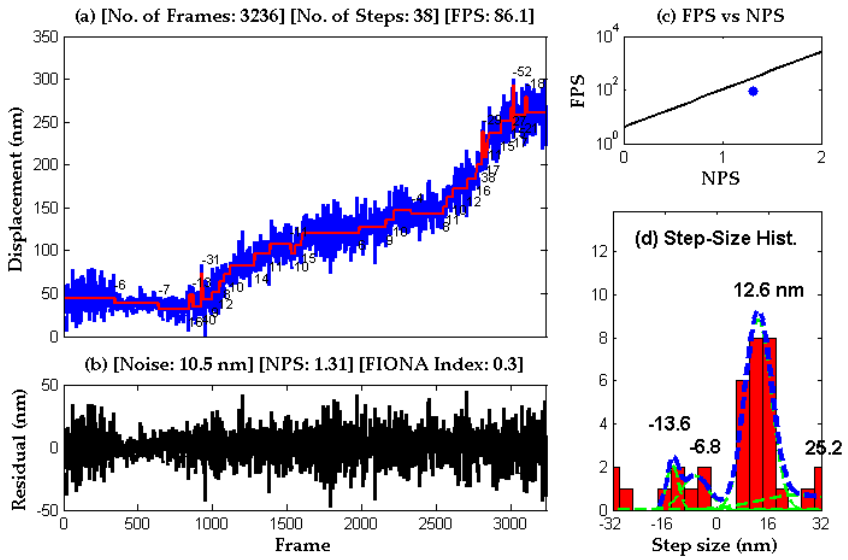

Figure 1.4: A typical stepping trace of kinesin with low FIONA Index (=0.3). Blue is the step-trace. Red is step-fit. The numbers next to the step fits are the step-sizes. (b) Residual graph subtracting the step-trace by the step-fit. (c) a semi-log graph of FPS vs. NPS. The straight line represents the line where FIONA Index = 1 and the blue dot plots the position of the FPS and NPS of the step-trace (d) Step-size histogram of the step-sizes obtained from the step-fits.

In our experience, a number of factors can yield a trace with low FIONA Index as in Figure 1.4. It may be the inherent noise in the trace, caused by the low signal; the sample is not properly focused; or microtubule fluctuation. Another factor is human error: choosing traces with sudden jumps caused by improper immobilization of microtubules; error in transforming 2D positional trace to a 1D staircase trace; or using traces when stage drifts are significant.

1.4.5 Effect of varying frame rates

To test the performance of FIONA Index, we perform the walking assay with kinesin for varying frame rates. We expect that as frame rate decreases, FIONA Index should decrease and the predicted step-size would become larger than the true 8.3 nm step. We use frame rates of 100 Hz, 40 Hz, 20 Hz, 10 Hz and 4 Hz.

Figure 1.5(a) shows the FPS vs. NPS graph for all the frame rates. Each point represents one trace. The different frame rates are color coded with yellow (100 Hz), light blue (40 Hz), magenta (20 Hz), dark blue (10 Hz) and 4 Hz (red). As the frame rate decreases from 100 Hz to 4 Hz, the FPS and NPS both decreases since FPS is proportional to frame rate and more photons are collected which reduces the noise.

For experiments with frame rates higher than 10 Hz, most of the points have their FIONA Indices greater than 1. For frame rates that are 10 Hz and below, the points are spread above and below the FIONA Index = 1 line, which means that some traces will have FIONA Indices greater than 1, and while others are less than 1.

Looking at the average FIONA Indices of the traces at varying frame rates in Figure 1.5(b), we notice that all of them have an average FIONA Index above 1, which means that the predicted step-size for all frame rates should be close to 8.3 nm. We note that the average FIONA Index increases from 2.46 to 3.04 as frame rate decreases from 100 Hz to 40 Hz, then decreases from 3.04 to 1.03 when frame rate decreases from 40 Hz to 4 Hz. One possible explanation is that the noise decreases much faster than frame rate from 100 Hz to 40 Hz, causing the FIONA Index to increase; while from 40 Hz to 4 Hz, the decrease in noise reaches a plateau as the frame rate keeps decreasing, causing the FIONA Index to decrease.

Figure 1.5(c) shows the step-sizes obtained at these frame rates. As expected, the step-sizes at all the frame rates are close to the true 8.3 nm step-size since all the FIONA Indices are greater than 1. At 4 Hz, the step size starts to be larger than 8.3 nm. We expect that at even lower frame rates, the predicted step-size will continue to increase. To confirm this, we sum together frames from the 100 Hz traces to generate traces with lower frame rates and report the result in the next section.

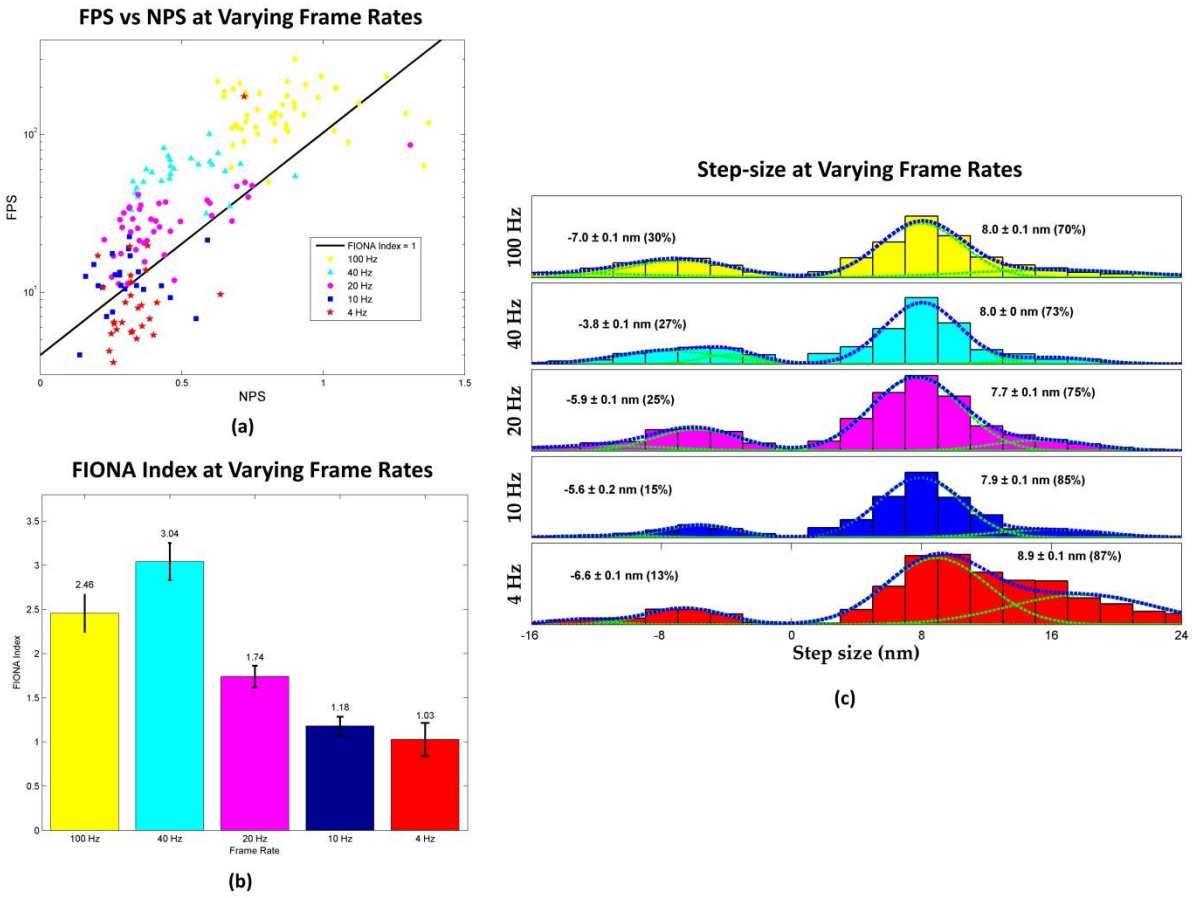

Figure 1.5: (a) FPS vs. NPS graph at varying frame rates. Each point represents one trace. The different frame rates are color coded with yellow (100 Hz), light blue (40 Hz), magenta (20 Hz), dark blue (10 Hz) and 4 Hz (red). (b) FIONA Index at varying frame rates. (c) Predicted step-size at varying frame rates.

1.4.6 Effect of integrating frames

By integrating frames 5x, 25x, 125x and 625x from the traces with the highest frame rate (100 Hz), we obtain traces at lower frame rates: 20 Hz, 4 Hz, 0.8 Hz, and 1.6 Hz. Figure 1.6(c) shows the changes in the predicted step-size as the integration factor increases. For 1x, 5x and 25x integration factors, the predicted step-sizes remain close to 8.3 nm. For 125x integration factor, the frame rate is low enough that there are significant skipped steps with large step-sizes, giving a predicted step-size of 10.7 nm. For 625x, there are too many skipped steps that there is essentially no step that is registered at 8 nm. All the step-sizes are bigger than 16 nm, and the predicted step-size is 24 nm.

Examining the FPS vs. NPS graph in Figure 1.6(a), we notice that the FPS consistently decreases when integration factor increases, while the NPS decreases then increases. The initial high value of NPS may be caused by high noise associated with kinesin cargo fluctuation or limitation in the number of photons collected at high frame rate. As integration factor increases to 5x and 25x, noise will decrease because

the fluctuations are averaged out and more photons are collected, yielding lower NPS. However after 25x integration factor, the FPS starts to be too low that there are a lot of skipped steps, generating imperfect step-size fits. These skipped steps and imperfect fits generate large residual graph similar to the one shown in Figure 1.4(b), giving rise to higher NPS.

Figure 1.6(b) shows the consistent decrease in the average FIONA Indices from 2.46 to 0.01 as the integration factor increases from 1x to 625x. As long as the FIONA Indices is above 1 (for 1x and 5x integration factor), the predicted step-sizes are close to the true step-size of 8.3 nm. It is worthwhile to note that the predicted step-size for the 25x integration factor is close to the true step-size of 8.3 nm, even though its average FIONA Index is 0.79, a value less than 1. This shows that certain traces with FIONA Indices less than 1—in this case, greater than 0.5— may still have predicted step-sizes close to the true step-size. For traces with 125x and 625x integration factor, their FIONA Indices are much less than 1 (0.11 and 0.01) and their predicted step-sizes are much greater than the true step-size of 8.3 nm (10.7 nm and 23.5 nm respectively).

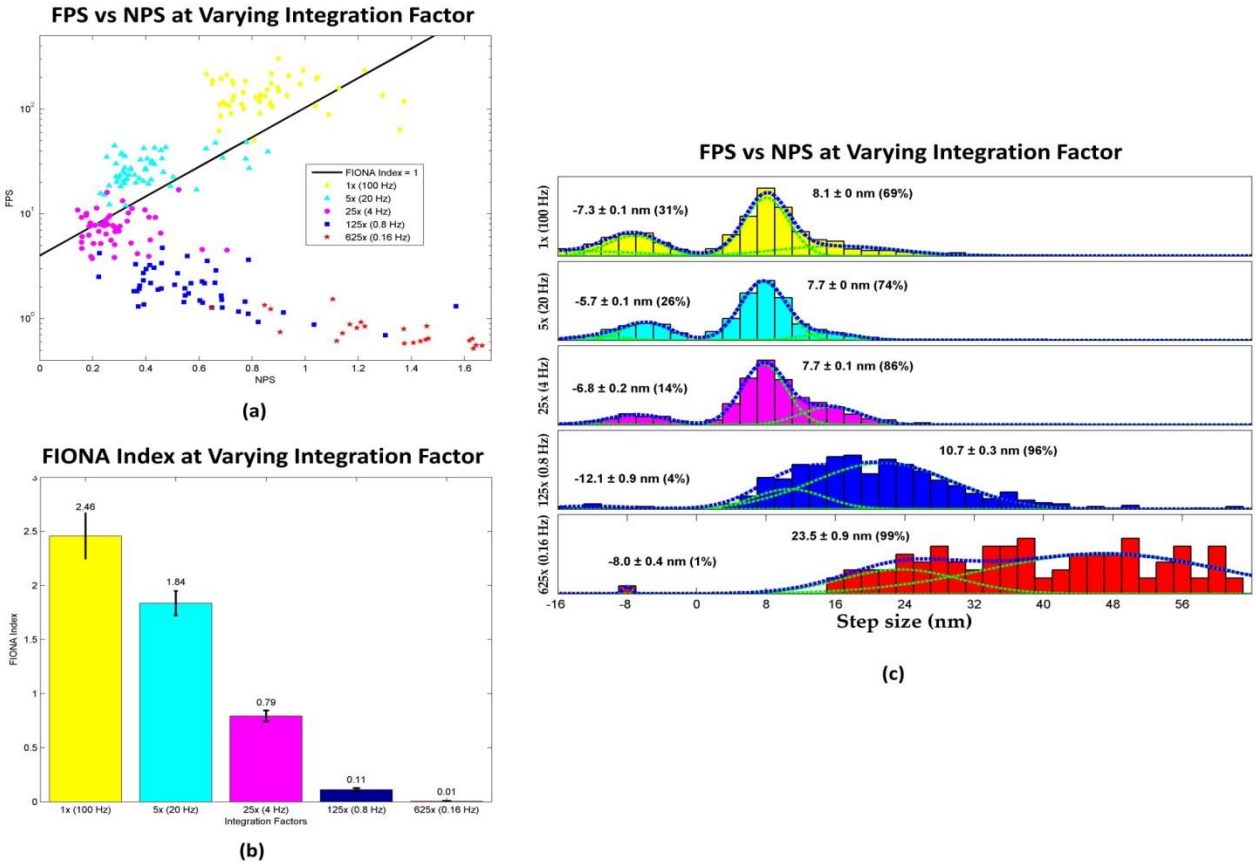

Figure 1.6: (a) FPS vs NPS graph at varying integration factors. (b) FIONA Index at varying integration factors. (c) Predicted step-size at varying integration factors.

1.5 Discussion

Finding the step-sizes of molecular motors requires the super-accuracy techniques to overcome the diffraction limit of light. Routine step-size measurements require prudent selection of the frame rate at a given ATP concentration, and minimizing noise in the experiment.

With FIONA Index, we can determine the optimal balance between frame rate and noise by looking into the frames per step (FPS) and noise per step-size (NPS) of each motor walking trace. By plotting the FPS vs. NPS graph with FIONA Index = 1 line, and calculating FIONA Index, we can:

1. Optimize experimental protocol for step-size experiment knowing the true step-size of molecular motor
2. Find the true step-size of molecular motor without prior knowledge of the step-size, being assured that the step-size predicted is a true step-size instead of one arising from skipped steps

1.5.1 Known step-size, optimizing experimental protocol

When the "true" step-size is known, we can calculate the FIONA Index, FPS and NPS using Equation (1), (2) and (3) then use these quantities to further optimize experimental parameters. To illustrate, suppose we conduct an experiment with a frame rate of 4 Hz and obtain a step-size histogram with a step-size of 8.9 nm as shown in the red histogram of Figure 1.5(c). A step-size of 8.9 nm is larger than the true step-size of 8.3 nm and we want to improve the experiment. What can we do?

This is when knowledge of the FIONA Index, FPS and NPS can inform us of what step to take next. The average FIONA Indices of the traces is 1.03, as shown in the red bar graph of Figure 1.5(b). This tells us that some of the traces have FIONA Indices less than 1, and some more than 1, and we confirm this by plotting the FPS vs NPS graph as shown in Figure 1.5(a).

Now knowing that the experiment contains a mixture of good and bad quality traces, we can take three different measures to improve the experiment. One is to lower the NPS, another is to increase the FPS, and the last one is to post-analytically select traces with FIONA Index > 1.

1.5.1.1 Reduce NPS

One way to improve FIONA Index is to reduce the NPS. Noise can arise from the finite amount of photons collected, fluctuation of the microtubule, or fluctuation of the fluorescent reporter itself. When noise is a factor, the simplest solution is to increase the laser power to collect more photons. This is limited by the photo-damage to kinesin caused by increased laser power, and also the inherent fluctuation in the microtubule and fluorophore as shown in the Appendix A.3. To summarize, there is a minimum NPS to a kinesin walking experiment (e.g. NPS 0.2 for experiment in Figure 1.6(a)), and once

we hit this minimum, we need to count on other ways to improve FIONA Index, which is by increasing FPS.

1.5.1.2 Increase FPS

We can increase FPS in two ways: 1) increasing the frame rate and 2) reducing the speed of the molecular motor by reducing the ATP concentration. Increasing the frame rate from 4 Hz to 10 Hz in Figure 1.5(c) leads to improvement in step-size from 8.9 nm to 7.9 nm, a closer value to the true step-size of 8.3 nm. Notice that for the 4 Hz traces in Figure 1.5(c), there are many skipped steps at 16 nm, which is largely absent when the frame rate is at 10 Hz.

A fair question to ask is how much should the FPS or the FIONA Index be increased. From Figure 1.5(c), we note that any frame faster than 4 Hz is sufficient to give us predicted step-size close to the true step-size. Collecting at 100 Hz is unnecessary as it only generate a large amount of data without significantly benefiting the step-size prediction. A side effect of increasing the FPS recklessly is increase in noise and potential for fitting noise that generate negative step-sizes. Figure 1.5(a) shows the constant increase in noise as the frame rate increases from 4 Hz to 100 Hz. Supplemental Figure A.3 shows that for high noise, some step-finding algorithms like Student's T-test will fit noise as a series of backward and forward steps with no net displacement, generating artifactual step-sizes. Supplemental Figure S6 shows that as FPS increases, especially when the frame length is greater than the FPS, we start to fit noise and generate aberrant negative step-sizes with its corresponding aberrant positive step-sizes.

Therefore, an optimal step-size experiment is one where the FPS is just enough to give FIONA Index around 1 to 2 while minimizing the NPS. For the experiment in Figure 1.5(a), the optimal frame rate is 20 Hz, which allows most of the points in the FPS vs. NPS plot to lie above the FIONA Index = 1 plot, while keeping the NPS low at around 0.4. This gives rise to a FIONA Index of 1.74 in Figure 1.5(b).

To find the optimal experimental protocol, we recommend collecting experiments at different frame rates, and plot the FPS vs. NPS and also the FIONA Index graphs as in Figure 1.5(a, b). Then choose the frame rate when the FPS vs. NPS plot just starts to have most of the points above the FIONA Index = 1 line, while keeping the NPS at its minimum to avoid fitting noise that gives rise to negative step-sizes.

1.5.1.3 Post-analysis correction

A very useful feature of the FIONA Index is the ability to post-analytically select traces with high FIONA Indices. This filters out traces with high NPS and low FPS, since in any experiment a fraction of motors will be attached to dimmer fluorophores generating high NPS, and some move faster than other motors giving low FPS. As a good example, we pool together traces collected by participants of the Center of Physics of Living Cell (CPLC) summer school in 2016. There are six participants trying their hands first time on the kinesin walking experiment. They collected a total of 106 walking traces, and the FPS vs. NPS graph, FIONA Index histogram and step-size histograms are shown in Figure 1.7. By choosing traces with

FIONA Indices more than 1, they are able to get kinesin step-size of 8.8 nm, in very close agreement with the expected step-size of 8.3 nm. Without the FIONA Index filter, the 106 traces would have generated a step-size of 9.6 nm. If we look only at those traces with FIONA Indices less than 1, the step-size generated is 12.1 nm.

From Figure 1.7(b, c), we notice that the majority of the traces (77%) have FIONA Indices less than 1. This may either be due to poor focusing, inaccurate pipetting that causes kinesin to walk faster than desired, or inexperience in choosing walking traces for kinesin. There are a number of traces that simply jumps from one spot to another, which is then mistakenly regarded as kinesin walking. We find this to be common among experimentalists who analyze kinesin walking data for the first time. With FIONA Index, we are able to separate high vs. low quality data based on the FPS and NPS of each trace.

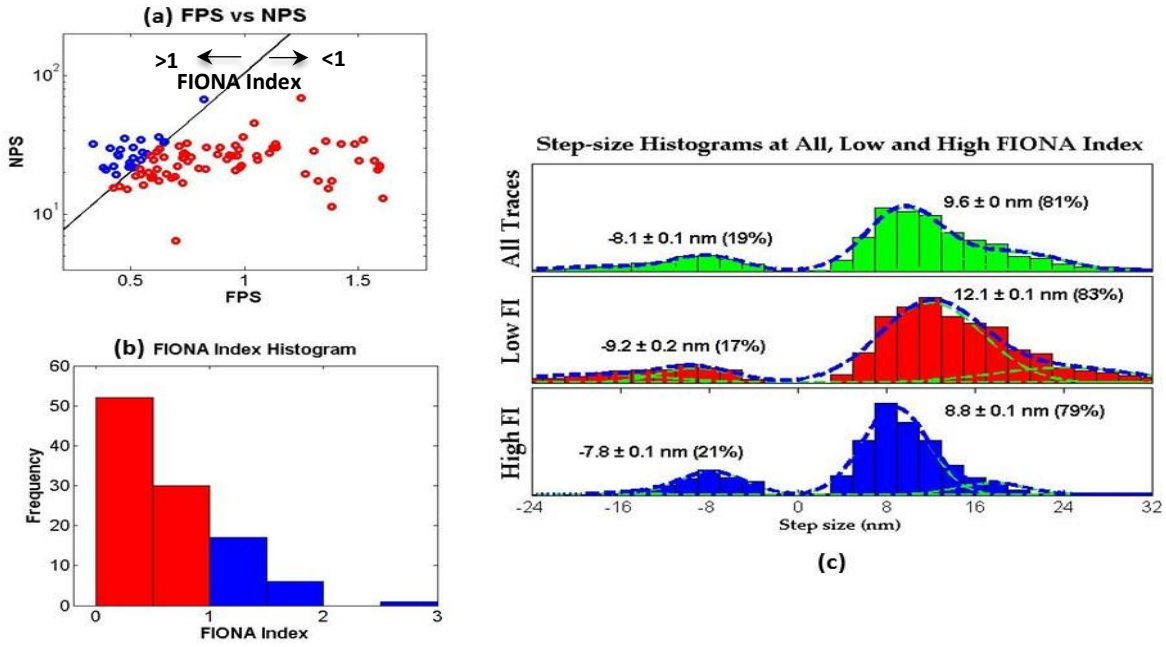

Figure 1.7: Kinesin stepping data from CPLC summer school 2016. Traces with FIONA Indices greater than 1 are marked blue, while those with FIONA Indices lower than 1 are marked red. (a) FPS vs. NPS graph of 106 traces. The black sloping line marks the cases where F IONA Indices = 1. (b) FIONA Index histogram of the 106 traces, with 77% of the traces having FIONA Indices less than 1, and 33% more than 1. (c) Step-size histograms of all the 106 traces (green), only those with FIONA Indices less than 1 (red) and only those with FIONA Indices more than 1 (blue).

1.5.2 Unknown step-size, finding the true step-size

We cannot use FIONA Index for motors with unknown step-size, since we need to have an assumed step-size to calculate FIONA Index. Instead, we can calculate a quantity called the smallest resolvable step (SRS), which is the minimum step that can be resolved for a given trace. Experiments finding unknown step-sizes should aim to obtain as low an SRS as possible. If the predicted step-size remains unchanged even when the SRS is half of the predicted step-size, we can be confident that the predicted step-size is the true step-size.

SRS is the step-size when FIONA Index = 1. Since there are two ways of calculating FPS, we can derive SRS in two ways:

$$SRS = \frac{3.25\ Noise}{\ln N_{frames} - \ln(4\ \frac{Distance}{SRS})}$$

or

$$SRS\left(\ln N_{frames} - \ln\left(4\ \frac{Distance}{SRS}\right)\right) - 3.25\ Noise = 0$$

The SRS of a trace will be the larger value of the two. Calculating the SRS for the 100 Hz data in section 1.4.6, we obtain SRS values shown in Figure 1.8(a). The smallest resolvable steps for the traces range between 4 and 21. We also plot the noise for each trace, and find that as the noise increases, SRS will also increase as expected. We divide the traces into 5 categories based on its SRS: 4-5 nm, 5-6 nm, 6-7 nm, 7-8.3 nm and 8.3-21 nm. Figure 1.8(b) shows the step-size histograms for all the five categories. When the SRS is more than 8.3 nm, the predicted step-size is 11.7 nm, larger than the expected 8.3 nm. When the SRS gets smaller and smaller to 7 nm, 6 nm, 5 nm and 4 nm, the predicted step-size remains unchanged at around 8 nm. Since the predicted step-size remains unchanged at smaller and smaller resolvable step, we have high confidence that this predicted step-size of ~8 nm is the true step-size of kinesin.

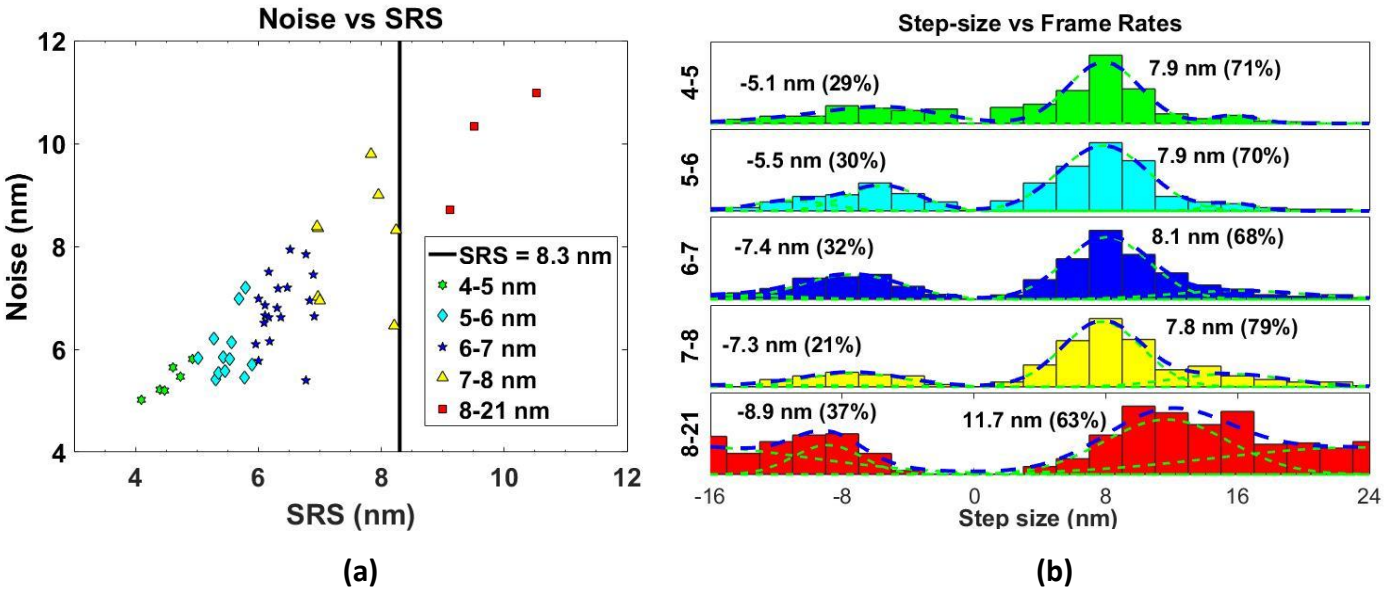

Figure 1.8: (a) Noise vs SRS graph for 100 Hz frame rate experiment. The SRS values range from 4 to 21 nm. We divide them into five categories based on the SRS value: 4-5, 5-6, 6-7, 7-8 and 8-21 nm. As noise increases, the SRS also increases. (b) Step-size histograms for traces in each of the SRS categories. At high SRS (>8), the step-size obtained is 11.7 nm, which is larger than the kinesin step-size of 8.3 nm. When the SRS decreases to less than 8 nm, step-size decreases to 8 nm and remains unchanged even when the SRS decreases to around 4-5 nm.

1.6 Conclusion

Experiments to find out step-sizes of molecular motors require fine balance between noise and frame rate. With FIONA Index, we now have a guide to find the optimal experimental setup either by changing the frame rate, changing the kinesin velocity, or reducing noise. FIONA Index also allows us to post-analytically filter out traces with high NPS and low FPS; it also allows molecular motor stepping experiments to be reproduced successfully even for those with limited research experience.

CHAPTER 2

NOISE OUT: REMOVING EXCESS DYES THROUGH MAGNETIC CYTOSKELETON AFFINITY (MICA) PURIFICATION

Until you remove the noise, you are going to miss a lot of signal

Seth Godin

2.1 Abstract

Single molecule research of molecular motors regularly requires labels ranging in size from small fluorophores to quantum dots (qdot) and large beads. Excess reporters may be an order of magnitude more than the labeled motor and need to be removed. Current centrifugation-based affinity purification is slow and requires a lot of sample. Herein we develop Magnetic Cytoskeleton Affinity (MiCA) purification that shortens purification time from 2.5 hours to 20 minutes and allows nanogram purification of protein, making it ideal for single molecule research requiring fast purification of small quantity of protein. We report 27% purification yield of kinesin and show that we can see microtubules gliding over individual kinesin-qdot after MiCA purification. We have also successfully purified as little as 30 ng dynein-dynactin-bicD2 (DDB) complex bound to qdot, which is a considerable advance considering the challenge typically associated with isolating dynein. The speed, versatility and ability to purify minute quantity of proteins make MiCA a promising technique for routine purification of molecular motor in a wide-range of downstream biomolecular application.

2.2 Introduction

Molecular motors are nanometer-sized machines that convert chemical energy into mechanical work. There are three families of cytoskeletal motor proteins - kinesin and dynein which walk along microtubule, and myosin which walks along actin filament. These motors are responsible for a wide range of motion inside the cell from membrane trafficking, mechanical signal transduction, to movement of the entire cell[22].

Single molecule studies offer powerful means of uncovering underlying mechanisms of motor movements, allowing us to learn about the step-sizes[1,3,10,23–28] and forces[12,26,28–32] generated by a single motor. To study individual motor, probes need to be attached to the motors. These probes can be fluorescent proteins[33–35], organic fluorophores[1,24,36,37], quantum dots[38–46], or DNA[46–48]. Excess probes give rise to background noise, and for applications requiring further conjugation of labeled motor to other substrate[47], it is important to remove the excess probes.

Current methods to remove excess probes include labeling and washing motors while bound to IgG Sepharose beads[37,45], or using microtubule affinity purification[46–48]. The drawbacks of these methods are the large sample volume and the long time needed to complete the removal. These are not optimal for single molecule study, since only a small amount of sample is needed for each single molecule experiment, and the leftover purified sample will either be wasted, or frozen for long term storage. Freeze-thaw damage often accompanies frozen sample, which reduces the fraction of active, labeled motor in the purified protein pool.

In order to maximize the number of active, labeled motor, it is important to have a point-of-use purification system that allows routine purification right before experiment. For such purification system to be successful, it needs to be (1) fast, (2) able to purify small sample quantity, and (3) able to purify labeled motor. To this end, we develop Magnetic Cytoskeleton Affinity (MiCA) purification using the magnetic separation technology that has gained traction in nucleic acid and protein purification in recent decade[49,50].

The key to a robust MiCA purification is finding a reliable way to attach the cytoskeleton to the magnetic beads to make the MiCA capture beads. We found that the best approach is to use moderately positive magnetic beads to bind to the negatively charged cytoskeleton, but not to the molecular motors. In our current study, we focus on the microtubule system, but the same conjugation scheme will likely work for the actin-myosin system.

Once the MiCA capture beads are synthesized, we performed MiCA purification on kinesin, kinesin bound to quantum dot (qdot), and dynein-dynactin-bicD2 (DDB) complex bound to qdot to show that we are able to achieve the three objectives above through (1) reduction of purification time by 7 times, (2) purification of nanogram amount of proteins, and (3) purification motors bound to large cargo such as quantum dot.

2.3 Materials and Methods

2.3.1 Microtubule affinity purification

One of the milestones in cytoskeleton transport is the discovery of kinesin in 1985 made possible through the microtubule affinity purification[51]. This purification strategy has been used for purification of kinesin in-vivo from squid axon [51], HeLa cells [52], Drosophila embryos [53,54], bovine brain [55], human neutrophils [56], and sea urchin early embryos and eggs [54,57]. In-vitro, this technique allows purification of kinesin to remove inactive kinesin. The working principle of microtubule affinity purification is illustrated in Figure 2-1(A). Details of the traditional microtubule affinity purification are described below:

(1) Long microtubules are first polymerized from 5 mg/mL tubulin at 37°C for 30 mins in the presence of 2 mM GTP. Polymerized microtubules are centrifuged at 13,000xg for 30 mins at room temperature, and the supernatant containing unpolymerized tubulins are removed while the pellet are reconstituted in BRB80 buffer (80 mM PIPES, 1 mM EGTA, 1 mM MgCl2, pH 6.9) supplemented with 1 mM GTP and 20 µM paclitaxel to give the final microtubule mix
(2) Microtubules are mixed with the motor sample containing active kinesin, inactive kinesin, excess fluorophores and kinesin labeled with fluorophore in the presence of 1 mM AMP-PNP, a non-hydrolysable analog of ATP. AMP-PNP causes kinesin to bind strongly to microtubule
(3) Microtubule and motor mixture are centrifuged at 13,000xg for 30 mins at room temperature. The microtubule, kinesin and any large fluorophore will be pelleted, while inactive kinesin will remain in solution
(4) The inactive kinesin is removed when the supernatant is taken out
(5) The pellet is washed with dilution buffer made up of BRB80 or DmB-BSA buffer containing 1 mM THP (Cat. 71194, EMD Millipore) and low amount of ATP (50 nM). DmB-BSA is dynein motility buffer (30 mM HEPES, 50 mM KAcetate, 2 mM MgAcetate, 1 mM EGTA, pH 7.2) supplemented with 8 mg/mL bovine serum albumin (BSA). Washing can either be done by pipetting gently a few times while trying to avoid disturbing the pellet or by a series of reconstitution and centrifugation. Once washed, elution buffer containing dilution buffer with 1-3 mM ATP is added, which causes kinesin to walk and be released from microtubule
(6) The mixture is centrifuged again at 13,000xg for 30 mins at room temperature. The microtubule and large fluorophore will be pelleted and active kinesin will remain in solution
(7) The active kinesin in the supernatant is transferred to a new centrifuge tube separate from the pellet

2.3.2 MiCA purification

MiCA purification is derived from the traditional microtubule affinity purification. The centrifugation steps (3 and 7) for the traditional purification are replaced with magnetic separation for MiCA purification. Details of the MiCA purification are illustrated in Figure 2-1(B) and described below:

(1) MiCA capture beads are formed by mixing short microtubules with moderately positive magnetic beads. The short microtubules are polymerized from 5 mg/mL tubulin at 37°C for 30 mins in the presence of 2 mM GMPCPP (non-hydrolysable analog of GTP), then sonicated for 3 mins
(2) Capture beads are mixed with the motor sample in the presence of 1 mM AMP-PNP
(3) Capture beads are pulled by magnet, leaving inactive kinesin and excess fluorophore in the solution
(4) The inactive kinesin and excess fluorophore are removed when the supernatant is taken out
(5) The pellet is washed with dilution buffer a few times, then eluted with 1-3 mM ATP, which releases kinesin from capture beads
(6) Capture beads are again pulled by magnet, leaving active and labeled kinesin in the solution
(7) The active and labeled kinesin in the supernatant is transferred to a new centrifuge tube separate from the pellet

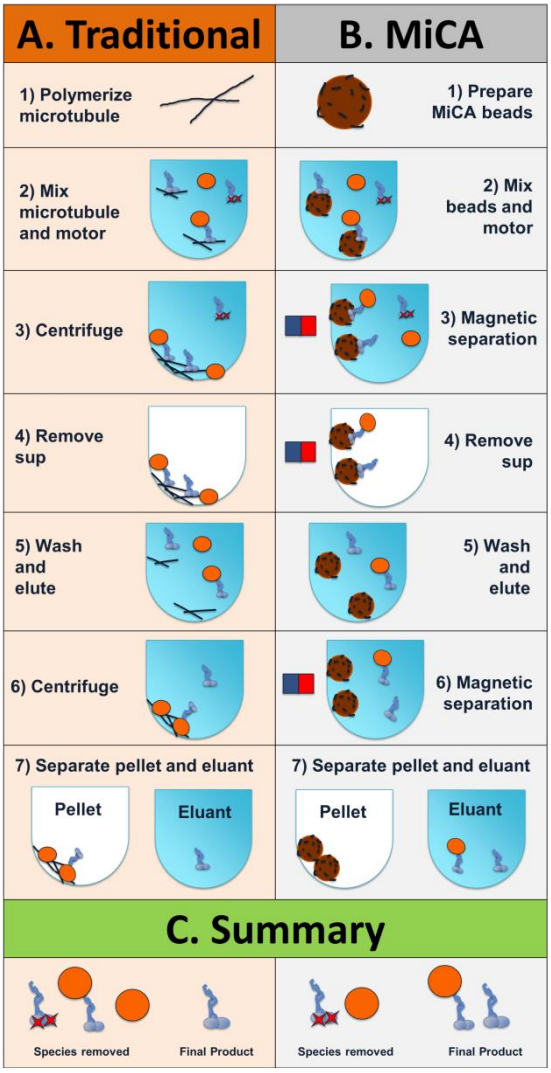

Figure 2-1: Comparison between (A) traditional microtubule affinity and (B) MiCA for kinesin purification. The centrifugation steps (3 and 7) for the traditional purification are replaced with magnetic separation for MiCA

purification. As summarized in panel (C), both methods remove inactive kinesin and excess fluorophores while retaining active kinesin. In addition, MiCA purification enables purification of kinesin attached to large fluorophore

2.3.3 Magnetic beads preparation

An important element to the robustness of MiCA purification is the magnetic beads used to bind microtubule. We use charge interaction to couple positively charged amine beads to the negatively charged microtubule. Commercial amine bead are too positively charged that it binds strongly not only to microtubule but also to kinesin, preventing kinesin from being eluted. We therefore reduce the positive charge by coupling PEG-amine to the magnetic beads, resulting in moderately positive beads that bind only to microtubule but not kinesin. The synthesis of this PEG-amine bead from commercial amine bead is illustrated in Figure 2-2(A).

Detailed protocol of the PEG-amine bead synthesis is outlined in Appendix B.1.1. Briefly, amine beads are washed with double-distilled water (ddH_2O), and then reacted with FMOC-NH-PEG-SVA. The reaction yields FMOC bead, which is washed with ddH_2O. FMOC bead is then deprotected with piperidine[58], yielding NH_2 in place of FMOC-NH group, generating PEG-amine bead used for MiCA purification. The PEG-amine bead can be stored at 4°C and is good for at least six months.

Figure 2-2(B) summarizes an SDS-PAGE electrophoresis binding experiment between PEG-amine beads and kinesin or microtubule. It shows that PEG-amine bead has preferential binding to microtubule but not kinesin. Detailed experimental protocol is described in Appendix B.1.2. Briefly, kinesin and microtubules are separately mixed with amine or PEG-amine bead, and the proteins left in supernatant (Sup) or stuck on final bead (Bead) are monitored. The initial amount of kinesin and microtubule are shown on lane 1. Amine bead binds very strongly to kinesin and microtubule that none is left in Sup on lane 2 and none is released from the Bead on lane 3 after mixing with SDS detergent and heated to 95°C. Incubating amine bead with BSA protein blocker does not prevent kinesin and microtubule from binding to amine bead, shown through the absence of the kinesin and microtubule bands in Sup on lane 4. However, BSA blocking reduces binding strength between amine bead and proteins, causing kinesin and microtubule to be released from Bead on lane 5 after incubation with detergent and heat. BSA binds non-specifically to amine beads, and some binds weakly that they readily detach from bead, leaving BSA bands in Sup and Bead on lane 4 and 5. PEG-amine bead binds preferentially to microtubule but not kinesin. Lane 7 shows a small fraction of kinesin and a large amount of microtubule left on Bead. Lane 6 shows that the majority of kinesin and only a small fraction of microtubule are left in Sup after binding to PEG-Amine bead. The PEG-Amine bead behaves in a similar manner with and without BSA blocking.

Figure 2-2(C) shows TIRF microscopy imaging of kinesin-Qdot and fluorescent microtubule binding to amine and PEG-amine surfaces functionalized on glass coverslip. The detailed experiment is outlined in Appendix B.1.3. Microtubule binds to both surfaces equally well, which is as expected. There are much more kinesin-qdot binding to the amine surface than the PEG-amine surface, indicating that amine surface would not be suitable for MiCA purification as kinesin will be lost to the surface. Control

experiment summarized in Appendix Figure B.1 shows that as PEG-amine concentration on the surface is reduced, less microtubule binds, confirming that binding of the microtubule to the surface is through presence of PEG-amine. Another control experiment shown in Appendix Figure B.2 concludes that kinesin-qdots walk well on PEG-amine surface (around 70% are motile) but not amine surface (only around 26% are motile).

Other than using PEG-amine bead, we also tried other conjugation method using EDC/amine chemistry and biotin-streptavidin interaction. They did not work well. We also found that not all commercial amine beads work for MiCA. These attempts are discussed further in Appendix B.1.3.

In general, positively charged beads will bind well to microtubule. Whether or not it is suitable for motor purification depends on the interaction of the bead with that motor. With the PEG-amine bead derived from MagSi-S NH2, we successfully purify kinesin-1 and DDB complex due to limited interaction between motors and the bead. The first experiment to conduct to see if a motor is suitable for purification with MiCA is to test if the motor binds to the PEG-amine bead. The less binding there is the better.

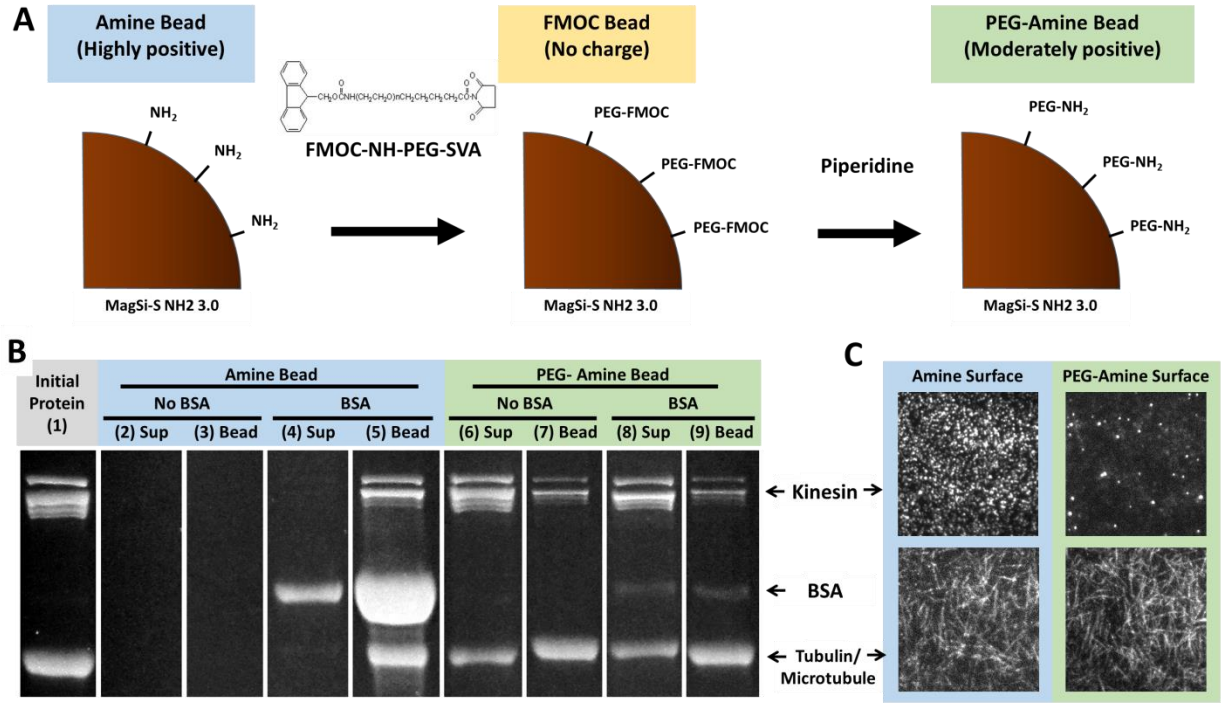

Figure 2-2: (A) Synthesis of magnetic bead used for MiCA purification. Amine bead binds not only to microtubule, but also to kinesin. For MiCA purification to work, bead should not bind kinesin. PEG-amine bead is thus synthesized to retain binding to microtubule but not kinesin. This is done by reacting commercial 3.0 µm amine bead (MagSi NH2 3.0) with FMOC-PEG3400-SVA to form PEG-FMOC bead. The FMOC group is then deprotected with piperidine to yield PEG-Amine bead. (B) Binding experiment of kinesin and microtubule to amine and PEG-amine beads observed through SDS-PAGE electrophoresis. Kinesin and microtubules are mixed with amine or PEG-amine bead, and the proteins left in supernatant (Sup) and stuck on final bead (Bead) are monitored. Starting with

the initial protein amount on lane 1, amine bead binds very strongly to kinesin and microtubule that none is left in Sup on lane 2 and none is released after the Bead is mixed with SDS detergent and heated to 95°C on lane 3. If the amine bead is first incubated with BSA protein blocker, both kinesin and microtubule still bind amine-bead, leaving none in Sup on lane 4, but they are readily released from Bead after incubation with detergent and heat shown on lane 5. Some BSA band can be seen left in Sup and releasing with kinesin and microtubule on lane 4 and 5. PEG-amine bead preferentially binds to microtubule but not kinesin, shown in lane 7 where a small fraction of kinesin and a large amount of microtubule bind to the Bead. Lane 6 shows that the majority of kinesin and small fraction of microtubule are left in Sup after binding to PEG-Amine bead. The PEG-Amine bead behaves almost identically with or without BSA blocking. (C) TIRF microscopy imaging of kinesin-Qdot and fluorescent microtubule binding to amine and PEG-amine functionalized on glass coverslip surface. Both surfaces bind to microtubule equally well, but the amine surface binds much more to the kinesin-Qdot than the PEG-amine surface.

2.3.4 Preparation of short microtubules

We define short microtubules as microtubules with average length less than 1 μm. MiCA purification can use both short and long microtubules. Short microtubules tend to stay in solution, which is why they cannot be used with traditional purification requiring long microtubules that sediment after centrifugation. Otherwise, motors will be lost when bound to the short microtubules that do not sediment.

In practice, we use short microtubules for MiCA purification, using sonication to shear long microtubules into short ones[59]. Long microtubule is prepared by polymerizing 8 μL tubulin (5 mg/mL) in 1 mM GMP-CPP for 30 minutes at 37°C. 15 μL GMP-Taxol buffer (20 μM paclitaxel, 1 mM GMP-CPP in BRB80) is then added and these long microtubules are sonicated. Supporting Figure B.3 shows that as sonication time increases from 0 min to 5 min, average microtubule length decreases from 4.0 μm to 0.40 μm. We typically sonicate microtubules from 3 to 5 minutes to prepare short microtubules.

The ability to use both short and long microtubules is advantageous for MiCA purification. The first two advantages are reduced preparation time and less microtubule lost. Microtubule after polymerization has a large length distribution. To prepare long microtubules, a 30-minute centrifugation is required to remove short microtubules that do not sediment. This step is skipped in MiCA purification, avoiding throwing away short microtubules. The centrifugation step is replaced with a shorter 3-5 minutes sonication. Control experiments in Figure B.4 confirm that short microtubules prepared through sonication and skipping centrifugation still allow kinesin binding and release. Figure B.4 also shows that kinesin do not release from tubulin, which means that free tubulin cannot be used for purification. It needs to be polymerized to microtubules first before being used for purification.

A third advantage is that the ability to use short microtubules allow freezing of microtubules for long term storage at -80°C. Each freeze-thaw cycle shortens the average length of microtubule, reducing the potency of long microtubules for traditional purification. Figure B.3 shows shortening of a 2 min sonicated microtubule from 0.74 μm to 0.44 μm after freeze-thawing. Since MiCA purification is not affected by shortening of microtubules, freezing for long term storage is now a reality. This allows a one-time preparation of microtubules to be aliquoted and used numerous times in the future, saving

significant amount of time. We have used the frozen microtubules 2-3 months after storage at -80°C and they are still viable for MiCA purification. Figure B.5 shows that freeze-thawing microtubule does not affect kinesin elution with MiCA purification. Freeze-thawing of the microtubule together with the magnetic bead, however, causes less kinesin to be eluted and more stuck on the magnetic bead. Presumably the magnetic bead or its PEG-amine layer is damaged due to freeze-thawing. Therefore we can only save time by freezing the microtubule but not the microtubule bound to the magnetic bead.

One last advantage of using short microtubule is it reduces the probability of motors walking into another motor and stick to each other. With shorter travel path, motors will detach once it reaches microtubule end. The chance of motors sticking to each other may increase when they are bound to qdot or other cargoes. Since MiCA purification enables purification of cargo-attached motors, having short microtubule means reducing chances of cargoes aggregating.

2.3.5 Preparation of kinesin

We use three different types of kinesin. All of them are truncated kinesins with biotin attached either to the C-terminus where the cargo binding domain of full length kinesin lies, or the N-terminus where the catalytic domain lies. The shortest kinesin used is K432, a 432 amino-acid fraction of *Drosophila* kinesin. The next two kinesins, K888 and K888-Het, are equally long with 888 amino acids from the mouse kinesin heavy chain. K888 is a homodimer with biotin on the C terminus of both monomers, while K888-Het is a heterodimer with biotin on the N-terminus of only one of the two monomers. The preparation of all kinesins is detailed in Appendix B.8.

2.3.6 Kinesin purification with traditional affinity and MiCA purifications and monitored with gel electrophoresis

Long microtubule is prepared by polymerizing 8 µL tubulin (5 mg/mL) in 1 mM GMP-CPP for 30 minutes at 37°C. 15 µL GMP-Taxol buffer (20 µM paclitaxel, 1 mM GMP-CPP in BRB80) is then added and the solution is divided into 2 tubes of 10 µL each. One tube is centrifuged for 30 mins at 13,000xg, and then reconstituted in 10 µL GMP-Taxol buffer to make the long microtubule. The other tube is sonicated for 3 min at room temperature to make the short microtubule. Any buffer coming into contact with microtubule should be warmed to room temperature.

MiCA capture bead is prepared by removing the buffer in 50 µL PEG-amine bead (10 mg/mL) and mixing in 6.25 µL short microtubule. The mixture is left to incubate for 5 min, and reconstituted in 5 µL dilution taxol buffer (20 µM paclitaxel, 1 mM THP, and 80 nM ATP in DmB). 5 µL DmB-BSA is then added, and the mixture incubated for 2 min followed by washing with 10 µL dilution taxol buffer. Finally the beads are reconstituted in 5 µL dilution taxol buffer to make a final volume of ~6 µL.

K888-Het is diluted 4x to ~3.75 µM in dilution-taxol buffer. For traditional affinity purification, 1 µL of this diluted K888-Het is mixed with 3.5 µL long microtubule, 1 µL AMP-PNP (8 mM), and 2.5 µL dilution

taxol buffer. For MiCA purification, 1 µL K888-Het (3.75 µM) is mixed with 6 µL MiCA capture bead and 1 µL AMP-PNP (8 mM). The mixtures are incubated for 5 min at room temperature in an end-to-end rotator.

The kinesin-microtubule and kinesin-bead are washed with 8 µL dilution taxol buffer twice. For traditional affinity purification, washing is done by centrifuging mixture at 13,000xg for 30 mins at room temperature to pellet the kinesin-microtubule, and then gently add and remove dilution taxol buffer without disturbing the pellet. For MiCA purification, washing is done by magnetic separation to pellet the kinesin-bead, then the buffer is removed and the pellet reconstituted in dilution taxol buffer.

Once washed, the pellets are reconstituted in 8 µL elution buffer (3 mM ATP in dilution taxol buffer) and left to incubate for 5 min. The eluants are collected through centrifugation or magnetic separation, and another 8 µL elution buffer is added and incubated for 5 min. The second batches of eluants are again collected.

The AMP-PNP supernatant, two wash batches, two elution batches, and proteins left in bead or pellet are then quantified with SDS-PAGE electrophoresis using Imperial™ protein stain (Cat. 24615, ThermoFisher Scientific).

2.3.7 Kinesin-qdot gliding assay

Kinesin-qdot is prepared by mixing 0.2 µL K888 (8.8 µM), 1 µL Qdot® 655 Streptavidin Conjugate (SA-Qd655, 1 µM), and 1.8 µL BSA-taxol buffer(20 µM paclitaxel, 1 mM THP, and 80 nM ATP in DmB-BSA). 2 µL short microtubules are thawed from a frozen aliquot of short microtubule prepared as in section 2.3.6. MiCA capture bead is prepared by mixing 2 µL short microtubules with 8 µL PEG-amine bead pellet (10 mg/mL) with its buffer removed. After 5 min incubation, the MiCA capture bead is washed 2x with 8 µL BSA-taxol buffer and reconstituted in 2 µL BSA-taxol buffer to give 3 µL final bead volume. Next, 4 µL kinesin-qdot is mixed with 3 µL MiCA capture bead and 1 µL AMP-PNP (8 mM), and then incubated for 5 min at room temperature. The mixture is then washed twice with 8 µL BSA-taxol buffer and 8 µL elution buffer (3 mM ATP in BSA-taxol buffer) is added. After 5 min incubation, the eluant is extracted that yields approximately 100 nM kinesin-qdot.

For the gliding assay, long fluorescent microtubule is prepared as in Appendix B.2, using HyLite 488 as the fluorescent tubulin. Approximately 0.2 nM kinesin-qdot before and after MiCA purification is added to biotin-PEG chamber and left to incubate for 5 min. The chamber is then washed with four chamber volume of BSA-taxol buffer, and imaging buffer containing 1 mM ATP, 10x dilution long microtubule, 1 mM THP, 20 µM paclitaxel, 50 µM biotin, 10 U/mL pyranose oxidase, 4000 U/mL catalase, 2% glucose is added. The chamber is then imaged on TIRF microscope with exposure time of 2 second on two EMCCD camera, one to collect the qdot fluorescence, another to collect the microtubule fluorescence. A set of nanohole images on both cameras are also collected for image registration.

For analysis, a transform function is obtained with the nanohole images, as shown in Appendix Figure B.6. The qdot images are then transformed so that they are registered with the microtubule images. The microtubule image is binarized, thinned to single pixel, then dilated to give it some width. The location of each qdot is found using TrackMate in ImageJ. Binary location of the qdots are then overlaid with binary microtubule images, and qdot points that overlap with microtubules for at least 8 frames are considered active.

2.3.8 MiCA purification of DDB-qdot

3 µL DDB (~20 nM or ~30 ng/µL dynein) is mixed with 3 µL SA-Qd705 (100 nM) and incubated for >3 hours. 2 µL frozen short microtubules are thawed and warmed with hand, and then mixed with 8 µL PEG-amine beads which has its buffer removed after magnetic pull. The mixture is incubated for 5 min at room temperature, then washed 2x with BSA-taxol buffer. On final wash, 7 µL BSA-taxol buffer is added to make 8 µL final solution. This bead solution is then aliquoted into 3 tubes in increasing volume: 0.4 µL, 1.6 µL and 6 µL, which are labeled as 1x, 4x and 15x beads. The buffers of these aliquots are then removed and 1 µL BSA-taxol is added to each. Next, 2 µL DDB-qdot is added to each bead sample, and the mixtures are left to incubate at room temperature for 10 minutes on an end-to-end rotator. The 3 µL supernatant is then removed and labeled 'Bind'. The pellet is washed twice with 3 µL BSA-taxol, labeled 'Wash 1' and 'Wash 2'. The final pellet is eluted twice with 3 µL elution buffer (1 mM ATP in BSA-taxol) and 5 min incubation. These are 'Elute 1' and 'Elute 2'.

The Bind, Wash 1 and Wash 2 samples are then mixed with 0.25 µL biotin (10 mM) to saturate all streptavidin binding sites on qdot, then flowed into microtubule chambers made from PEG-biotin slide layered with streptavidin and long biotin-fluorescent microtubule. DDB-qdots in these samples will bind to microtubules on the chamber. Elute 1 and Elute 2 are diluted twice in imaging buffer, yielding final solution with 0.6 mM ATP, 1 mM THP, 20 µM paclitaxel, 50 µM biotin, 10 U/mL pyranose oxidase, 4000 U/mL catalase, and 2% glucose in DmB-BSA. These final solutions are then flowed into microtubule chamber. All images are recorded on TIRF microscope after ~5 min from infusion into microtubule chamber. Particle counting is done with TrackMate in ImageJ. Signal to noise ratios (SNR) and precision values are obtained by fitting 2d Gaussians to 16 dots from each Bind and Elute 1 movie. This is done using in-house program in Matlab. Each dot consists of 22 to 200 frames that are 0.5s apart in time. The amplitudes and background noises from the Gaussian fits and raw images are used to compute the SNR and precision values.

2.4 Results

2.4.1 MiCA reduces purification time 7 times

Figure 2-3(A) summarizes the time needed for traditional affinity vs MiCA purification. Total purification time reduces from 130 min for traditional affinity to 19 min for MiCA purification. Initial microtubule

polymerization and centrifugation step that takes 60 min in traditional affinity is replaced with a 5 min MiCA capture bead preparation using short microtubules stored at -80°C. The binding and elution step takes the same time for both traditional affinity and MiCA purification, but the wash and eluant extraction takes 15 times longer for traditional affinity than MiCA. This is because the 30 min centrifugation time in traditional affinity is replaced with a 2 min magnetic separation in MiCA purification.

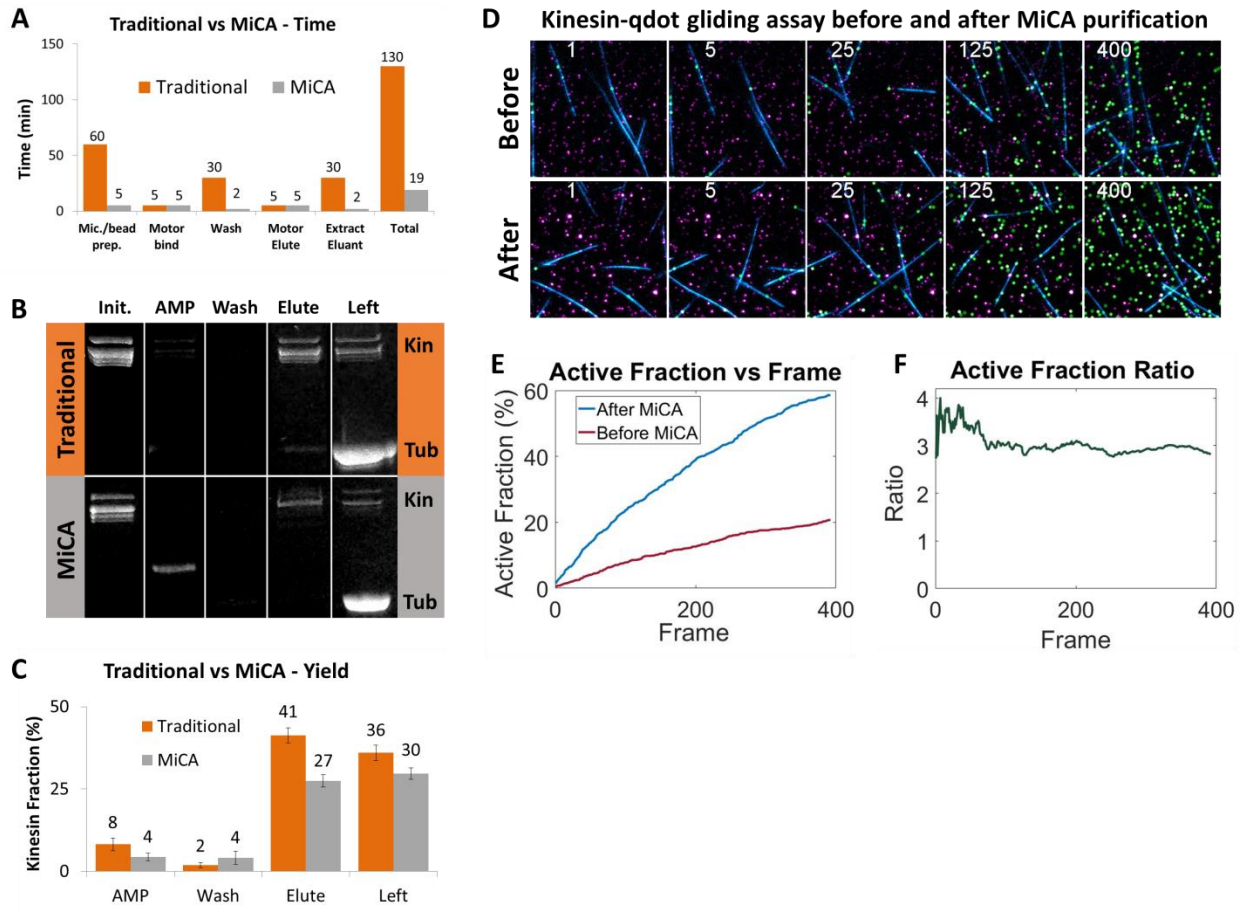

Figure 2-3: (A) Purification time comparison between traditional affinity vs MiCA purification. MiCA purification allows 7x reduction in total preparation time, from 130 min to 19 min. (B-C) Yield comparison between traditional affinity and MiCA purification. The quantity of kinesin at each bind (AMP), wash, elute and leftover phases are tracked. Very small amount of kinesin is seen in the bind and wash phase, showing that kinesin is efficiently bound to microtubule/ MiCA capture bead. Kinesin yield with MiCA (27% in elute) is 1.5x less to that for traditional affinity purification (41%). The error bars are obtained from gel results of 2-5 experiments. (D-F) Gliding assay for kinesin-qdot before and after MiCA purification. Kinesin is mixed with qdot in 1 to 1.1 ratio. Due to statistical nature of binding, not all qdot has kinesin bound. After MiCA, free qdots are removed. Panel (D) shows qdot fluorescence in magenta, microtubule in blue and active kinesin that has moved microtubule is post-marked with green. Time marker on upper left hand corner is in frame. Each frame is 2 s. Over time, more kinesins are involved in transport. More qdots are active after MiCA compared to before. Panel (E) shows the active fraction before and after MiCA. At the end of experiment, as many as 60% of qdots after MiCA are active, compared to around 20% before MiCA. Over time, there are around 3x more active fraction after MiCA than before MiCA, as shown in panel (F).

2.4.2 MiCA delivers 27% kinesin yield

Figure 2-3(B-C) shows traditional affinity and MiCA purification experiments monitored through SDS gel electrophoresis. The yield for each is shown on the Elute lane. The yield for MiCA is 27%, 1.5x less than that of traditional affinity purification, which is 41%. The initial protein amount is shown on the first lane. This initial amount of kinesin is then bound to the microtubule or magnetic bead by addition of AMP-PNP. The second lane (AMP) shows the amount of protein left in the supernatant and not binding to the microtubule or magnetic bead. Most kinesins bind to the magnetic beads. Only 8% and 4% of kinesins are left in supernatant for traditional affinity and MiCA purification. After the binding step, the kinesin-bound microtubule or magnetic beads are washed. The wash lane shows that minimal protein is lost (2% and 4%) at this step. Once washed, the kinesin is eluted with ATP, and both the amount eluted and amount left in beads are monitored in the Elute and Left lane. The amount eluted (41% and 27%) are comparable to the amount left on microtubule or magnetic bead (36% and 30%). Sometimes we run a second elution step to get more motors eluted.

2.4.3 MiCA allows single molecule observation of kinesin gliding

Figure 2-3(D-F) shows a gliding experiment using kinesin-qdot before and after MiCA purification. Figure 2-3(D) shows fluorescence of qdot (magenta) and microtubule (blue) overlaid with green dots to mark location of active kinesin. The active kinesins are identified post-analytically. Qdots that co-localize with microtubule for at least 8 frames are considered active. Before MiCA purification, free qdots are not removed. Figure 2-3(E) shows that at the end of the gliding experiment, only 20% of qdots before MiCA purification are actively gliding microtubule, compared to 60% after MiCA purification. Figure 2-3(F) shows that at any period of time approximate 3 times as many qdots are active after MiCA compared to before MiCA purification.

As far as we know, this is the first gliding assay where individual kinesin-qdot are observed gliding microtubule. Rahul et al. performed gliding assay with a mixture of kinesin-GFP and kinesin[60], but no experiment has been done where all the kinesins on the surface can be accounted for with a stable, long-lasting fluorophore.

2.4.4 MiCA allows purification of as little as 30 ng DDB-qdot

DDB is difficult to isolate and its purification yield is typically much less than kinesin. DDB also needs to be mixed with an excess amount of qdot (5-10x more) in order to bind non-specifically to qdot. Despite these complexities, DDB-qdot is successfully purified with MiCA, demonstrating that: 1) MiCA is able to purify very small quantity of precious protein; 2) MiCA allows purification of traditionally challenging protein; and 3) MiCA can increase signal to noise ratio through removal of excess qdots.

Figure 2-4 shows MiCA purification of 30 ng DDB-qdot with increasing amount of MiCA capture bead (1x, 4x and 15x) to find out which amount is best for the amount of DDB-qdot used. The amount of DDB-qdot left after binding to MiCA capture beads (Bind), left in second wash (Wash 2), and eluting through first and second elution (Elute 1, 2) are shown in (A) and quantified in (B). Looking at panel (B), we note that there are a lot of DDB-qdots left after the Bind phase, shown by the high DDB-qdot count in Bind compared to other phases. Two wash cycles effectively remove the unbound DDB-qdot, shown by the relatively low DDB-qdot count in Wash 2. Upon addition of ATP, DDB-qdots elute from MiCA capture beads. More DDB-qdots release into the first elution than the second one.

As the amount of MiCA capture beads increase from 1 to 4 to 15x, more DDB-qdot binds to the beads and less is left in the Bind sample. In terms of elution in Elute 1, the greatest amount of DDB-qdot released is with the 4x bead amount, followed by 15x, then 1x. This shows that when there is too little MiCA capture bead added (1x), too much DDB-qdots are lost unbound to the beads, and very little elutes out. When there is too much MiCA capture bead added (15x), the excess bead likely makes it difficult for the DDB-qdot to release during the elution phase through rebinding events. This experiment shows that there is an optimal amount of beads for a given quantity of proteins to be purified.

Panel (C) shows the kymographs for DDB-qdots at each phase and bead amount. DDB-qdots are mostly stationary during the Bind and Wash 2 phase, but are active during Elute 1 and 2 phases. Note that DDB-qdots can be diffusing on microtubule even without ATP, shown by the kymograph on Wash 2 with 4x Bead.

Panel (D) compares the signal to noise (SNR) and precision obtained from qdots before MiCA (or during Bind phase) and after MiCA (Elute 1 phase). There is high background before MiCA is applied due to excess qdots in the background. These are removed on subsequent washes and elution. High background causes low SNR and poor localization precision. Panel (D) shows the SNR before MiCA (11) being 5x less than after MiCA (55). Precision achieved before MiCA (17 nm) is ~3x worse than after MiCA (5 nm). Through quick removal of excess dye, MiCA purification can become a routine technique used to achieve high signal to noise ratio in single molecule fluorescence experiments.

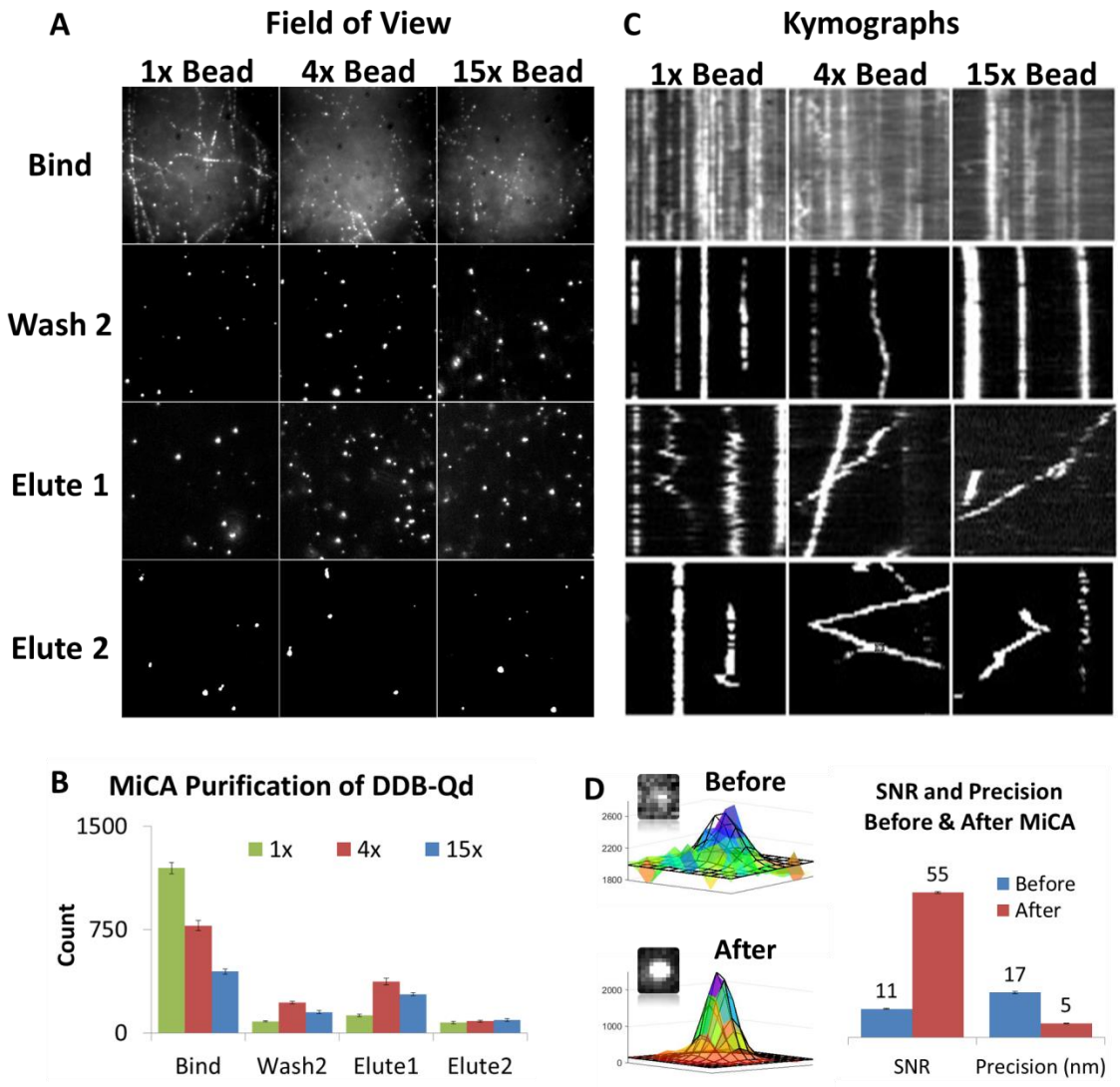

Figure 2-4: MiCA purification of DDB-qdot. (A-B) DDB-qdot purification with increasing amount of MiCA capture bead mixed with fixed amount of DDB-qdot. The amount of DDB-qdot left after binding to MiCA capture beads (Bind), left in second wash (Wash 2), and eluting through first and second elution (Elute 1 and 2) are shown in (A) and quantified in (B). As the MiCA capture bead increases from 1x to 4x and 15x, more DDB-qdots bind to the beads and less are left in the Bind supernatant. After 2 wash cycles, most free qdots and unbound DDB-qdots are removed. Elution yields the most DDB-qdot from the 4x sample, followed by 15x, then 1x sample. The kymograph on the panel (C) shows that the DDB-qdots are mostly stationary in Bind and Wash 2, but are active in Elute 1 and 2. This is also shown in Supporting Movie S2. Panel (D) compares the signal to noise (SNR) and precision obtained from qdots before MiCA (Bind) and after MiCA (Elute 1). There is high background before MiCA is applied due to excess qdots in the background. These are removed on subsequent washes and elution. High background causes low SNR and poor localization precision. Panel (D) shows the SNR before MiCA (11) being 5x less than after MiCA (55). Precision achieved before MiCA (17 nm) is ~3x worse than after MiCA (5 nm). 7-16 frames are collected to quantify the number of qdots in panel (B). 1500-1800 qdot frames are collected to quantify the SNR and precision in panel (D).

2.5 Discussion

2.5.1 General strategy to optimize MiCA purification

Initial attempts at MiCA purification were met with failure due to poor microtubule binding to magnetic beads. With PEG-amine magnetic bead, a robust MiCA capture bead is made. When a new motor construct or a new batch of MiCA capture bead is prepared, we follow the strategy below to optimize protein yield:

1. *(Critical)* Test cytoskeleton and motor binding to PEG-amine beads
    - Follow experiment shown in Figure 2-2(B). Cytoskeleton should bind well to PEG-amine bead, but not motors.
2. Do a titration experiment to determine the ratio of cytoskeleton to PEG-amine bead. Use 1.5-2x excess cytoskeleton to PEG-amine beads to make MiCA capture bead
3. *(Critical)* Using a fixed quantity of protein, vary the amount of MiCA capture bead to find out the amount that gives the best yield
    - The protein quantity should be large enough to be detectable. More are needed with gel electrophoresis experiments than single molecule TIRF experiments.
    - Yield can be very low if too little or too much MiCA capture bead is used. There is an optimal point, as shown in Figure 2-2(B) and Appendix Figure B.7(F).
4. *(Critical)* The following factors highly affect elution efficiency:
    - Elution ATP concentration. Appendix Figure B.7(D) shows that as ATP concentration increases from 0.1 mM to 1 mM and 10 mM, yield increases from 13% to 27% and 39%. Higher ATP concentration gives greater yield.
    - Elution volume. Appendix Figure B.7(B) shows that as elution volume increases from 2 µL to 4 µL and 8 µL, yield increases from 19% to 26% and 27%. Higher elution volume gives greater yield at the expense of diluting the purified protein.
    - Elution time. Appendix Figure B.7(C) shows that as elution time increases from 1 min to 5 min and 30 min, the yield increases from 12% to 27%, then decreases to 23%. There is an optimal time for elution. Longer time is not necessarily better as ATP may start to run out, or motors become inactive or lost to tubes or beads.
    - Microtubule sonication time. Appendix Figure B.8(D) shows that increasing microtubule sonication time from 0 min to 3 min and 6 min increases yield from 30% to 36% and 46%. Increasing sonication time reduces microtubule length, and shorter microtubules likely promote motor release due to short travel path that reduces motors' processivity.
5. The following factors has little effect on elution efficiency:
    - Motor binding time. Appendix Figure B.8(A-B) shows that as kinesin binding time increases from 1 min to 5 min and 30 min, yield increases slightly from 10% to 12%, then stays at 12%. Note that this result may be different for motors other than kinesin.
    - AMP-PNP concentration. Appendix Figure B.8(F) shows that as AMP-PNP concentration increases from 0.5 mM to 2 mM and 5 mM, elution yields remain steady s at 59%, 60% and 58%.

- BSA blocking of MiCA capture bead. Appendix Figure B.8(D) shows that the elution efficiencies with and without BSA blocking are the same (36%). BSA blocking does not improve or adversely affect purification yield.

2.5.2 Limitation of MiCA purification

We have shown the effectiveness of MiCA purification for single molecule application through purification of kinesin-qdot and DDB-qdot. There are two key limitations for MiCA that may prevent it from wider application. One is in the disruption of cytoskeleton binding to the PEG-amine magnetic bead. For effective purification, the cytoskeleton should remain bound to the bead at all time. However, the charge-charge interaction between cytoskeleton and PEG-amine bead can be disrupted by various buffer components. Appendix Figure B.9 shows that 82% and 27% of microtubules are dislodged from bead when 0.5x and 0.1x working concentration of casein is used. Appendix Figure B.9 also shows that as potassium chloride (KCl) concentration increases from 15 mM to 60 mM and 300 mM, the fraction of microtubules released from bead increases from 14% to 28% and 45%. For these reasons, buffers used for MiCA purification should not contain casein or high salt. Since high salt is sometimes used to elute motors from cytoskeleton, this presents one limitation for MiCA purification. Despite this, a wide range of motors can be eluted from their cytoskeletons using ATP, and we show that ATP does not disrupt microtubule binding to PEG-amine bead, as shown in Appendix Figure B.9.

A second limitation for MiCA purification is the loss of motors to the PEG-amine bead. Even though currently all the motors we have tested have minimal binding to the PEG-amine bead, there may be motors that are highly negatively charged, which will bind to the positively charged bead.

We have not tested the application of MiCA to purify motors from cell extract. All the motors we have tested on so far have been previously isolated before MiCA purification is applied. The two limitations above are relevant for applying MiCA on cell extract. As long as the cell extracts do not contain components that will disrupt microtubule-bead interaction, and the motors to be purified do not bind strongly to the bead itself, we predict that MiCA purification can be successfully applied for motor purification from cell extracts as well.

2.6 Conclusion

MiCA purification is ideal for point-of-use purification of molecular motor either by itself or attached to a cargo. It is fast and able to purify small quantity of motors. In this paper, we show successful purification of kinesin, kinesin-qdot and DDB-qdot with MiCA. The purification yield is as high as 41%, and it is able to purify as little as 30 ng of DDB-qdot. MiCA purification shortens purification time from 2.5 hours to 20 minutes, lending itself to routine purification of molecular motor for a wide-range of single molecule and biomolecular experiments.

CHAPTER 3

IN THE QUIET: FLUORESCENT FORCE GLIDING ASSAY TO STUDY COLLECTIVE MOTOR BEHAVIOR

Sometimes you need to sit lonely on the floor in a quiet room in order to hear your own voice and not let it drown in the noise of others.

Charlotte Eriksson

3.1 Abstract

Recent single molecule techniques have uncovered the force-velocity behavior of individual molecular motor. However, there is still limited understanding of how motors work collectively to transport cargo inside a cell. Multiple kinesin transporting a cargo, for instance, are shown to have lower velocity compared to single kinesin when no load is present. But in the presence of an opposing force, multiple kinesin have higher velocity than single kinesin. To understand this counter-intuitive observation, it is critical to directly observe force contribution of individual motor in a multi-motor transport. In this chapter we present a proof of concept for a fluorescent force gliding assay to study how motors work together. In this assay, we use kinesin-qdots purified with Magnetic Cytoskeleton Affinity (MiCA) purification and attached to coverslip surface via long DNAs that act as force probes. As kinesin-qdot exerts a force on microtubule, the reactive force displaces it in the opposite direction. Monitoring qdot displacement provides insight to the force contribution of individual motor. Our preliminary result shows that individual kinesin cycles between supplying force and drag on an advancing microtubule, even though the net effect of collective kinesin is to propel microtubule forward. This assay has the potential to study how different types of motor work together.

3.2 Introduction

Many cellular movements depend on collective transport of one or more types of molecular motors. Kinesin and dynein are known to work together to transport mitochondria[61] and cell nucleus[62] bidirectionally. Lipid droplets[63,64] and pigment granules[65] depend on transport by microtubule and actin-based motors. Collective transport of motors depends not only on properties of individual motors, but also on the interaction between motors. Recent advances in single molecule techniques have helped uncover step-sizes[1,24] and force behaviors[31,66–68] of individual motor, but the exact mechanism of how two motors of similar or different type work together remain largely unknown. For this reason we develop a fluorescent force gliding assay that is capable of observing force behavior of individual motor in a multi-motor transport.

3.3 Materials and Methods

To set up the fluorescent force gliding assay, we use MiCA purification from Chapter 2 to isolate kinesin-qdot, which are then bound to a long DNA with 1565 base pairs having biotin and dig conjugated at each end, as shown in Figure 3.1. Kinesin-qdot binds to DNA via biotin-streptavidin interaction, and the DNA binds to the coverslip via dig-anti dig interaction. The anti-dig coverslip surface is prepared on a biotin-PEG coverslip suffused with streptavidin, washed, and then covered with anti-dig-biotin.

When microtubules are flowed into the kinesin-qdot chamber, a fraction of the microtubule will bind to the kinesin-qdot and glide along the surface due to active transport by the kinesin-qdot. When the kinesin-qdot exerts a force on the microtubule, it will be displaced in the opposite direction because it is bound to a flexible DNA tether. When two or more kinesins work together, we can identify which kinesins are responsible for microtubule movement by finding the kinesins which are displaced in the opposite direction as the microtubule. Kinesins which are displaced in the same direction as microtubule drags the microtubule backward instead of supplying force forward.

Using this assay, we can zoom into the dynamic action of each kinesin as they bind on, unbind from, drag, and supply force on microtubule. As we find out in later section, no one kinesin remains the sole force provider of an entire microtubule movement. Instead, kinesins frequently switch role and alternate between supplying force on, dragging, and unbinding from microtubule.

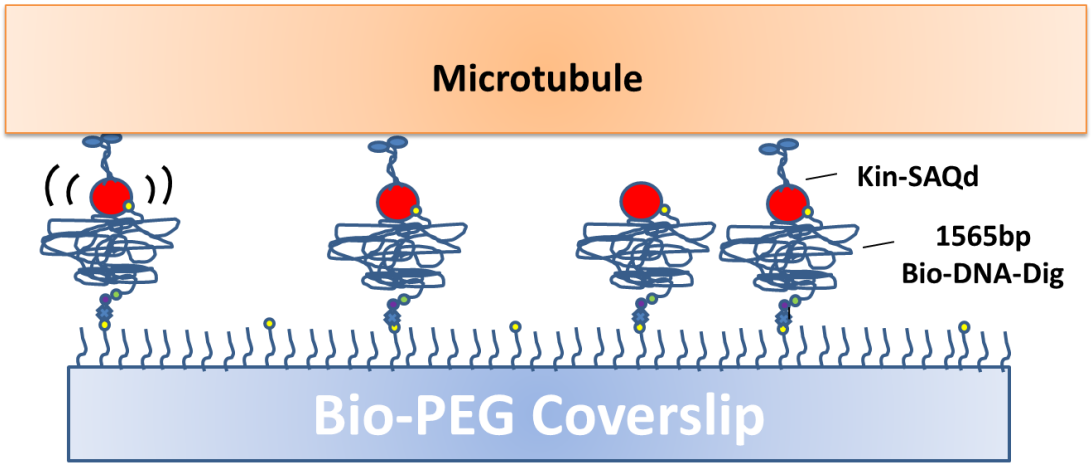

Figure 3.1: Schematic diagram of fluorescent force gliding assay. Kinesin-qdot isolated using MiCA purification is held by long DNA acting as a force probe. As kinesin-qdot walk on microtubule, it will move microtubule forward while displacing itself backward. This displacement can be recorded to show force exerted by individual kinesin.

3.4 Results

As a proof of concept, we show one representative trace from the fluorescent force gliding experiment in Figure 3.2. Images at frame 1, 89, 112 and 200 of the movie are shown in Figure 3.2(a), with microtubule in green and kinesin-qdot in red. The three kinesin-qdots are labeled 1, 2 and 3 to facilitate identification. At frame 1, no microtubule binds to any kinesin yet. At frame 89, a microtubule is in the midst of being moved by kinesin 2. White arrow indicates the direction of force by kinesin on the microtubule. Yellow arrow indicates the direction of microtubule movement. Notice that kinesin 2 is displaced backward from its original position in frame 1 as it is pushing the microtubule forward. In frame 112, kinesin 1 and 2 supplies forward force together, but kinesin 3 pushes the microtubule back. Finally at frame 200, kinesin 3 supplies force forward while kinesin 2 drags the microtubule back.

Figure 3.2(b) shows the displacement of each kinesin 1, 2 and 3 over time. Downward movement indicates backward displacement, which means forward push on microtubule. The lines at frame 1, 89, 112 and 200 are provided for comparison with Figure 3.2(a).

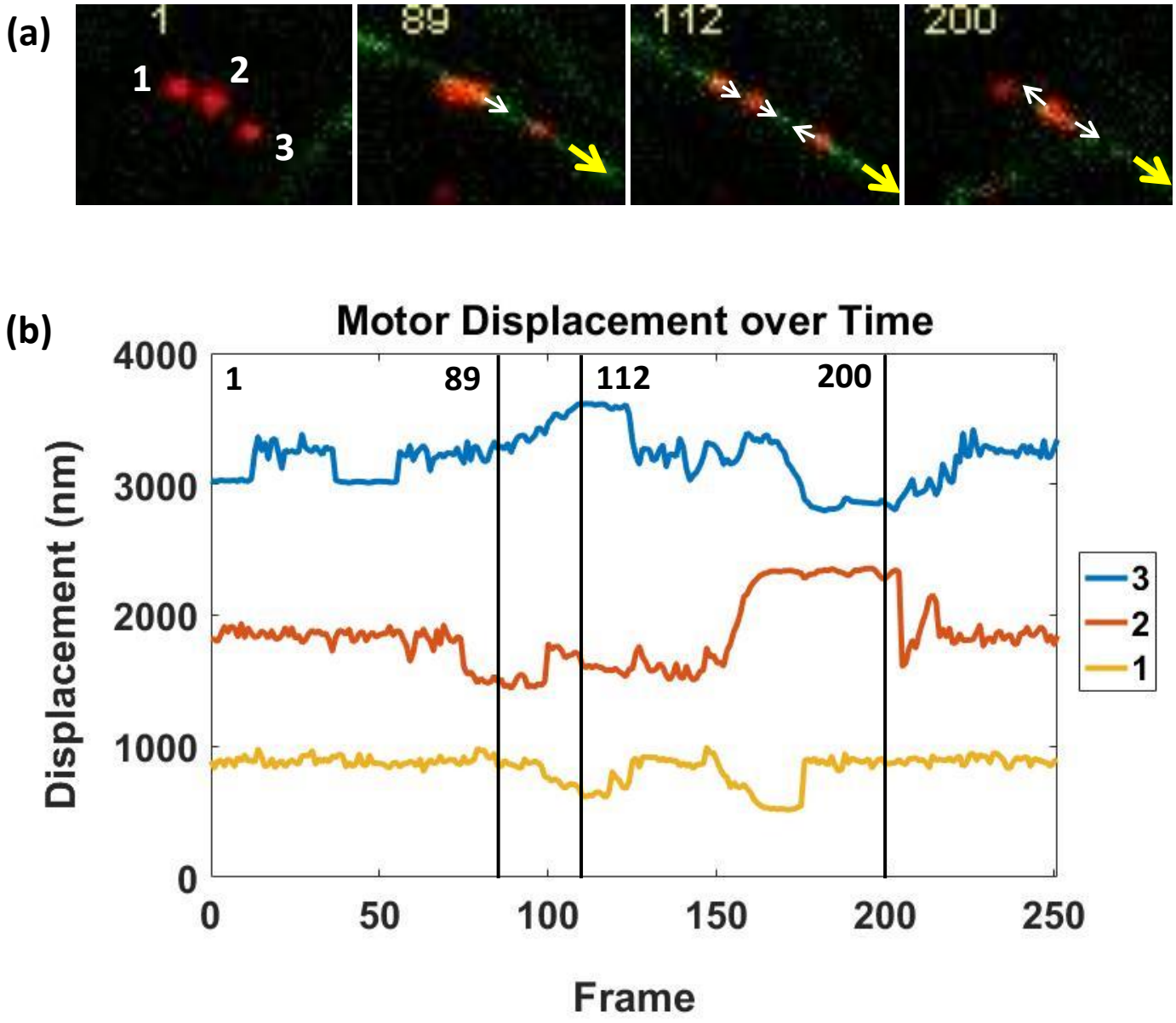

Figure 3.2: Three kinesins moving a microtubule observed with fluorescent force gliding assay. (a) Images at frame 1, 89, 112 and 200 of the movie. Microtubule is in green and kinesin-qdot is in red. The three spots are labeled 1, 2 and 3. At frame 1, no microtubule binds to any of the kinesin yet. At frame 89, a microtubule is in the midst of being moved by kinesin 2. The white arrow indicates the direction of force by kinesin on the microtubule. The yellow arrow indicates the direction of microtubule movement. Notice that kinesin 2 is displaced backward from its original position in frame 1 as it is pushing the microtubule forward. In frame 112, kinesin 1 and 2 supplies force forward, but kinesin 3 pushes the microtubule back. Finally at frame 200, kinesin 3 supplies force forward while kinesin 2 drags microtubule back. (b) Displacement of each kinesin 1, 2 and 3 over time. Downward movement indicates backward displacement, which means forward push on microtubule. The lines at frame 1, 89, 112 and 200 are provided for comparison with (a).

3.5 Discussion

From the fluorescent force gliding result shown in Figure 3.2, we notice that kinesins take turn as the force provider for microtubule. Microtubule first engages kinesin 2, and kinesin 2 is the sole force provider in frame 89. From this point on, the force provider switches to kinesin 1 and 2 in frame 112, kinesin 1 only in frame 165, and kinesin 3 only in frame 200. All the kinesins are involved as the force provider at one point or another. Likewise, all the kinesins with the exception of kinesin 1 are also involved in dragging the microtubule backward. The microtubule is continuously moved forward in the same direction while the kinesins are switching roles.

From this proof of concept, we can see that the fluorescent force gliding assay has the potential of studying detailed motor interactions in multiple motor transport. This is useful in uncovering how different types of molecular motors work together, particularly how kinesin and dynein cooperate to produce bidirectional motion.

3.6 Conclusion

In this chapter we show the proof of concept for a fluorescent force gliding assay to study how molecular motors work together. This assay makes use of the MiCA purification outlined in Chapter 2, and can be used to study cooperation of different types of molecular motors.

Hate is the consequence of fear; we fear something before we hate it; a child who fears noises becomes a man who hates noise.

Cyril Connolly

APPENDIX A: SUPPLEMENTARY MATERIAL FOR CHAPTER 1

A.1 Threshold FPS at zero noise

We look at the special instance when there is zero-noise during stepping. This tells us the minimum number of frames in between steps that we need in an ideal situation when there is no noise.

To prevent skipped steps, there must be at least one frame in between steps. This does not mean that an average FPS of 1 frame per step suffices to prevent skipped steps. Since dwell time distribution is exponential, an average FPS of 1 frame per step will have 63% of the steps having dwell time less than 1 frame, while 37% have a dwell time more than or equal to 1 frame. The probability of steps having dwell time more than 1 frame increases as we increase the average FPS, as shown in Figure A.1. At an average FPS of 6, as many as 85% of steps will have dwell time more than 1 frame, allowing most if not all step-finding algorithm to predict the correct step-size of 8 nm. In fact, all three step-finding algorithms under study correctly predict a step-size of 8 nm at FPS 6.

Different step-finding algorithms perform differently at zero noise. For T-test, HMM, and SIC-stepfinder, the threshold FPS at zero noise are 2, 2 and 6 respectively, as shown in Figure A.2. We can also see that for all stepping algorithms, the fraction of steps found at the correct step-size of 8 nm is smallest at FPS 1, and there are steadily more steps found at 8 nm as FPS increases. T-test and HMM performs better than SIC-stepfinder at zero noise.

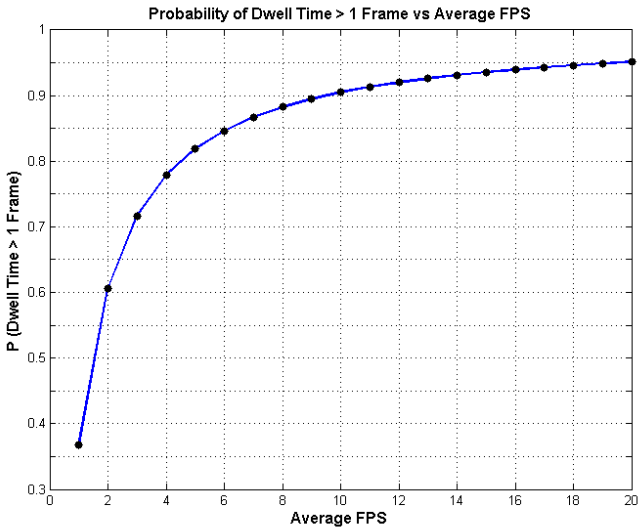

Figure A.1: The probability of steps having dwell time greater than 1 frame increases as average FPS increases. At FPS of 1 frame per step, only 37% of the steps have dwell-time greater than 1 frame. At FPS of 6 frames per step, as many as 85% of all steps have dwell-time greater than 1 frame.

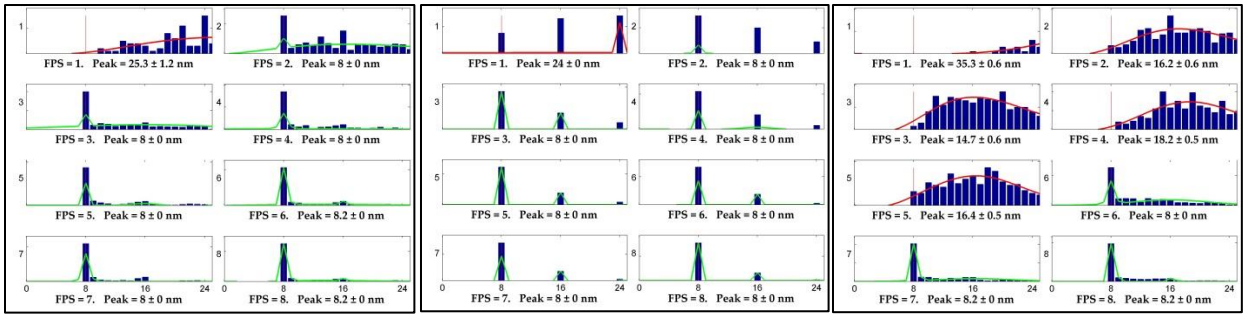

(a) T-test **(b) HMM** **(c) SIC-Stepfinder**

Figure A.2: At zero noise, the threshold FPS for (a) T-test, (b) HMM and (c) SIC-stepfinder is 2, 2 and 6 respectively. X-axis is the step-size in nm. Y-axis is the step frequency.

A.2 Behavior at high noise

Imaging at high frame rate in a cellular environment[3] often yield traces with high noise. This is because we cannot lower the ATP concentration in a cell, and has to increase the frame rate at the expense of noise to capture stepping motions. It is therefore worthwhile to study the behavior of step-finding algorithms at high noise. Figure A.3 shows the step-size histograms of simulated kinesin stepping with high noise of 10 nm. As expected, all three step-finding algorithms report larger step-sizes than the true step-size (8 nm). One surprising finding is that the Student's t-test returns negative in addition to positive step-sizes, while HMM and SIC-stepfinder only report positive step-sizes. The negative step-size reported by t-test is an artifact of overfitting where noise is fitted as a series of backward and forward steps with no net displacement. HMM and SIC-stepfinder is therefore much preferred for step-finding at high noise.

When analyzing data involving bidirectional motion (as in the case of kinesin and dynein in tug-of-war), this finding is useful for us to avoid using step-finding algorithm that is prone to overfitting, as the back and forth motion seen may simply be an artifact of noise rather than real bidirectional motion.

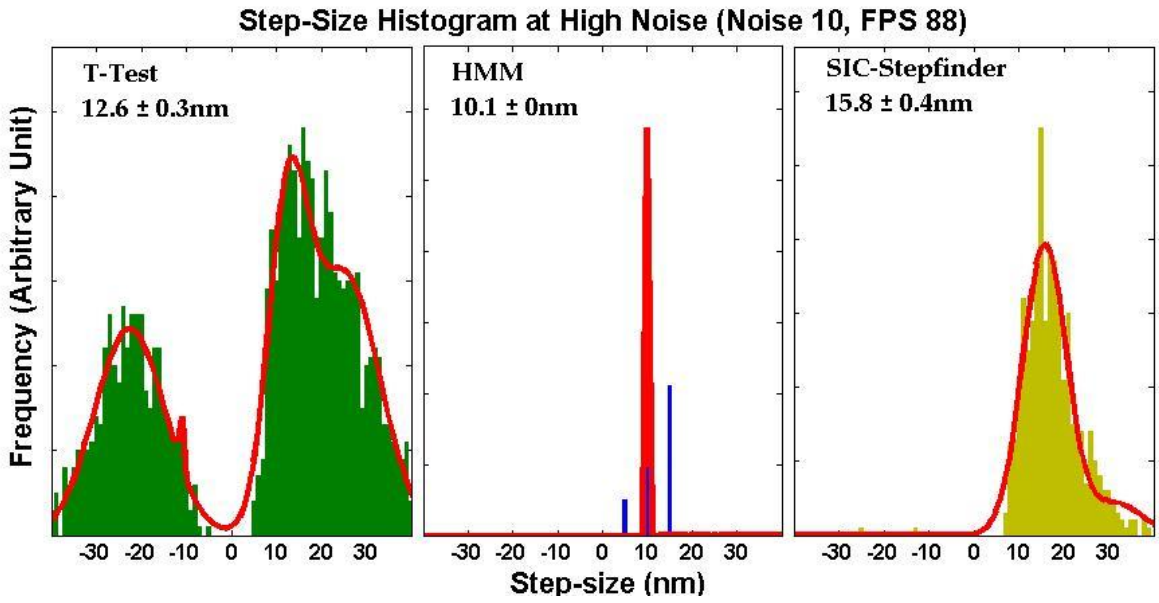

Figure A.3: Behavior of t-test, HMM and SIC-stepfinder at high noise of 10.

A.3 Inherent noise from microtubules and fluorophore

Noise is an integral part of an experiment. The smaller the step-sizes we are trying to resolve, the more significant is the effect of noise. In a kinesin walking experiment, noise can arise from the fluctuation of the microtubule itself, and also from the finite brightness of the fluorophore. To gauge the extent of noise inherent in the microtubule-Qdot system, we attach Qdot® 655 streptavidin conjugate to HiLyte 488-biotin-microtubule and then immobilize the Qdot-microtubules on streptavidin suffused biotin-PEG slides with varying biotin concentrations (0.001%, 0.01%, 0.1% and 1% biotin-PEG). We then measure the noise that arises from the immobilized Qdot-microtubules.

We seek to find the noise contribution to the kinesin-Qdot walking assay by looking at the fluctuations contributed solely by microtubule fluctuation and also Qdot photon count. By attaching Qdot directly to microtubule, we exclude noise associated with the fluctuation of the kinesin stalk. We analyze the Qdot fluctuations on four different biotin-PEG surface (0.001%, 0.01%, 0.1% and 1% biotin-PEG to PEG ratio) to see the effect of varying biotin-PEG concentrations to how firmly microtubules are fixed to the surfaced. When we decrease the biotin concentration from 1% to 0.001% we see gradual decrease in the number of microtubules per field of view. We would expect that there will be less biotin-streptavidin attachment of microtubule to the surface for lower biotin concentration, but the result in (a) says otherwise. At 10 Hz frame rate, the noise from microtubule varies from 3 nm to 5 nm, gradually increasing when the biotin-PEG concentration increases from 0.001% to 1%. We collected only 7 data points from each experiment for this quick experiment, but what we learn from this experiment is that increasing the biotin availability on the surface does not necessarily reduce the microtubule fluctuations.

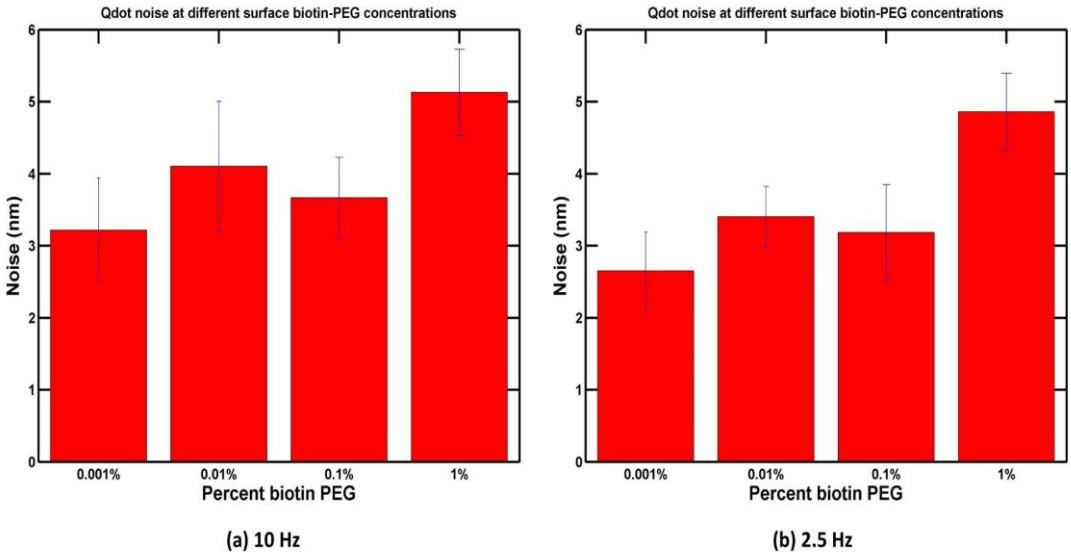

Figure A.4: Noises from QD-microtubules

When we reduce the frame rate to 2.5 Hz by integrating the 10 Hz data frames 4x, we get around 4% to 15% better NPS for each experiment, as shown in (b). There are 4x as many photons collected for 2.5 Hz compared to 10 Hz, and if the photon noise is the limiting factor, the NPS would have improved 2x. The fact that there is only a modest increase in the NPS shows that photon noise is not the limiting factor, and that it is either the microtubule fluctuation or the stage drift that is responsible for the noise in our experiment. For this Qdot-microtubule experiment, the drift is minimized by smoothing the track using Matlab smooth function with robust local regression using weighted linear least squares and a 2nd degree polynomial model.

The 3 nm to 5 nm noise at 10 Hz frame rate correspond to NPS of 0.375 to 0.625. Examining Figure 1.6(a) from the main document, we notice that the noise from 20 Hz, 4 Hz and 0.8 Hz falls within this range. The minimum NPS obtained is around 0.2, close to the 0.375 to 0.625 variation from this experiment. All these point to the fact that microtubule fluctuation and Qdot finite photon count contribute largely to the noise in kinesin walking experiment. We can expect the minimum amount of NPS obtained from experiments to be greater than 0.2. This means that to improve step-size prediction, we can only improve the NPS to a certain extent. Once NPS is at the minimum, we will need to increase the FPS.

A.4 Simulation at other step-sizes

In order to make sure that the step-fitting applies to other step-sizes, and is not biased only to 8 nm step-size, we perform other simulations at step-size of 1.5 nm and 35 nm to see if we get similar relationship between FPS and NPS. Figure A.5 shows FPS vs. NPS relationship for a simulated motor

having step-size of 1.5 nm (red square), 8 nm (blue diamond) and 35 nm (green triangle), with step-fitting done with SIC-stepfinder. We note that the FPS vs. NPS relationship for 1.5 nm and 35 nm step-sizes are similar to the one for 8 nm step-size.

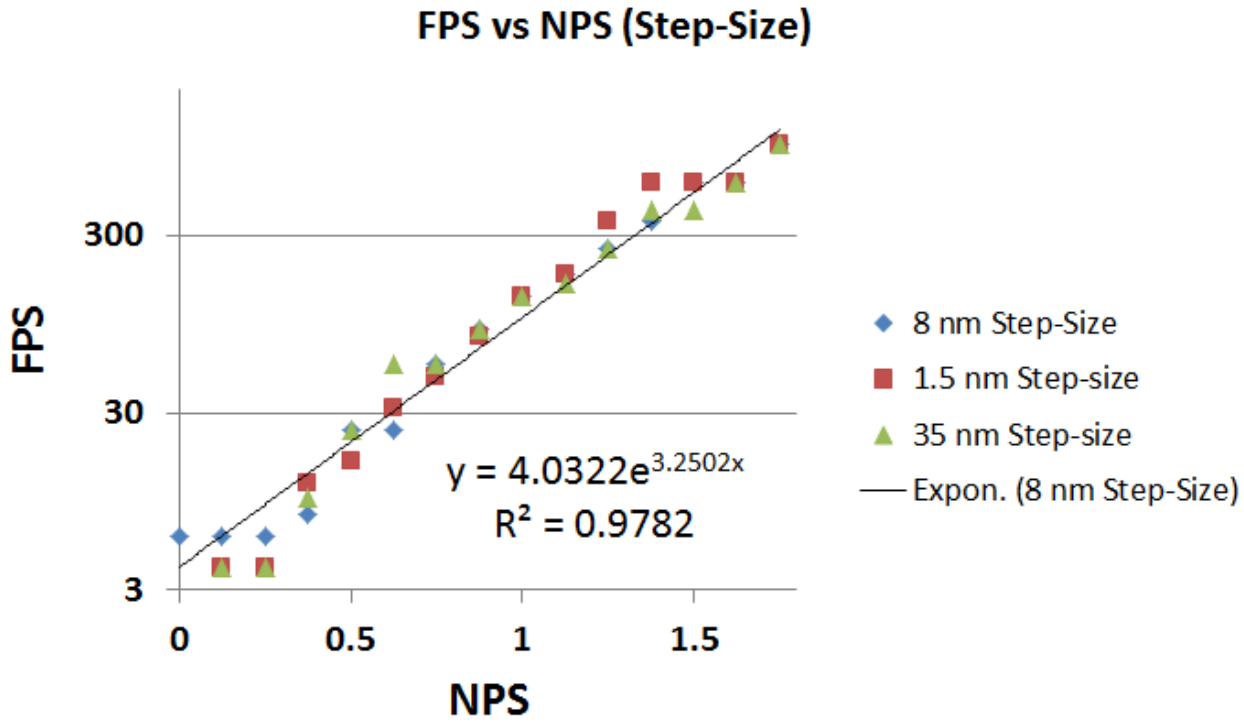

Figure A.5: FPS vs. NPS relationship for simulated traces with step sizes of 1.5 nm (red square), 8 nm (blue diamond), and 35 nm (green triangle). The exponential fit for the 8 nm step-size is also shown in black line. The FPS vs. NPS relationship for the 1.5 nm and 35 nm step-sizes are similar to the one for 8 nm step-size

A.5 Effect of varying frame lengths

Experiments with different frame rates give rise to data sets with varying frame lengths. Concerned that different frame lengths will affect the way step-finding algorithms analyze the data, we investigated the effect of making one data set into smaller sets with shorter frame lengths. We used the data from FPS 144 with noises of 1 nm, 8 nm and 14 nm, then analyze for the predicted step-sizes at frame lengths of 100, 400, 1600, 6400, 25600 and 100000 frames.

Using SIC-stepfinder for step-fitting, when frame lengths are varied from 100 frames to 400, 1600, 6400, 25600 and 100000 frames, we notice that better step-fits are produced with frame lengths greater than the FPS. When the frame lengths are less than the FPS, more negative steps are produced. In Figure A.6(a,b), we notice that when the frame lengths are 100 frames, there are significantly more negative step-sizes than when the frame lengths are 400 frames. Further increase in frame lengths result in less occurrence of negative step-sizes.

The negative step-sizes likely arise from the SIC-stepfinder algorithm trying to force fit a step when there is no step at all. The result is noise-fitting, which generates positive and negative step-sizes equal in magnitude, resulting in zero net displacement. This effect is most apparent in (a) for frame length of 100. Here we notice that there is a real peak at 8 nm, and two peaks at both –2 nm and 2 nm which are equal in frequency, likely arising from fitting noise.

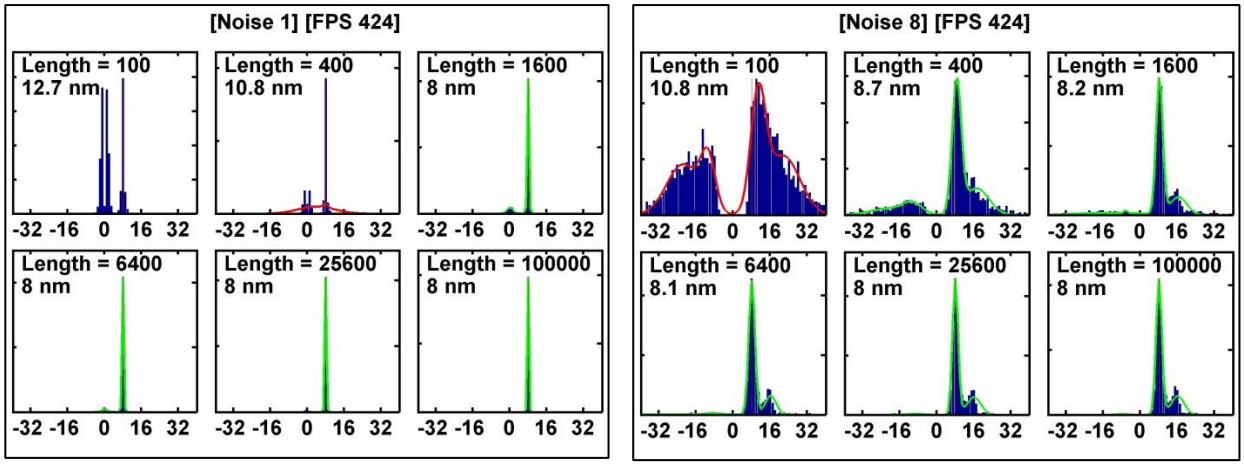

Figure A.6: Step-size histograms of traces at FPS 424 with noises of (a) 1 nm and (b) 8 nm, with frame lengths of 100, 400, 1600, 6400, 25600 and 100000 frames.

A.6 Formulating FIONA Index using dwell-time

It is now known that kinesin steps with hand-over-hand mechanism[2,69], rather than inchworm mechanism[70]. To distinguish hand-over-hand vs inchworm, kinesin can be labeled on the foot. Kinesin step-size will be 16 nm with a hidden 0 nm step if it is handover-hand, and 8 nm if it is inchworm. The dwell-time histogram for hand-over-hand will show an initial rise then fall because there is a hidden step. For inchworm mechanism, the dwell-time histogram will be exponential. Figure A.7 shows the dwell-time histograms for each stepping mechanism. Determining the correct kinesin stepping mechanism requires data collection at high enough frame rate to ensure there is no skipped steps. Simulations show that even for an inchworm mechanism with expected 8 nm step-size and an exponential dwell-time, we can obtain step-size and dwell-time profiles similar to that of hand-over-hand when the FPS is low. Figure A.8 shows that at FPS 4, the step-size obtained is 14.4 nm, with a dwell-time histogram that has a rise then fall profile. At higher FPS, however, the step-size converges to 8 nm, and the dwell-time becomes exponential.

If we compare the step-size histograms to the dwell-time histograms, we note that the step-size is predicted accurately at lower FPS (16) compared to dwell-time (104). Indeed, we can also use dwell-time to formulate FIONA Index, and this will be a more stringent criterion than using step-size. Figure A.9 shows the FPS vs NPS plot when we use dwell-time as the criteria for threshold FPS. Comparing this to Figure 1.2, we see that at every NPS, we generally need higher threshold FPS to get the correct dwell-time histogram (exponential) than the correct step-size (8 nm).

Therefore, if only the step-size is important, we can make do with less stringent criteria for threshold FPS and use Figure 1.2 to derive the FIONA Index equation. If dwell-time is equally important, we will need to use more stringent criteria for threshold FPS and use Figure A.9 to derive the FIONA Index equation.

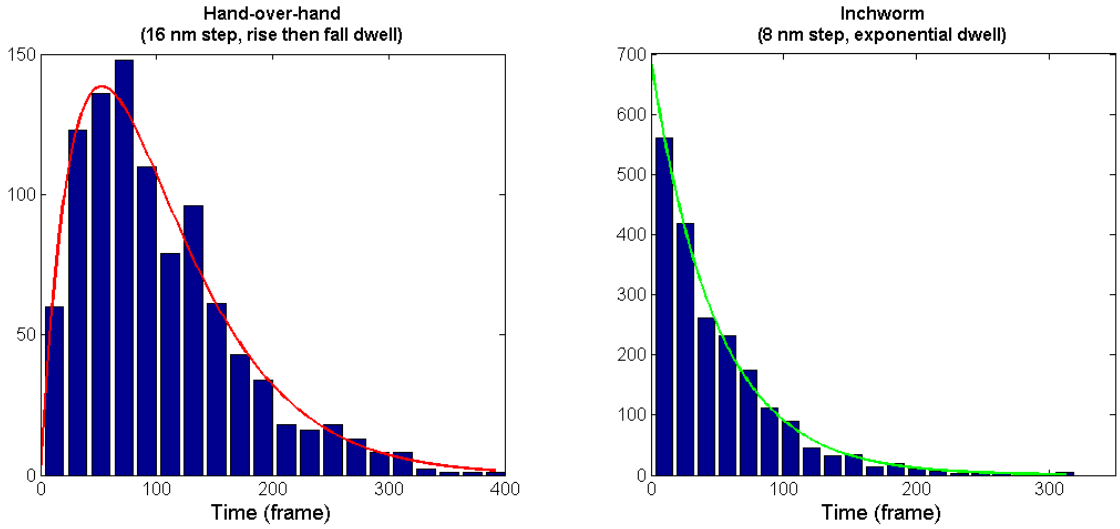

Figure A.7: Dwell-time histograms of foot-labeled-kinesin with hand-over-hand and inchworm mechanism

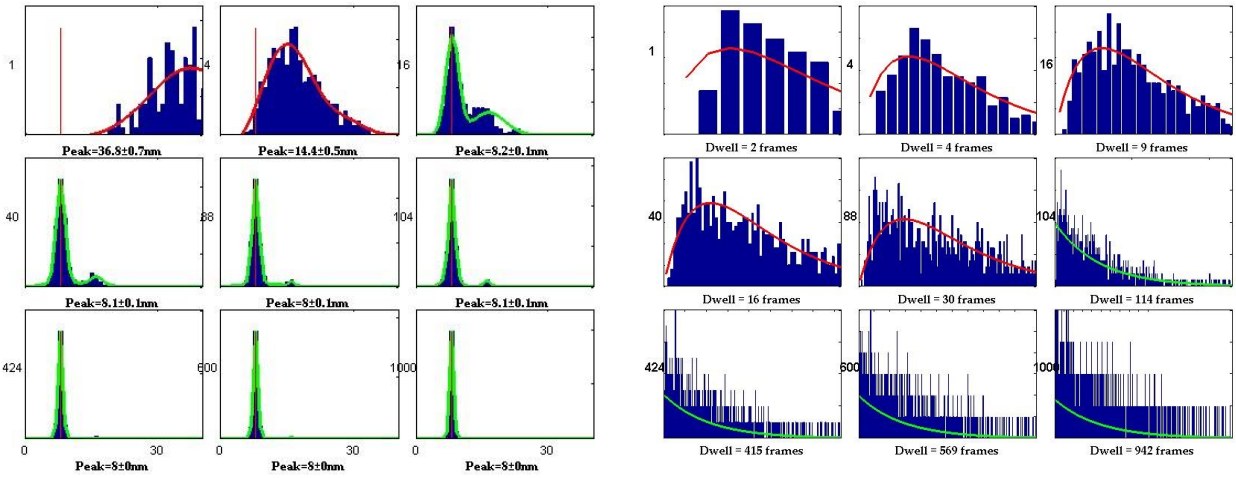

(a) Step-size histograms **(b) Dwell-time histograms**

Figure A.8: (a) Step-size histograms and (b) Dwell-time histograms of simulated kinesin inchworm stepping at FPS 1, 4, 16, 40, 88, 104, 424, 600, and 1000, with a noise of 3 nm.

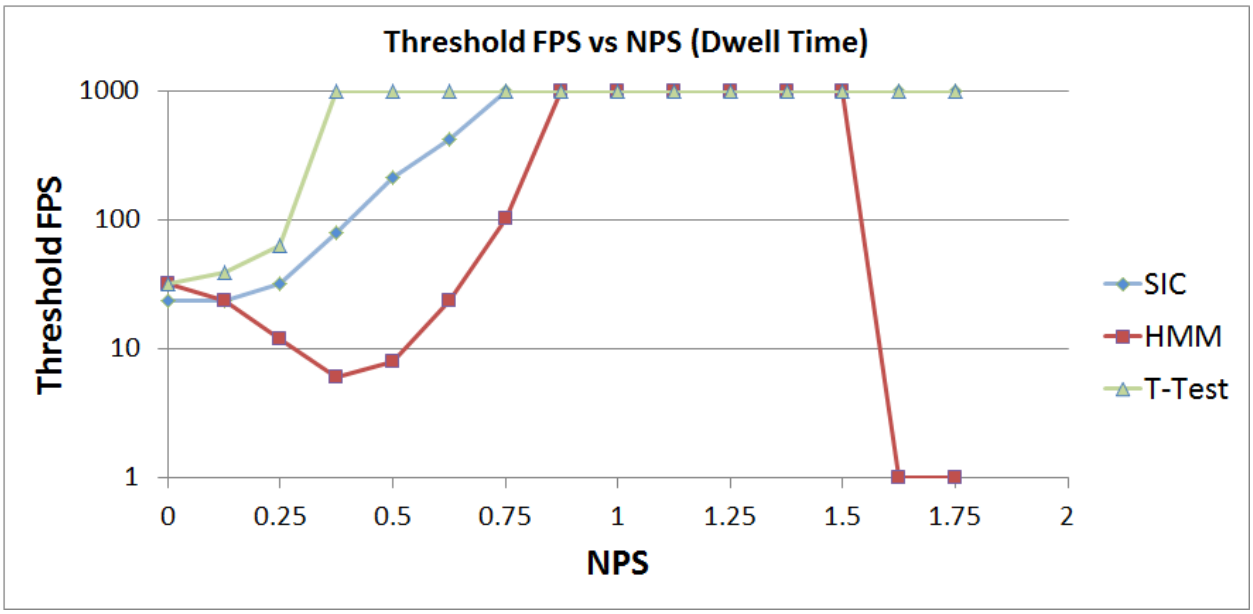

Figure A.9: A semi-log plot of threshold FPS at different NPS for T-test, HMM and SIC stepfinder, using dwell-time as the criteria for threshold FPS

To know yourself as the Being underneath the thinker, the stillness underneath the mental noise, the love and joy underneath the pain, is freedom, salvation, enlightenment.

Eckhart Tolle

APPENDIX B: SUPPLEMENTARY MATERIAL FOR CHAPTER 2

B.1 Magnetic beads preparation

B.1.1 PEG-amine bead synthesis

To synthesize the PEG-amine bead, PEG solution is first prepared by dissolving 50 mg FMOC-NH-PEG-SVA (Laysan Bio, Inc.) in 150 µL freshly prepared sodium bicarbonate buffer (100 mM). The solution is centrifuged at 7,200xg for 1 minute to remove undissolved powder. 1 mL of 3 µm MagSi-S NH2 (10 mg/mL) bead is washed three times with 0.5 mL double-distilled water (ddH_2O) through magnetic separation and buffer exchange. The bead pellet is then washed in 0.1 mL sodium bicarbonate buffer (100 mM). The FMOC-NH-PEG-SVA solution is then added to and mixed thoroughly with the washed bead pellet, taking care to avoid the undissolved PEG at the bottom of the tube (*Note S1*). The mixture is sonicated in a bath sonicator for 1 minute, and then incubated on an end-to-end rotator at room temperature for 3 hours, yielding the FMOC bead shown in Figure 2-2(A). The next step is to deprotect the FMOC group to yield an amine group. This is done by first washing the FMOC beads 2 times with 0.5 mL ddH_2O, and then adding 2 mL of 20% piperidine in DMF to the bead pellet (*Note S2*). The mixture is incubated on end-to-end rotator at room temperature for 2 hours, washed 4 times with 0.5 mL ddH_2O, and the final bead pellets are reconstituted in 1 mL DmB buffer.

Note S1: The succinimidyl valerate (SVA) group in the FMOC-NH-PEG-SVA is an active ester that reacts to the primary amine on the amine bead

Note S2: It is important for this deprotection step to be done in a glass vial since organic solvent used for deprotection may eat into eppendorf tubes. We use HPLC Agilent 2mL Vials with Teflon screw cap from the very beginning of the synthesis, and use neodymium disc magnets (0.220"D x 0.250"T from buymagnets.com) wrapped with tape with the sticky side out for the magnetic pulling

B.1.2 Protocol: kinesin and microtubule binding to beads with gel electrophoresis

Prepare eight Eppendorf tubes. Add amine bead (10 mg/mL) to four tubes (4 µL each) and PEG-amine bead (10 mg/mL) to another 4 tubes (4 µL each). Out of the four tubes for the amine or PEG-amine beads, two will be used for the BSA experiment, another two for experiment without BSA. Out of the two tubes for the BSA or no BSA experiment, one will be to test for kinesin binding and another will be for microtubule binding.

For the BSA experiment, 2 µL DmB-BSA are added to the beads pellet after the original buffers are removed with magnetic pulling. The beads and BSA are incubated for 10 minutes at room temperature on an end-to-end rotator and then washed with 8 µL DmB. The beads are then mixed with either kinesin or microtubule following the protocol below.

For the kinesin binding experiment, the original buffers in the bead (amine or PEG-amine, with or without BSA) are removed with magnetic pulling, and 2 µL kinesins (K888-Het, 1.5 µM) are added and incubated for 10 minutes at room temperature on an end-to-end rotator.

For the microtubule binding experiment, the original buffers in the bead (amine or PEG-amine, with or without BSA) are removed with magnetic pulling, and 2 µL short microtubules (0.8 mg/mL, sonicated for 3 mins) are added and incubated for 10 minutes at room temperature on an end-to-end rotator.

Laemmli-BME buffer is prepared by mixing 95 µL 2x Laemlli buffer with 5 µL BME. DmB-Laemmli-BME buffer is prepared by mixing 50 µL Laemlli-BME buffer with 50 µL DmB.

The kinesins and microtubules supernatant (2 µL each) from each experimental category are removed, combined together, and washed with 2 µL DmB, which is also removed and combined with the supernatant. This mixture is added to 8 µL Laemmli-BME buffer. 8 µL DmB-Laemmli-BME buffer is added to the kinesin bead pellet to reconstitute the pellet, which is then mixed with the microtubule bead pellet. All the samples are heated at 95°C for 5 minutes using a PCR machine with lid heated to 97°C. Gel electrophoresis are carried out using precast gel (12% Mini-PROTEAN® TGX™ Precast Protein Gels, 15-well, 15 µl) and Imperial Protein Stain (ThermoFisher Scientific).

B.1.3 Protocol: kinesin and microtubule binding to amine/ PEG-amine surfaces with TIRFM

Long fluorescent microtubule is prepared following protocol in Appendix B.2. Amine and PEG-amine surfaces are prepared following protocol in Appendix B.3. To prepare kinesin-qdot, 1.14 µL kinesin (K888, 0.44 µM) is mixed with 0.5 µL Qdot® 655 Streptavidin Conjugate (1 µM, Cat No: Q10121MP, ThermoFisher Scientific) and 2.86 µL dilution buffer (DmB-BSA with 16 µM ATP and 1 mM THP). The mixture is allowed to incubate for 30 minutes before 0.5 µL biotin (10 mM) is added to saturate streptavidin binding site on the qdot.

Sample chambers are constructed by sticking the amine and PEG-amine coverslips to glass sides using double-sided tape. We can typically make 7 to 11 chambers with 1 to 2 µL volume using one coverslip (22x22 mm). For microtubule binding experiment, microtubule is diluted 20 times from stock in taxol buffer and added to the amine or PEG-amine chamber, incubated 5 minutes, then washed with 5 µL imaging buffer (50 nM PCD (P8279-25UN, Sigma Aldrich), 0.5 mg/mL PCA (37580, Sigma Aldrich), 2 µM paclitaxel, 1 mM THP, 80 µM ATP, and 50 µM biotin in DmB-BSA). For kinesin binding experiment, 5 nM kinesin-qdot is added to the amine or PEG-amine chamber to fill the chamber volume, incubated 5 minutes, and then washed with 5 µL imaging buffer. Images are recorded on Andor iXon^{EM} camera using internally built TIRFM.

B.1.4 Other MiCA capture beads conjugation attempted

We tried covalently conjugating beads to microtubule using EDC/ amine chemistry, but microtubules tend to depolymerize in the low pH used for conjugation. We also tried using streptavidin magnetic beads to bind biotinylated microtubule, but the coupling is inefficient and it complicates purification of biotinylated motors coupled to streptavidin probes.

Not all commercial amine beads are suited for MiCA. We had success with 0.6 and 3.0 µm MagSi-S NH2 from Amsbio LLC, but not BcMag™ Amine-Terminated Magnetic Beads from Bioclone Inc. PEG-amine beads synthesized using the BcMag™ amine beads still binds to both kinesin and microtubule after modification.

B.2 Preparation of long fluorescent microtubules

Biotin-Fluorescent-Microtubule is prepared by mixing biotin-tubulin (Cat. T333P, Cytoskeleton, Inc.), fluorescent tubulin and plain tubulin (Cat. T240, Cytoskeleton, Inc.) in 0.125:0.04:1 ratio at 7.2 mg/mL total tubulin concentration, then aliquoted to 1.1 µL aliquots and flash frozen in liquid nitrogen. When needed, one tube is quickly thawed on hand and 0.5 µL GlyTP (6.4 mM GTP in 32% glycerol) is added to the 1.1 µL tubulin mix. Final concentrations of tubulin, glycerol and GTP are 5 mg/mL, 10% and 2 mM respectively. The tubulin mix is incubated at 37°C for 30 mins, after which 15 µL warm (room temperature) GTP-taxol buffer (20 µM paclitaxel and 1 mM GTP in BRB80) is added. The mixture is then centrifuged at 13,000xg for 30 minutes to pellet the microtubule. The supernatant is discarded and the pellet is washed with 10 µL warm GTP-taxol buffer without disturbing the pellet. Finally 8 µL warm GTP-taxol buffer is added to reconstitute the pellet to obtain microtubule used for experiment.

B.3 Experiments on amine and PEG-amine coverslips

B.3.1 Preparation of amine and PEG-amine surfaces on glass coverslips

Cleaning coverslips: Place 8 coverslips (22x22 mm) in Teflon holder and clean with 1 M KOH and sonicate 20 mins. Meanwhile, get out aminosilane (CAS 1760-24-3 United Chem. Tech) and FMOC-NH-PEG-SVA from freezer to equilibrate to room temperature. Pour KOH into waste container. Refill holder with ddH2O. Rinse 7 times. Dry all coverslips using lab-made centrifuge dryer by spinning at 200xg for 2 mins at room temperature. Plasma clean all the coverslips in Teflon holder for 3 minutes and place coverslips in a dry 100 mL beaker.

Aminosilanization: Clean a 100 mL beaker with water and methanol, and then dry with nitrogen gas. Add 75 mL methanol to the beaker, then add 1.5 mL aminosilane and 3.75 mL acetic acid with glass pipette in fume hood. Pour aminosilane mix over the coverslips until they are covered. Incubate 10 minutes, then sonicate 1 minute and incubate another 10 minutes. Pour off liquid mix into waste container. Refill with methanol. Pour off methanol into waste container. Repeat 1 time. Refill with water. Pour out water and refill. Repeat 7 times. Dry all coverslips using centrifuge dryer with 200xg spin for 2 mins at room temperature. At this point, the coverslips are covered with amine surface. Set 4 coverslips aside and modify another 4 with FMOC-NH-PEG-SVA.

Prepare PEG solution: Weigh 10 mg sodium bicarbonate (fresh each time) and add 1.2 mL ddH_2O (makes 100 mM sodium bicarbonate). Weigh 18 mg FMOC-NH-PEG-3400-SVA and add 75 µL sodium bicarbonate buffer. Mix by vortexing, then centrifuge for 1 minute at 7200xg to remove undissolved solid. This yields around 84 µL FMOC-NH-PEG-3400-SVA.

Coverslip PEGylation: Take out an empty pipette box with water in the wells to prevent PEG evaporation. Lay one aminosilane coverslip on the dry surface above the water. Add 30 µL PEG mixture to center of one aminosilane coverslip. Spread a bit with pipet tip and avoid forming bubble. Sandwich another aminosilane coverslip on top, watching out for bubbles (can tap to edges or press slightly to get rid of bubbles). Repeat with another coverslip sandwich. Close plastic box and wait 3 hours. After 3 hours, take sandwich apart (remember which side is coated with PEG!) and put them on Teflon holder, marking the side where the PEG is coated. Wash 7 times with ddH_2O. Dry all coverslips using centrifuge dryer. At this point, PEG-FMOC surface is prepared

FMOC deprotection: Prepare 20% piperidine solution by mixing 64 mL DMF and 16 mL piperidine in a 100 mL beaker. Place coverslips in solution, cover beaker with parafilm, and incubate for 2 hours. Wash once with DMF, then 7 times with ddH_2O, and finally dry with centrifuge dryer. Dispose the piperidine solution in a dedicated waste container. At this point, PEG-amine surface is prepared.

Storage: Place individual coverslip with the PEG-amine side up in a small plastic container just big enough to hold one coverslip. Parafilm container to prevent coverslip contact with moisture. All aminosilane and PEG coverslips can be stored at -20°C freezer for prolonged period of time (1 year or longer). Upon use, allow coverslip to equilibrate to room temp to prevent condensation on coverslip surface.

B.3.2 Microtubule binding to PEG-amine surfaces at different PEG-amine concentrations

To make sure that microtubule binding to PEG-amine surfaces is specific to the PEG-amine, we decrease the PEG-amine concentration and look at microtubule binding to these surfaces. Appendix Figure B.1 shows that as PEG-amine concentration decreases from 100% to 25%, 5% and 1%, the number of microtubules binding to these surfaces decrease. Addition of casein, which is known to dislodge microtubule from amine surfaces[71], causes some but not all of the microtubules to release.

The PEG-amine surfaces at lower PEG-amine concentrations (1%, 5% and 25%) are prepared in a similar way as the 100% PEG-amine using the protocol in Appendix B.3.1. The only difference is that instead of using solely FMOC-NH-PEG-3400-SVA, MPEG-SVA-2000 (Laysan Bio, Inc.) is added to reduce the final PEG-amine concentration.

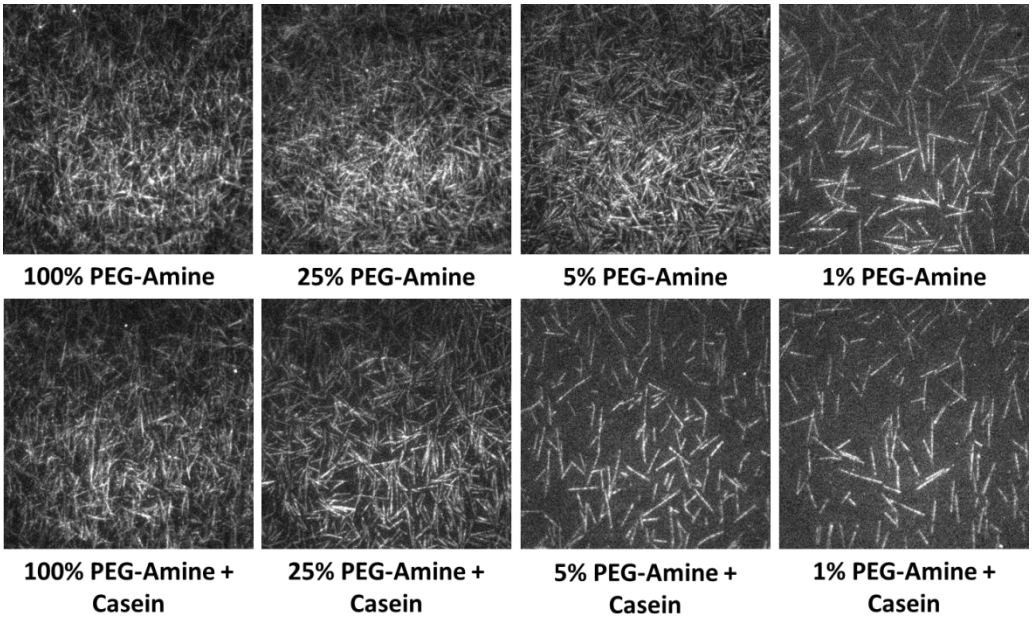

Figure B.1: Binding of microtubule to PEG-amine surfaces at different concentrations. As PEG-amine concentration decreases, less microtubule binds. Addition of casein causes microtubule to release from the surface.

B.3.3 Kinesin motility on amine and PEG-amine surfaces

We investigate kinesin-qdot motility on the amine and PEG amine surfaces to determine if kinesin-qdot bound to the microtubule on these surfaces are still motile. Figure B.2 shows the result of this experiment. When amine surface is used, only around 26% of kinesin-qdots are motile, showing that many of the kinesin-qdots become immotile due to interaction with the amine surface. With 100%, 25% and 5% PEG-amine, as many as 67% to 80% of kinesin-qdots are motile, showing that these PEG-amine concentrations can be used to immobilize microtubule and still allow kinesin motility. With 1% PEG-amine, only 24% kinesin-qdots are motile, likely because too few microtubules bind to the surface and the ones detected are non-specifically bound to the surface instead of binding to microtubule.

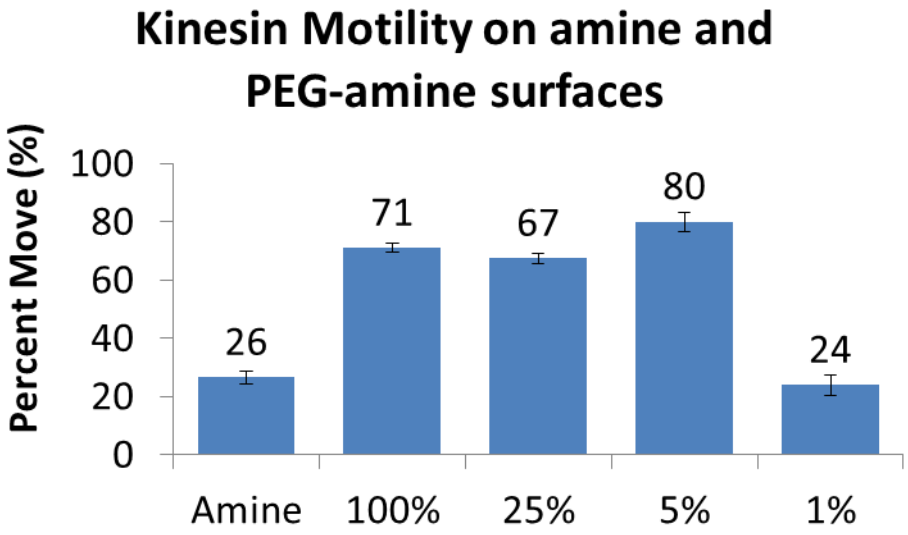

Figure B.2: Kinesin motility on amine and PEG-amine surfaces. When amine surface is used, only around 26% of kinesin-qdots are motile, showing that many of the kinesin-qdots either bind non-specifically to the amine surface, or the microtubule bound to amine surface does not support motility. With 100%, 25% and 5% PEG-amine, as much as 67% to 80% kinesin-qdots are motile, showing that these PEG-amine concentrations can be used to immobilize microtubule that still allow kinesin motility. With 1% PEG-amine, only 24% kinesin-qdots are motile, likely because too few microtubules bind to the surface and the ones detected are non-specifically bound to the surface instead of binding to microtubule. Error bars are generated from 200-1500 stuck and moving dots on each surface.

B.4 Preparation of PEG-biotin coverslips

The PEG-biotin coverslip is made with 1% PEG-biotin and 99% just PEG. We find that this biotin quantity on the surface is enough to immobilize microtubules and other proteins through the biotin-streptavidin interaction.

To make 8 PEG-biotin coverslips, the PEG-amine coverslip preparation protocol in Appendix B.3 is followed, with a change in the PEG solution preparation. Instead of using FMOC-NH-PEG-3400-SVA, 25.7 mg MPEG-SVA-2000 (Laysan Bio, Inc.) is mixed with 0.64 mg Biotin-PEG-SVA-5000 (Laysan Bio, Inc.) and 107 µL sodium bicarbonate buffer to make 1% Biotin-PEG solution. 30 µL of the solution is then added and sandwiched between coverslips, and the coverslips are incubated, washed, dried and stored as in Appendix B.3. The FMOC deprotection step is skipped.

B.5 Effect of sonication and freeze-thawing on microtubule length

Long fluorescent microtubules are prepared as in Appendix B.2, just that no biotin tubulin is used, only HiLyte 488 fluorescent tubulin (Cat. TL488M-A, Cytoskeleton, Inc.) and plain tubulin in 0.04:1 ratio. Also, instead of using GlyTP (glycerol + GTP), we use GMP-CPP, a non-hydrolysable analog of GTP. GMP-CPP microtubules are more stable than GTP microtubules, but the final microtubules obtained are stiffer[72,73] and slightly shorter than GTP microtubules. Briefly, 1.1 µL of HiLyte488-Tubulin mix (7.4 mg/mL) are mixed with 0.5 µL GMPCPP (6.4 mM). The tubulin mix is incubated at 37°C for 30 mins then centrifuged at 13,000xg for 30 minutes after mixing with 15 µL warm GMP-taxol buffer (20 µM paclitaxel and 0.2 mM GMPCPP in BRB80). The supernatant is discarded and the pellet is washed with 10 µL warm GMP-taxol buffer then reconstituted with 8 µL warm GMP-taxol buffer.

The microtubules are then subjected to sonication in a bath sonicator at 0, 1, 2 and 5 minutes after diluting 50 times in taxol buffer (20 µM paclitaxel in BRB80). Note that different sonicators and different areas of the same sonicator have different power. For reproducibility, use the same area on the same sonicator each time after proper degassing. We use Branson 2510 Ultrasonic cleaner and made a float adaptor to position the tubes at the stronger sonication area each time.

The 2 min sample is divided into two aliquots, and one is subjected to freeze-thawing to investigate the effect of freeze-thawing on microtubule length.

The microtubules after sonication and freeze-thawing are flowed into an aminosilane chamber made following protocol in Appendix B.3. They are imaged on a TIRFM setup with Andor iXon^{EM} EMCCD camera using 0.5s exposure time, 100 EM gain and a green laser.

A Matlab code (CountMicrotubules.m) is written to analyze the microtubule length and provided in the supporting information. Briefly, each microtubule image is binarized and the microtubule filaments are thinned into single pixel region. The microtubule length is calculated by summing the areas of the pixels occupied by single microtubule. The mean and standard error of the mean are then calculated from all the microtubule lengths and reported in Figure B.3. Accompanying microtubule images are also included in Figure B.3 to the left of the microtubule length histogram.

Figure B.3 shows that increasing the sonication time decreases average microtubule length. Starting with an average of 4.04 µm length with no sonication, microtubule length decreases to 1.24 µm, 0.74 µm and 0.40 µm at 1 min, 2 min and 5 min sonication. Freeze-thawing also decrease the microtubule length for the 2 min sample, from 0.74 µm before freeze-thaw, to 0.44 µm after freeze-thaw.

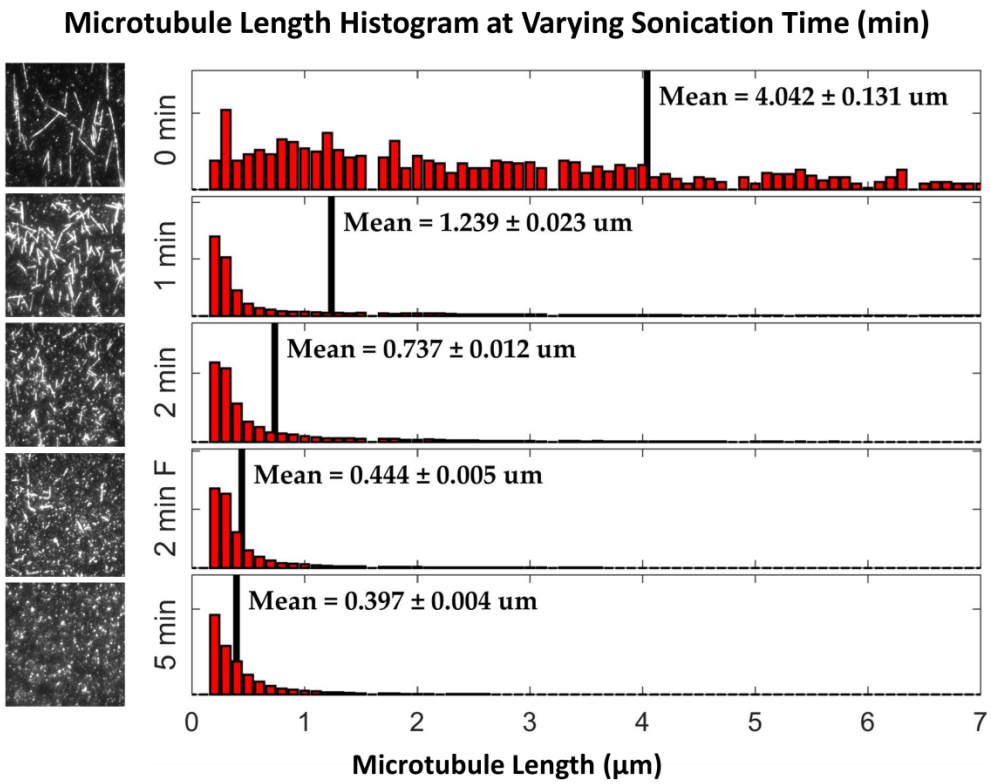

Figure B.3: Microtubule length at varying sonication time. As sonication time increases, the microtubules are sheared and become shorter. Freeze-thawing microtubule (2 min F) also has the effect of reducing the average length of microtubule, as compared to one without freeze-thawing (2 min).

B.6 Bind and release of kinesin-qdot to tubulin and various microtubule preparations

For these experiments, kinesin-qdot is bound and released from tubulin and various microtubule preparations. The tubulin comes from biotin-tubulin (Cat. T333P, Cytoskeleton, Inc.). The centrifuged microtubules are prepared from 0.125: 0.04: 1 ratio of biotin: HiLyte488: tubulin, made as in Appendix B.2, with GMPCPP (6.4 mM) replacing GlyTP. The non-centrifuged microtubules are prepared similar to the centrifuged microtubule, just that the 30 minutes centrifugation step at the end is skipped. The sonicated microtubules are prepared similar to the centrifuged microtubule, just that TMR-tubulin (TL590M, Cytoskeleton, Inc.) is used in place of HyLite 488-tubulin. Additionally, the microtubules are sonicated for 0 min, 2 min and 5 min in a bath sonicator.

Kinesin-qdot is made by mixing 1 µL K432 kinesin (4 µM) with 0.5 µL Qdot® 655 Streptavidin Conjugate (SA-Qd655) and 8.5 µL dilution buffer (DmB-BSA with 1 mM THP and 16 µM ATP). The mixture is incubated on ice for 30 minutes, and then 0.25 µL biotin (10 mM) is added to saturate the streptavidin binding site in SA-Qd655.

PEG-biotin chamber is made from PEG-biotin coverslip (Appendix B.4). Streptavidin (600 nM) is added to chamber and left incubated for 5 min. The chamber is washed with 5 chamber volumes of DmB-BSA. Two chamber volumes of tubulin or microtubule (10 times dilution from stock in BSA-taxol buffer (20 μM paclitaxel in DmB-BSA)) is flowed in and left incubated for 5 min. The chamber is then washed with 4 chamber volumes of BSA-taxol-biotin buffer (20 μM paclitaxel and 200 μM biotin in DmB-BSA). Two chamber volumes of kinesin-AMP solution (0.625 or 5 nM kinesin-qdot, 1 mM AMP-PNP, 20 μM paclitaxel, 0.1 μM PCD (protocatechuate 3,4-dioxygenase - Cat. P8279-25UN, Sigma Aldrich), 1.5 mg/mL PCA (protocatechuic acid - Cat. 37580, Sigma Aldrich)) is added and the chamber is recorded on a TIRFM setup to get the AMP-PNP (binding) images. After AMP-PNP imaging, two chamber volumes of ATP solution (1 mM ATP, 20 μM paclitaxel, 0.1 μM PCD, 1.5 mg/mL PCA) is added and the chamber is recorded to get the ATP (release) images.

The results of these experiments are shown in Figure B.4. Figure B.4(A-B) shows that kinesin-qdot binds well to tubulin, non-centrifuged and centrifuged microtubule, but releases well only for non-centrifuged and centrifuged microtubule (only 0.3% and 6.2% kinesin-qdot remains). As much as 74.1% kinesin-qdot is still stuck to tubulin after ATP release buffer is added. This experiment informs us that MiCA purification cannot be done using pure tubulin.

The next set of experiments investigates bind and release scenario from sonicated microtubules. As shown in Figure B.3, 5 min sonicated microtubules can be 10 times shorter than non-sonicated ones. It is possible that the sonication breaks the microtubule down to pure tubulin, which cannot release kinesin-qdot. Figure B.4 (C-D), however, shows that increasing sonication time has no effect on the bind and release of kinesin-qdot. Practically all kinesin-qdot releases from microtubules sonicated from 0 to 5 min (only less than 15% kinesin-qdot remains after ATP elution for all).

All in all, the kinesin-qdot bind and release experiments in Figure B.4 show us that kinesin can bind to any tubulin or microtubule, and can release from any microtubule be it sonicated or not, or centrifuged or not. However, kinesin-qdot cannot release from tubulin once bound.

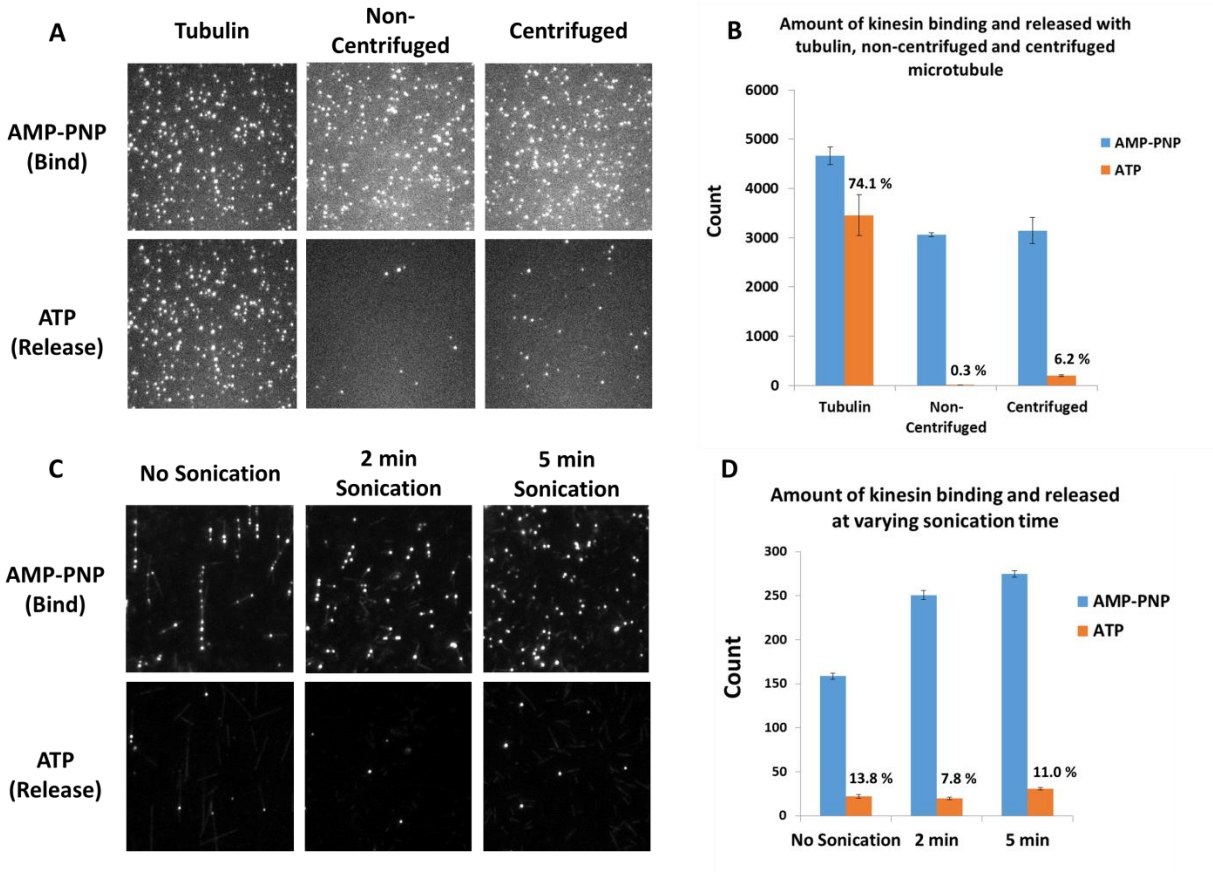

Figure B.4: Kinesin-qdot bind and release experiments on different microtubule and tubulin surfaces. (A & B) Comparison of kinesin binding to and releasing from tubulin and microtubules without and with short microtubules removed through centrifugation. Kinesin-qdot can bind to all tubulin or microtubules. It does not release well from tubulin (74.1% remains bound), but releases well from microtubules without or with centrifugation (only 0.3% and 6.2% remains bound). (C & D) Bind and release experiment using microtubules with varying sonication time. Sonication does not affect kinesin-qdot release. Only 13.8%, 7.8% and 11.0% kinesin-qdot remains after elution with ATP for microtubules with 0 min, 2 min and 5 min sonication. Error bars for panels B and D are the standard error of the mean of the number of kinesin-qdot detected from 3 to 6 fields of view in every experiment.

B.7 Effect of freeze-thawing microtubules on kinesin elution

For this experiment, three MiCA capture beads are prepared. One with freeze-thawing short microtubule while bound to PEG-amine bead, called FTBoth. One with freeze-thawing only the microtubule, called FTMic and another with no freeze-thawing, called NoFT.

To start, 45 µL PEG-amine bead (10 mg/mL) is washed with 30 µL GMP-taxol buffer and reconstituted in 14 µL GMP-taxol buffer to make a 15 µL solution. 10 µL of this is then mixed with 6 µL short microtubules with 5 min sonication and left to incubate for 5 min. This gives us the NoFT. FTBoth is

made by flash-freezing 8 µL of NoFT in liquid nitrogen and thawing it. FTMic is made by mixing 5 µL washed PEG-amine bead with 3 µL thawed sample of frozen short microtubule, and then the mixture is incubated for 5 min.

All three beads are washed with 5 µL GMP-taxol buffer, then 2.5 µL warm DmB-BSA added. The solution is incubated for 1 min, and then washed with 5 µL GMP-taxol buffer and reconstituted in 5 µL GMP-taxol buffer to give a final volume of 6 µL. K888-Het (3.75 µM) and 1 µL AMP-PNP (8 mM) are then mixed with each of these 6 µL MiCA capture beads, and then incubated for 5 min on an end-to-end rotator. The beads are then washed twice with 8 µL GMP-taxol buffer and eluted with 8 µL elution buffer (3 mM ATP in GMP-taxol buffer).

The elution, and proteins left in bead are then quantified with SDS-PAGE electrophoresis using Imperial™ protein stain and shown in Figure B.5. Compared to the amount left in bead, FTBoth has the least fraction eluting (49%), while FTMic and NoFT have 68% and 59% elutiing. The low yield for FTBoth may be caused by damage to the magnetic beads or PEG during freeze-thawing of the PEG-amine bead. Since freeze-thawing just the microtubule does not adversely affect elution efficiency, we start to use frozen microtubules for routine MiCA purification. This saves the short microtubule preparation time, since they can now be made just once in a large batch, then aliquoted into small aliquots and taken out before any MiCA purification.

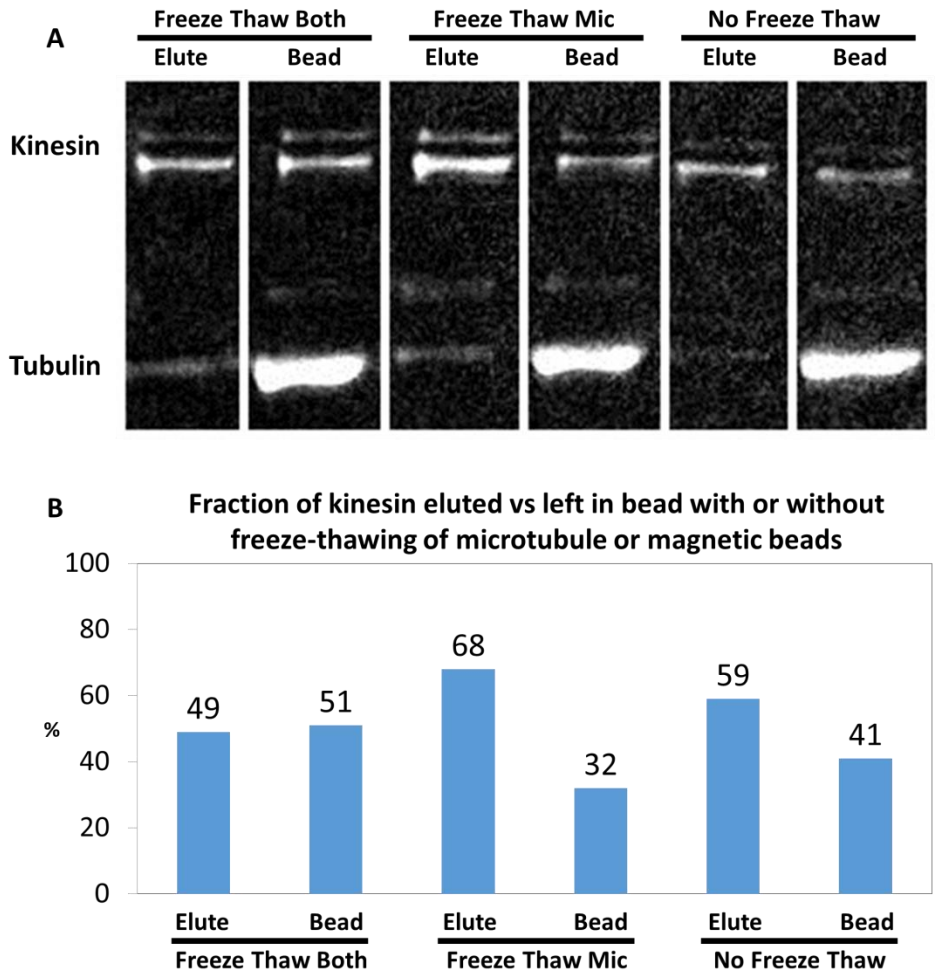

Figure B.5: Effect of freeze-thawing of MiCA capture beads on kinesin elution. Three MiCA capture beads are compared. The first undergoes freeze-thawing on both microtubule and magnetic bead when microtubule is bound to the bead. The second only has the microtubule but not the magnetic bead undergoing freeze-thaw. The third undergoes no freeze-thaw at all. (A) Gel bands showing the amount kinesin and tubulin that release with the elution buffer (Elute) or remain on bead (Bead) after MiCA purification. The greater the fraction of kinesin eluting vs. staying on bead the better. (B) Quantifying the fraction of kinesin eluted vs. remaining on bead. No freeze-thaw and freeze-thawing only microtubule allows more kinesin eluting than staying on bead. When both microtubule and magnetic bead is frozen and thawed, less kinesin elutes than stays on bead.

B.8 Preparation of kinesin

B.8.1 Preparation of K888 and K888-Het

For K888 homodimer, the mouse kinesin heavy chain (accession number BC090841) and light chain (accession number BC014845) were cloned separately into the baculovirus transfer vector pAcSG2 (BD Biosciences). The constitutively active kinesin (kinesin ΔC) was truncated after Ala^{888}. For expression of a homodimeric kinesin with two identical heavy chains, a C terminal biotin-tag was added for attachment

to streptavidin Qdots, followed by a FLAG epitope at its C-terminus to facilitate purification. The biotin tag is an 88 amino acid sequence segment from the Escherichia coli biotin carboxyl carrier protein[74], which is biotinated at a single lysine during expression in Sf9 cells.

For K888 heterodimer (K888-Het), two versions of the kinesin heavy were cloned to enable isolation of a heterodimer that contained a biotin tag on only one of its two heads. One heavy chain had an N-terminal biotin-tag, and a C-terminal HIS_6 tag. The second heavy chain had only a C-terminal FLAG-tag. Both heavy chains were truncated after Ala^{888}.The mouse kinesin light chain was cloned with YFP at the C-terminus for use with the heavy chain heterodimer, and with no YFP for expression of the heavy chain homodimer. Recombinant baculovirus was prepared by standard protocols.

Sf9 cells were infected with the heavy and light chain recombinant baculovirus, or in the case of the heterodimer, three recombinant baculovirus; two coding for kinesin heavy chain, and one coding for the light chain. The medium was supplemented with 0.2 mg/ml biotin, harvested after 72 h, and lysed by sonication in 10 mM imidazole, pH 7.4, 0.3 M NaCl, 1 mM EGTA, 5 mM MgCl2, 7% (w/v) sucrose, 2 mM DTT, 0.5 mM 4-(2-aminoethyl) benzenesulfonyl fluoride, 5 µg/ml leupeptin prior to clarifying at 200,000 X g for 40 min. The supernatant was purified by FLAG-affinity chromatography (Sigma- Aldrich). The column was washed with 10 mM imidazole, pH 7.4, 0.3 M NaCl, and 1 mM EGTA. Kinesin was eluted from the column in the same buffer containing 0.1 mg/ml FLAG peptide. For the homodimer, the fractions of interest were combined, concentrated with an Amicon centrifugal filter device (Millipore), and dialyzed against 10 mM imidazole, pH 7.4, 0.2 M NaCl, 1 mM tris(2-carboxyethyl)phosphine TCEP), 55% (v/v) glycerol,1 mM DTT, 1 µg/ml leupeptin and 50 µM MgATP for storage at -80°C. For the heterodimer, the first 15 ml of wash buffer contained excess non-bound light chain and other impurities, and was discarded. The desired heterodimeric kinesin containing a biotin tag on only one of its two heads, and a FLAG tag only on the heavy chain lacking a biotin tag, did not bind tightly to the FLAG resin, and eluted in the next 50 ml of wash. Fractions were concentrated as above, and the concentrated heterodimer was dialyzed in the same 55% glycerol buffer as the homodimer.

B.8.2 Preparation of K432

Recombinant truncated kinesin DNA with 432 amino acids fragment from *Drosophila* kinesin is made with biotin and 6xHis tag at the C-terminus[75] . The DNA is cloned into pET17b vector and transformed into BL21(DE3) bacterial cells. Cells are grown in LB (Luria-Bertani) media at 37°C until OD600 reaches 0.6, after which they are induced with IPTG (0.25 mM) for 4 to 5 hours at 37°C. The cells are then harvested, lysed with probe sonication after incubation for 15 minutes on ice in lysis buffer (10 mM Imidazole, 50 mM TRIS, 250 mM NaCl, 1 mM MgCl2, 40 µM ATP, 1 mg/mL lysozyme, and 1 mM PMSF, pH 8.0), and the cell debris removed through centrifugation at 10,000xg for 30 mins at 4°C. The lysate is incubated with Ni-NTA resins at 4°C for an hour, loaded on a column, and washed 3x with wash buffer (20 mM Imidazole, 50 mM TRIS, 250 mM NaCl, 1 mM MgCl2, 40 µM ATP, pH 8.0). Kinesin is eluted with elution buffer (250 mM Imidazole, 50 mM TRIS, 250 mM NaCl, 1 mM MgCl2, 40 µM ATP, pH 8.0) and the

fractions of interest are combined. Equal volume of 20% sucrose solution is added and the kinesin is flash frozen and stored at -80°C.

B.9 Image registration

Approximately 1200 points are collected from each nanohole channel for image registration. Figure B.6 shows a representative image before and after image registration. The qdot channel is registered onto the microtubule channel such that when combined, the dots on both channels colocalize. For image registration, the cp2tform function in Matlab is used with local weighted mean as the transform type. Once the transform function is obtained, it is applied to all the qdot images to transform them so that they are registered with their corresponding microtubule images.

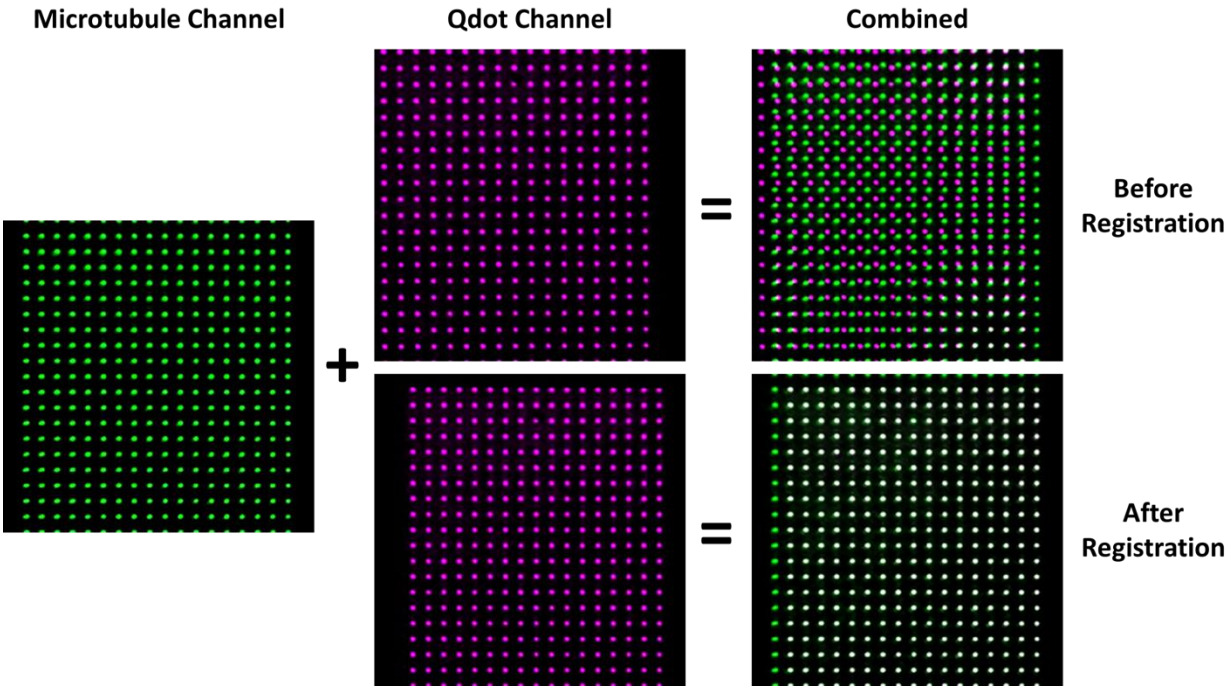

Figure B.6: Nanohole images from the microtubule and qdot channel shown in green and magenta. Image shown is one quarter size of the full 512x512 pixel collected during experiment. The qdot channel is transformed using cp2tform function in Matlab with local weighted mean transform type. Before registration, each dot in the qdot channel do not colocalize with the microtubule channel. After registration, the dots in the qdot channel colocalize well with the microtubule channel.

B.10 MiCA purification optimization

B.10.1 Varying elution volume, time and ATP concentration

In this experiment, nine different elution conditions varying three parameters are investigated: three with varying time (1 min, 5 min and 30 min), three with varying volume (2 µL, 4 µL and 8 µL) and three with varying ATP concentrations (0.1 mM, 1 mM and 10 mM). The default parameters are 5 min elution time, 8 µL elution volume and 1 mM elution ATP concentration. This default condition is common for all three parameters, allowing us to collect only 7 experiments since the result from this default condition can be applied to all three parameters. The experimental setup is summarized in Figure B.7(A).

MiCA capture bead is prepared by removing the buffer in 120 µL PEG-amine bead (10 mg/mL) and mixing in 16 µL short microtubule with 5 min sonication. The mixture is left to incubate for 5 min, washed with 20 µL dilution-taxol buffer, and then incubated in 10 µL DmB-BSA for 1 min. It is again washed with 20 µL dilution-taxol buffer before reconstituting in 12 µL dilution-taxol buffer to make a final volume of 15 µL. The mixture is mixed with 1 µL AMP-PNP (20 mM) and 4 µL K888-Het (3 µM), then incubated for 5 min at room temperature. After washing twice with 20 µL dilution-taxol buffer, the mixture is reconstituted in 20 µL dilution-taxol buffer and aliquoted into 7 tubes of 2.5 µL each. Seven different experiments are conducted with varying elution condition, with the default condition as described above. The other experiments are: 1 min and 30 min elution time, 2 µL and 4 µL elution volume, and 0.1 mM and 10 mM ATP concentrations. The eluants are then quantified with SDS-PAGE electrophoresis using ImperialTM protein stain.

Figure B.7(A) shows the gel result from experiments varying elution conditions, and Figure B.7(B-D) quantify their corresponding purification yields. Figure B.7(B) shows that as elution volume increases from 2 µL to 4 µL and 8 µL, yield increases from 19% to 26% and 27%. This shows that low elution volume adversely affects elution yield. Larger elution volume gives greater yield at the expense of diluting the eluant. For our experiments, it is desirable to get optimal yield at high concentration, so 4 µL is a good compromise as the yield is only 1% less than that eluted with 8 µL volume, but the concentration is twice as high.

Figure B.7(C) shows that as elution time increases from 1 min to 5 min and 30 min, the yield increases from 12% to 27%, then decreases to 23%. 5 min is thus the optimal elution time. The yield decreases at long elution time (30 min) likely because some kinesin become inactive and get stuck to microtubule, or some are lost to the tube or the bead. It is also likely that ATP starts to run out at longer elution time.

Figure B.7(D) shows that as ATP concentration increases from 0.1 mM to 1 mM and 10 mM, kinesin yield increases consistently from 13% to 27% and 39%. If yield is the only priority, we should use as high an ATP concentration as possible. In some experiments, however, low ATP concentration is needed in the eluant, and yield would be sacrificed.

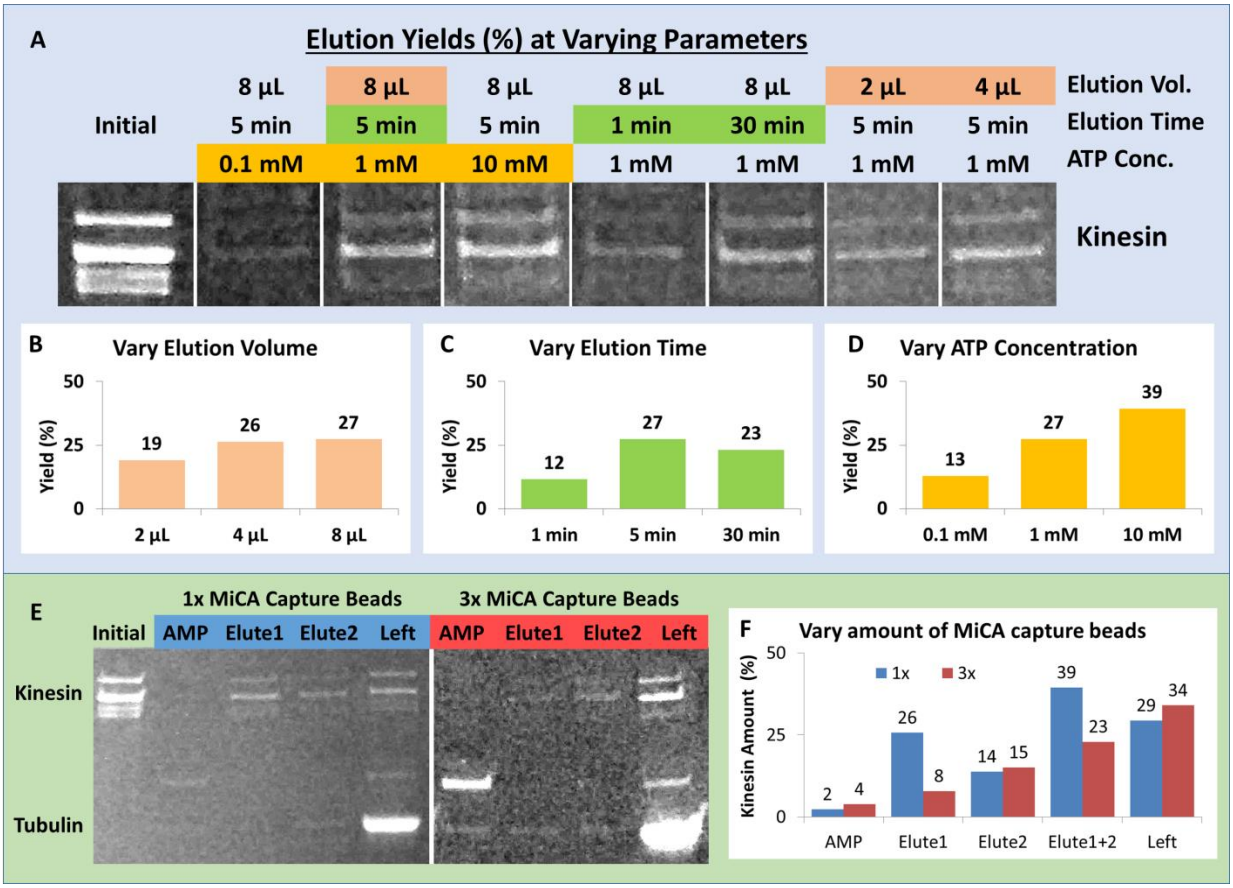

Figure B.7: (A) Gel image showing changes in MiCA purification yield when varying elution volume, time and ATP concentration. Yields are quantified in (B-D). (B) As elution volume increases from 2 µL to 4 µL and 8 µL, yield increases from 19% to 26% and 27%. Too low an elution volume will adversely affect elution yield. Up till a certain volume (4 µL in this case), increasing volume would not increase yield significantly. (C) Too short an elution time (1 min) will adversely affect yield. 5 min seems to be an optimal time. When the elution is too long (30 min), yield decreases, perhaps because some kinesin becomes inactive and are stuck to microtubule, or some are lost stuck to the tube or the bead. (D) Increasing ATP concentration increases kinesin yield, from 13% at 0.1 mM, to 27% and 39% at 1 mM and 10 mM. (E) Gel image showing the amount of kinesin detected at different purification phases while varying the amount of MiCA capture beads (1x and 3x). The amount of kinesin is quantified in (F). When the amount of bead increases three times, total yield (Elute 1+2) decreases from 39% to 23%. This is because extra beads increase the likelihood of kinesin rebinding to the microtubules on beads after unbinding. In this experiment, MiCA capture bead is in excess relative to kinesin. When MiCA capture bead is the limiting factor, increasing MiCA capture bead would increase yield.

B.10.2 Varying the amount of MiCA capture beads

In this experiment, the amount of MiCA capture bead is varied (1x and 3x amount), and its effect on elution yield is investigated. MiCA capture beads are prepared by removing the buffer in 20 µL/ 60 µL PEG-amine bead (10 mg/mL) and mixing in 2 µL/ 6 µL short microtubule. The mixtures are left to incubate for 5 min, washed with 8 µL dilution-taxol buffer, and then incubated in 4 µL DmB-BSA for 1

min. It is again washed with 8 µL dilution-taxol buffer before reconstituting in 2 µL dilution-taxol buffer to make a final volume of 3 µL. The mixture is mixed with 1 µL AMP-PNP (6 mM) and 2 µL K888-Het (0.75 µM), then incubated for 5 min at room temperature. After washing twice with 8 µL dilution-taxol buffer, the mixture is eluted twice with 4 µL elution buffer (1 mM ATP in dilution-taxol buffer), incubating 5 min each elution. The AMP-PNP supernatants, eluants, and proteins left in beads are then quantified with SDS-PAGE electrophoresis.

Figure B.7(E) shows the gel result from experiments varying MiCA capture beads. Figure B.7(F) quantifies the corresponding amounts of kinesin. Figure B.7(F) shows that when the amount of MiCA capture bead increases three times, total yield (Elute 1+2) decreases from 39% to 23%. This suggests the existence of an optimal amount of MiCA capture bead for a given amount of protein to be purified, consistent with the result from DDB-qdot purification shown in Figure 2-4(B). Too low is not good since there is not enough microtubules to capture all motors. Too high is also not good since it increases the likelihood of motors rebinding to the microtubules after unbinding.

B.10.3 Varying kinesin binding time

In this experiment, the kinesin binding time to microtubule in the presence of AMP-PNP is varied (1, 5 and 30 min), and its effect on elution yield is investigated. MiCA capture bead is prepared by removing the buffer in 80 µL PEG-amine bead (10 mg/mL) and mixing in 10 µL short microtubule. The mixture is left to incubate for 5 min, washed with 10 µL dilution-taxol buffer, and then incubated in 5 µL DmB-BSA for 1 min. It is again washed with 10 µL dilution-taxol buffer before reconstituting in 10 µL dilution-taxol buffer to make a final volume of 12 µL. The mixture is mixed with 3 µL AMP-PNP (6 mM) and 6 µL K888-Het (1.5 µM), then separated into 3 aliquots of 6 µL each. At each 1, 5 or 30 min, one aliquot is washed twice with 8 µL dilution-taxol buffer, then eluted twice with 4 µL elution buffer (1 mM ATP in dilution-taxol buffer), incubating 5 min each elution. The AMP-PNP supernatants, eluants, and proteins left in beads are then quantified with SDS-PAGE electrophoresis.

Figure B.8(A-B) shows that kinesin binding time minimally affects elution efficiency. Yield increases slightly from 10% to 12% as the binding time increases from 1 min to 5 min, and stay at 12% as binding time increases further to 30 min.

B.10.4 Varying microtubule sonication and use of BSA

In this experiment, the sonication of the short microtubules binding to PEG-amine bead is varied (0 min, 3 min and 6 min), and its effect on elution yield is investigated. The 3 min experiment is also duplicated and another set is done without BSA to block the MiCA capture bead.

Four aliquots of MiCA capture beads are prepared by removing the buffer in 96 µL PEG-amine bead (10 mg/mL) and mixing in 12 µL short microtubules (0 min, 3 min, 3 min (2^{nd}) and 6 min sonication). The mixtures are left to incubate for 5 min, washed with 10 µL BSA-taxol buffer for 0 min, 3 min and 6 min,

while for the 3 min (2^{nd}), 10 µL dilution-taxol buffer is used for wash. The mixtures are incubated for 1 min before another wash with 10 µL dilution-taxol buffer for all four aliquots. All are then reconstituted in 2 µL dilution-taxol buffer to make a final volume of 3 µL. The mixtures are mixed with 1 µL AMP-PNP (3 mM) and 2 µL K888-Het (1.5 µM), then incubated for 5 min. The mixtures are then washed twice with 8 µL dilution-taxol buffer, then eluted twice with 4 µL elution buffer (1 mM ATP in dilution-taxol buffer), incubating 5 min each elution. The AMP-PNP supernatants, eluants, and proteins left in beads are then quantified with SDS-PAGE electrophoresis.

Figure B.8(C-D) shows that Increasing microtubule sonication time from 0 min to 3 min and 6 min increases yield from 30% to 36% and 46%. This means that using shorter microtubules through longer sonication allows more kinesin to elute. This may be due to the short travel path motors have to walk on before releasing. As shown in the inset of Figure B.8(D), the amount of tubulin on each bead does not follow a consistent trend, which means that the increase in yield does not come from more microtubule binding to the beads at longer sonication.

The elution efficiencies with and without BSA blocking at 3 min sonication are the same (36%). Blocking with BSA does not improve or adversely affect purification yield. This result is helpful for experiments where BSA is essential to maintain protein activity, like that of dynein.

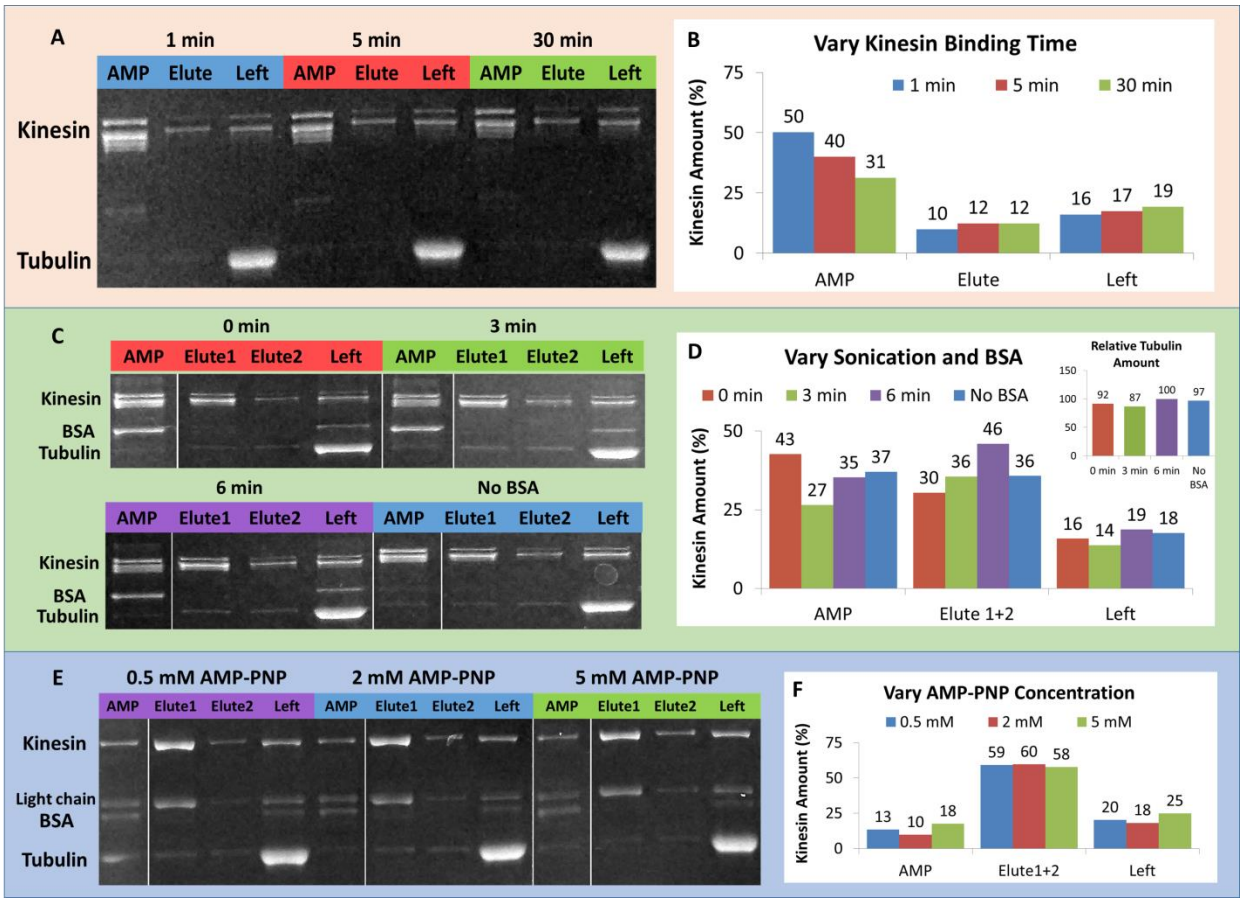

Figure B.8: (A,C,E) Gel images for experiments investigating kinesin yield by varying binding time (A), microtubule sonication time (C) and AMP-PNP concentration (E). (B,D,F) The corresponding quantification of bands shown in (A,C,E). (A-B) Binding time minimally affects elution efficiency. Yield increases slightly from 10% to 12% as the binding time increases from 1 min to 5 min, and stays at 12% as the binding time increases further to 30 min. (C-D) Increasing microtubule sonication time from 0 min to 3 min and 6 min increases yield from 30% to 36% and 46%. Using shorter microtubules through longer sonication allows more kinesin to elute. The 3 min experiment is duplicated without BSA blocking, and the elution efficiency with and without BSA blocking are the same (36%). Blocking with BSA does not improve or adversely affect yield. (E-F) Increasing AMP-PNP concentration from 0.5 mM to 5 mM does not increase elution yield. Yields maintain at around 59% when the AMP-PNP concentrations are at 0.5 mM, 2 mM or 5 mM.

B.10.5 Varying AMP-PNP concentration

In this experiment, the AMP-PNP concentration during kinesin binding is varied (0.5 mM, 2 mM and 5 mM), and its effect on elution yield is investigated. MiCA capture bead is prepared by removing the buffer in 72 µL PEG-amine bead (10 mg/mL) and mixing in 12 µL short microtubule. The mixture is left to incubate for 5 min, washed with 20 µL BSA-taxol buffer, and then incubated in 20 µL BSA-taxol buffer for 1 min. It is then washed with 20 µL dilution-taxol buffer before reconstituting in 10 µL dilution-taxol buffer to make a final volume of 12 µL. The mixture is then divided into three aliquots of 3 µL, and to

each aliquot, 1 µL AMP-PNP (3 mM, 12 mM or 30 mM) and 2 µL K888 (3.5 µM) are added. All aliquots are washed twice with 8 µL dilution-taxol buffer, then eluted twice with 8 µL elution buffer (1 mM ATP in dilution-taxol buffer), incubating 5 min each elution. The AMP-PNP supernatants, eluants, and proteins left in beads are then quantified with SDS-PAGE electrophoresis.

Figure B.8(E-F) shows that increasing AMP-PNP concentration from 0.5 mM to 5 mM does not increase elution yield. Yields remain approximately constant around 59% regardless of the AMP-PNP concentrations between 0.5 mM to 5 mM range. We can thus choose to use AMP-PNP concentration as low as 0.5 mM so that no trace AMP-PNP can be found in the elution buffer.

B.11 Microtubule release with casein, KCl and ATP

For MiCA purification to work, buffers that elute motors should not dislodge microtubule from the MiCA beads. Typically motors are eluted with ATP (1-5 mM) and high salt (50-300 mM potassium chloride (KCl)). In this experiment, we investigate if ATP and KCl dislodge microtubule. Additionally, we also test if casein dislodges microtubule, as casein is known to disrupt the charge-charge interaction between microtubule and the positively charged amine surface[71].

Seven aliquots of MiCA capture beads are prepared by removing the buffer in 6 µL PEG-amine bead (10 mg/mL) and mixing in 3 µL short microtubule (5x diluted from the usual stock described in Section 2.3.4). The mixtures are left to incubate for 10 min, then 3 µL of casein (0.1x and 0.5x working concentration), KCl (15 mM, 60 mM and 300 mM), and ATP (1 mM and 5 mM) are added to each aliquot. After 5 min incubation, the supernatant and the proteins left in beads are quantified with SDS-PAGE electrophoresis.

Figure B.9 shows the gel result (A) and the fraction of microtubule released (B) from this experiment. The fraction released is calculated by taking the ratio between the amount left in supernatant and the amount left on bead. When 0.5x and 0.1x working concentration of casein is added, 82% and 27% of microtubules are dislodged. It is clear that casein causes microtubule unbinding from the PEG-amine bead, so any buffers containing casein should be used with caution to prevent unwanted unbinding of microtubules. Figure B.9(B) also shows that as KCl concentration increases from 15 mM to 60 mM and 300 mM, the fraction of microtubules released increases from 14% to 28% and 45%. High salt therefore also causes microtubule release from the PEG-amine bead, and its use in elution buffers should be avoided. Lastly, as ATP concentration is increased from 1 mM to 5 mM, the amount of microtubules released remains minimal at 10% and 7%. This shows that we can increase ATP up to 5 mM without worrying it dislodging the microtubules.

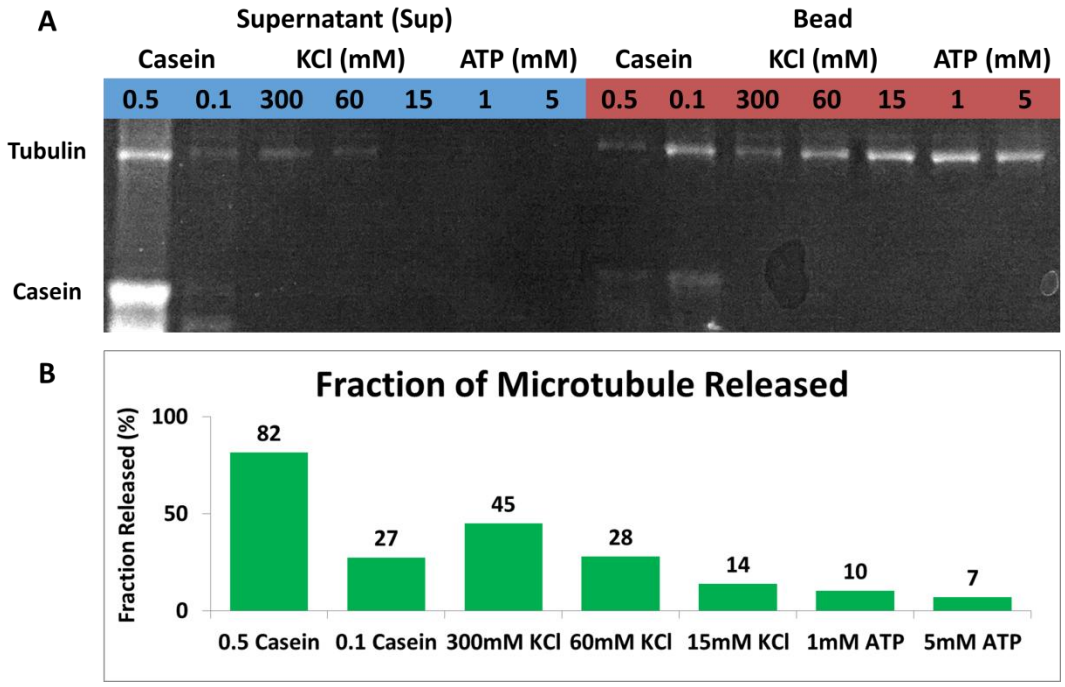

Figure B.9: (A) Gel image for microtubule unbinding experiment. The fraction of microtubule released shown in panel (B) is calculated by taking the ratio between the amount left in supernatant and the amount still stuck on bead. Casein is known to dislodge microtubules from positively charged surfaces[71]. When 0.5x and 0.1x working concentration of casein is added, 82% and 27% of microtubules are dislodged. Potassium chloride (KCl) increases the ionic strength of the buffer, thus decreasing the charge-charge interaction between microtubule and PEG-amine bead. As KCl concentration increases from 15 mM to 60 mM and 300 mM, the fraction of microtubules released increases from 14% to 28% and 45%. ATP is used to elute kinesin, and fortunately as the concentration of ATP increases from 1 mM to 5 mM, the fraction of microtubule released remains minimal at 10% and 7%.

REFERENCES

1. Yildiz A, Forkey JN, McKinney SA, Ha T, Goldman YE, Selvin PR. Myosin V Walks Hand-Over-Hand: Single Fluorophore Imaging with 1.5-nm Localization. Science. 2003;300(5628):2061–2065.

2. Yildiz A, Tomishige M, Vale RD, Selvin PR. Kinesin Walks Hand-Over-Hand. Science. 2004;303(5658):676–678.

3. Kural C, Kim H, Syed S, Goshima G, Gelfand VI, Selvin PR. Kinesin and Dynein Move a Peroxisome in Vivo: A Tug-of-War or Coordinated Movement? Science. 2005;308(5727):1469–1472.

4. Bruno A, Bruno L, Levi V. Extracting the Stepping Dynamics of Molecular Motors in Living Cells from Trajectories of Single Particles. Cell Biochemistry and Biophysics. 2012;65(1):1–11.

5. Kalafut B, Visscher K. An objective, model-independent method for detection of non-uniform steps in noisy signals. Computer Physics Communications. 2008;179(10):716–723.

6. Müllner FE, Syed S, Selvin PR, Sigworth FJ. Improved Hidden Markov Models for Molecular Motors, Part 1: Basic Theory. Biophysical Journal. 2010;99(11):3684–3695.

7. Syed S, Müllner FE, Selvin PR, Sigworth FJ. Improved Hidden Markov Models for Molecular Motors, Part 2: Extensions and Application to Experimental Data. Biophysical Journal. 2010;99(11):3696–3703.

8. Carter NJ, Cross RA. Mechanics of the kinesin step. Nature. 2005;435(7040):308–312.

9. Carter BC, Vershinin M, Gross SP. A Comparison of Step-Detection Methods: How Well Can You Do? Biophysical Journal. 2008;94(1):306–319.

10. Svoboda K, Schmidt CF, Schnapp BJ, Block SM. Direct observation of kinesin stepping by optical trapping interferometry. Nature. 1993;365(6448):721–727.

11. Cai D, Verhey KJ, Meyhöfer E. Tracking Single Kinesin Molecules in the Cytoplasm of Mammalian Cells. Biophysical Journal. 2007;92(12):4137–4144.

12. Svoboda K, Block SM. Force and velocity measured for single kinesin molecules. Cell. 1994;77(5):773–784.

13. Hua W, Young EC, Fleming ML, Gelles J. Coupling of kinesin steps to ATP hydrolysis. Nature. 1997;388(6640):390–393.

14. Kerssemakers JWJ, Laura Munteanu E, Laan L, Noetzel TL, Janson ME, Dogterom M. Assembly dynamics of microtubules at molecular resolution. Nature. 2006;442(7103):709–712.

15. Sadler BM, Swami A. Analysis of multiscale products for step detection and estimation. IEEE Transactions on Information Theory. 1999;45(3):1043–1051.

16. Rabiner LR. A tutorial on hidden Markov models and selected applications in speech recognition. Proceedings of the IEEE. 1989;77(2):257–286.

17. Hughey R, Krogh A. Hidden Markov models for sequence analysis: extension and analysis of the basic method. Computer applications in the biosciences : CABIOS. 1996;12(2):95–107.

18. Chung S-H, Gage PW. Signal processing techniques for channel current analysis based on hidden markov models. In: Enzymology B-M in, editor. Vol. 293. Academic Press; 1998. p. 420–437. (Ion Channels Part B). http://www.sciencedirect.com/science/article/pii/S0076687998930270

19. Fredkin DR, Rice JA. Maximum Likelihood Estimation and Identification Directly from Single-Channel Recordings. Proceedings of the Royal Society of London B: Biological Sciences. 1992;249(1325):125–132.

20. Qin F. Restoration of Single-Channel Currents Using the Segmental k-Means Method Based on Hidden Markov Modeling. Biophysical Journal. 2004;86(3):1488–1501.

21. Venkataramanan L, Sigworth FJ. Applying hidden Markov models to the analysis of single ion channel activity. Biophysical Journal. 2002;82(4):1930–1942.

22. Veigel C, Schmidt CF. Moving into the cell: single-molecule studies of molecular motors in complex environments. Nature Reviews Molecular Cell Biology. 2011;12(3):163–176.

23. Finer JT, Simmons RM, Spudich JA. Single myosin molecule mechanics: piconewton forces and nanometre steps. Nature. 1994;368(6467):113–119.

24. Yildiz A, Tomishige M, Vale RD, Selvin PR. Kinesin Walks Hand-Over-Hand. Science. 2004;303(5658):676–678.

25. Molloy JE, Burns JE, Kendrick-Jones J, Tregear RT, White DCS. Movement and force produced by a single myosin head. Nature. 1995;378(6553):209–212.

26. Block SM. Kinesin Motor Mechanics: Binding, Stepping, Tracking, Gating, and Limping. Biophysical Journal. 2007;92(9):2986–2995.

27. Gennerich A, Vale RD. Walking the walk: how kinesin and dynein coordinate their steps. Current Opinion in Cell Biology. 2009;21(1):59–67. (Cell structure and dynamics).

28. Sellers JR, Veigel C. Walking with myosin V. Current Opinion in Cell Biology. 2006;18(1):68–73. (Cell structure and dynamics).

29. Mehta AD, Rock RS, Rief M, Spudich JA, Mooseker MS, Cheney RE. Myosin-V is a processive actin-based motor. Nature. 1999;400(6744):590–593.

30. Altman D, Sweeney HL, Spudich JA. The Mechanism of Myosin VI Translocation and Its Load-Induced Anchoring. Cell. 2004;116(5):737–749.

31. Gennerich A, Carter AP, Reck-Peterson SL, Vale RD. Force-Induced Bidirectional Stepping of Cytoplasmic Dynein. Cell. 2007;131(5):952–965.

32. Veigel C, Wang F, Bartoo ML, Sellers JR, Molloy JE. The gated gait of the processive molecular motor, myosin V. Nature Cell Biology. 2002;4(1):59–65.

33. Telley IA, Bieling P, Surrey T. Obstacles on the Microtubule Reduce the Processivity of Kinesin-1 in a Minimal In Vitro System and in Cell Extract. Biophysical Journal. 2009;96(8):3341–3353.

34. Norris SR, Núñez MF, Verhey KJ. Influence of Fluorescent Tag on the Motility Properties of Kinesin-1 in Single-Molecule Assays. Biophysical Journal. 2015;108(5):1133–1143.

35. Pierce DW, Hom-Booher N, Vale RD. Imaging individual green fluorescent proteins. Nature. 1997;388(6640):338–338.

36. Vale RD, Funatsu T, Pierce DW, Romberg L, Harada Y, Yanagida T. Direct observation of single kinesin molecules moving along microtubules. Nature. 1996;380(6573):451–453.

37. Qiu W, Derr ND, Goodman BS, Villa E, Wu D, Shih W, Reck-Peterson SL. Dynein achieves processive motion using both stochastic and coordinated stepping. Nature Structural & Molecular Biology. 2012;19(2):193–200.

38. Sikora A, Canova FF, Kim K, Nakazawa H, Umetsu M, Kumagai I, Adschiri T, Hwang W, Teizer W. Behavior of Kinesin Driven Quantum Dots Trapped in a Microtubule Loop. ACS Nano. 2015;9(11):11003–11013.

39. Seitz A, Surrey T. Processive movement of single kinesins on crowded microtubules visualized using quantum dots. The EMBO Journal. 2006;25(2):267–277.

40. Yildiz A, Vale RD. Tracking Movements of the Microtubule Motors Kinesin and Dynein Using Total Internal Reflection Fluorescence Microscopy. Cold Spring Harbor Protocols. 2015;2015(9):pdb.prot086355.

41. Ori-McKenney KM, Xu J, Gross SP, Vallee RB. A cytoplasmic dynein tail mutation impairs motor processivity. Nature Cell Biology. 2010;12(12):1228–1234.

42. Can S, Dewitt MA, Yildiz A. Bidirectional helical motility of cytoplasmic dynein around microtubules. eLife. 2014;3:e03205.

43. Ohyanagi T, Shima T, Okada Y, Tsukasaki Y, Komatsuzaki A, Tsuboi S, Jin T. Compact and stable SNAP ligand-conjugated quantum dots as a fluorescent probe for single-molecule imaging of dynein motor protein. Chemical Communications. 2015;51(80):14836–14839.

44. Ali MY, Vilfan A, Trybus KM, Warshaw DM. Cargo Transport by Two Coupled Myosin Va Motors on Actin Filaments and Bundles. Biophysical Journal. 2016;111(10):2228–2240.

45. DeWitt MA, Chang AY, Combs PA, Yildiz A. Cytoplasmic Dynein Moves Through Uncoordinated Stepping of the AAA+ Ring Domains. Science. 2012;335(6065):221–225.

46. Belyy V, Schlager MA, Foster H, Reimer AE, Carter AP, Yildiz A. The mammalian dynein-dynactin complex is a strong opponent to kinesin in a tug-of-war competition. Nature Cell Biology. 2016;18(9):1018–1024.

47. Derr ND, Goodman BS, Jungmann R, Leschziner AE, Shih WM, Reck-Peterson SL. Tug-of-War in Motor Protein Ensembles Revealed with a Programmable DNA Origami Scaffold. Science. 2012;338(6107):662–665.

48. Belyy V, Hendel NL, Chien A, Yildiz A. Cytoplasmic dynein transports cargos via load-sharing between the heads. Nature Communications. 2014;5:5544.

49. Berensmeier S. Magnetic particles for the separation and purification of nucleic acids. Applied Microbiology and Biotechnology. 2006;73(3):495–504.

50. Safarik I, Safarikova M. Magnetic techniques for the isolation and purification of proteins and peptides. BioMagnetic Research and Technology. 2004;2:7.

51. Vale RD, Reese TS, Sheetz MP. Identification of a novel force-generating protein, kinesin, involved in microtubule-based motility. Cell. 1985;42(1):39–50.

52. DeLuca JG, Newton CN, Himes RH, Jordan MA, Wilson L. Purification and Characterization of Native Conventional Kinesin, HSET, and CENP-E from Mitotic HeLa Cells. Journal of Biological Chemistry. 2001;276(30):28014–28021.

53. Sigua R, Tripathy S, Anand P, Gross SP. Isolation and Purification of Kinesin from Drosophila Embryos. Journal of Visualized Experiments : JoVE. 2012 [accessed 2016 Oct 30];(62). http://www.ncbi.nlm.nih.gov/pmc/articles/PMC3466667/

54. Tao L, Scholey JM. Purification and assay of mitotic motors. Methods. 2010;51(2):233–241. (Methods Related to Mitotic Spindle Research).

55. Kuznetsov S, Gelfand V. Purification of Kinesin from the Brain. In: Vernos I, editor. Kinesin Protocols. Humana Press; 2001. p. 1–7. (Methods in Molecular Biology™). http://dx.doi.org/10.1385/1-59259-069-1%3A1

56. Rothwell SW, Deal CC, Pinto J, Wright DG. Affinity purification and subcellular localization of kinesin in human neutrophils. Journal of Leukocyte Biology. 1993;53(4):372–380.

57. Buster D, Scholey JM. Purification and assay of kinesin from sea urchin eggs and early embryos. J Cell Sci. 1991;1991(Supplement 14):109–115.

58. Fields G. Methods for Removing the Fmoc Group. In: Pennington M, Dunn B, editors. Peptide Synthesis Protocols. Humana Press; 1995. p. 17–27. (Methods in Molecular Biology). http://dx.doi.org/10.1385/0-89603-273-6%3A17

59. David-Pfeuty T, Laporte J, Pantaloni D. GTPase activity at ends of microtubules. Nature. 1978;272(5650):282–284.

60. Grover R, Fischer J, Schwarz FW, Walter WJ, Schwille P, Diez S. Transport efficiency of membrane-anchored kinesin-1 motors depends on motor density and diffusivity. Proceedings of the National Academy of Sciences. 2016;113(46):E7185–E7193.

61. Morris RL, Hollenbeck PJ. The regulation of bidirectional mitochondrial transport is coordinated with axonal outgrowth. Journal of Cell Science. 1993;104(3):917–927.

62. Tanenbaum ME, Akhmanova A, Medema RH. Bi-directional transport of the nucleus by dynein and kinesin-1. Communicative & Integrative Biology. 2011;4(1):21–25.

63. Gross SP, Tuma MC, Deacon SW, Serpinskaya AS, Reilein AR, Gelfand VI. Interactions and regulation of molecular motors in Xenopus melanophores. The Journal of cell biology. 2002;156(5):855–865.

64. Welte MA, Gross SP, Postner M, Block SM, Wieschaus EF. Developmental Regulation of Vesicle Transport in Drosophila Embryos: Forces and Kinetics. Cell. 1998;92(4):547–557.

65. Nascimento AA, Roland JT, Gelfand VI. PIGMENT CELLS: A Model for the Study of Organelle Transport. Annual Review of Cell and Developmental Biology. 2003;19(1):469–491.

66. Blehm BH, Schroer TA, Trybus KM, Chemla YR, Selvin PR. In vivo optical trapping indicates kinesin's stall force is reduced by dynein during intracellular transport. Proceedings of the National Academy of Sciences. 2013;110(9):3381–3386.

67. Coppin CM, Pierce DW, Hsu L, Vale RD. The load dependence of kinesin's mechanical cycle. Proceedings of the National Academy of Sciences. 1997;94(16):8539–8544.

68. Block SM, Asbury CL, Shaevitz JW, Lang MJ. Probing the kinesin reaction cycle with a 2D optical force clamp. Proceedings of the National Academy of Sciences. 2003;100(5):2351–2356.

69. Asbury CL, Fehr AN, Block SM. Kinesin Moves by an Asymmetric Hand-Over-Hand Mechanism. Science (New York, N.Y.). 2003;302(5653):2130–2134.

70. Hua W, Chung J, Gelles J. Distinguishing inchworm and hand-over-hand processive kinesin movement by neck rotation measurements. Science (New York, N.Y.). 2002;295(5556):844–848.

71. Nicholas M, Rao L, Gennerich A. Covalent Immobilization of Microtubules on Glass Surfaces for Molecular Motor Force Measurements and Other Single-Molecule Assays. In: Sharp DJ, editor. Mitosis. Springer New York; 2014. p. 137–169. (Methods in Molecular Biology). http://dx.doi.org/10.1007/978-1-4939-0329-0_9

72. Kawaguchi K, Yamaguchi A. Temperature dependence rigidity of non-taxol stabilized single microtubules. Biochemical and Biophysical Research Communications. 2010;402(1):66–69.

73. Hawkins TL, Sept D, Mogessie B, Straube A, Ross JL. Mechanical Properties of Doubly Stabilized Microtubule Filaments. Biophysical Journal. 2013;104(7):1517–1528.

74. Cronan JE. Biotination of proteins in vivo. A post-translational modification to label, purify, and study proteins. Journal of Biological Chemistry. 1990;265(18):10327–10333.

75. Simonson PD. Using photo-instability to quantify fluorophores and achieve super-resolution imaging. 2011.